Heriot-Watt University

Numerical approximation of SDEs & the stochastic Swift-Hohenberg equation

by

Iyabo Ann Adamu

Submitted for the degree of
Doctor of Philosophy
on completion of research in the
Department of Mathematics,
School of Mathematical and Computer Sciences,
Heriot-Watt University

July 2011

Declaration

I hereby declare that the work presented in this thesis was carried out by myself at Heriot-Watt University, except where due acknowledgement is made, and not been submitted for any other degree.

Signature of Iyabo Ann Adamu:

Signature of Supervisor:

Abstract

We consider the numerical approximation of stochastic differential equations interpreted both in the Itô and Stratonovich sense and develop three stochastic time-integration techniques based on the deterministic exponential time differencing schemes. Two of the numerical schemes are suited for the simulations of Itô stochastic ordinary differential equations (SODEs) and they are referred to as the stochastic exponential time differencing schemes, SETD0 and SETD1. The third numerical scheme is a new numerical method we propose for the simulations of Stratonovich SODEs. We call this scheme, the Exponential Stratonovich Integrator (ESI).

We investigate numerically the convergence of these three numerical methods, in addition to three standard approximation schemes and also compare the accuracy and efficiency of these schemes. The effect of small noise is also studied.

We study the theoretical convergence of the stochastic exponential time differencing scheme (SETD0) for parabolic stochastic partial differential equations (SPDEs) with infinite-dimensional additive noise and one-dimensional multiplicative noise. We obtain a strong error temporal estimate of $O(\Delta t^{\theta} + \epsilon \Delta t^{\theta} + \epsilon^2 \Delta t^{1/2})$ for SPDEs forced with a one-dimensional multiplicative noise and also obtain a strong error temporal estimate of $O(\Delta t^{\theta} + \epsilon^2 \Delta t)$ for SPDEs forced with an infinite-dimensional additive noise. We examine convergence for second-order and fourth-order SPDEs.

We consider the effects of spatially correlated and uncorrelated noise on bifurcations for SPDEs. In particular, we study a fourth-order SPDE, the Swift-Hohenberg equation, and allow the control parameter to fluctuate. Numerical simulations show a shift in the pinning region with multiplicative noise.

Dedication

In memory of my late father, Mr M. M. O. Bello, who gave me his best for my education.

Acknowlegdements

First and foremost, I give all the thanks and honour to God Almighty who has helped and sustained me throughout my life and studies.

My deep and sincere appreciation goes to my supervisor Professor Gabriel J. Lord for his outstanding supervision, invaluable guidance, support and encouragement throughout my PhD studies. I am also grateful for his suggestions and comments while reading the draft of this thesis.

I would like to thank the Heriot-Watt University for awarding me, the James-Watt Scholarship which covered my tuition and maintenance fees.

My earnest gratitude goes to my loving husband, Mr Timothy Adamu, who is also my best friend. I appreciate his unending support, encouragement, understanding and motivation throughout the period of my studies. In the process of writing-up this thesis, I was pregnant with our son, Davidson Tavershima Oluwademilade Adamu. He has in his own little ways helped me in coping better with my obligation to taking care of him and also getting the thesis finished, by being a strong and joyful child. While working on the laptop with him, he usually loves to help me in the typesetting of the thesis, by striking the computer keyboard.

Special thanks to my mother, Mrs Ruth E. Bello and my siblings- Babarinde, Abiodun, Olufunmilayo and Korede Bello for their prayers and love. I thank my parent-inlaws, Mr & Mrs Jonathan Adamu and my sibling-inlaws, Terkimbi, Blessing, Dooshima, Doofan Adamu for their constant prayers and support.

I thank my friends and colleagues in the School of MACS. I thank Dr A. Tambue in particular, for the discussions on our similar research interests. I acknowledge the members of staff of the Department of Mathematics, Heriot-Watt University. I thank the African Institute of Mathematics Sciences (AIMS) for its interest in my career.

Table of Contents

List of Figures

List of Tables

Chapter 1

Introduction.

Before the 1950's, deterministic differential equations were typically used to describe the dynamics of the systems which occur in applications. However, it is obvious that in the world we live in today, phenomena that arise are not always deterministic in nature.

Noise, sometimes referred to as fluctuations or randomness, has now been found to be important in lots of phenomena, thus it has become important to include random effects when modelling diverse physical phenomena that arise in engineering, aeronautics, physics, biology, meteorology, oceanography, environmental sciences, etc. Equations which take into account time dependent random fluctuations are referred to as stochastic differential equations.

Over the past decades, there has been an increase in the study and research of the numerical solutions of stochastic differential equations (SDEs). More recently, there is growing interest in stochastic partial differential equations (SPDEs). In general, there are very few SDEs for which analytical solutions can be obtained and this is also true for SPDEs. Hence, the need to develop numerical methods for the solution of these equations. Noise paths can be generated from the computer. Many approaches for the numerical solutions are either based on computing many sample paths and then determining the accuracy of a trajectory or based on computing approximation to the probability distribution of the solution, and then determine various statistical measures. The treatment of stochastic differential equation is very different from

the deterministic setting. Consequently, understanding fully the theory, analysis and solution of this problem is not an easy task, and so we believe that development of numerical methods to generate solutions to stochastic differential equations will lead to a better understanding of the subject of stochastic differential equations [25].
This thesis is mainly concerned with the study of numerical approximations to stochastic ordinary and partial differential equations.
We shall review the literature on the numerical approximations of SPDEs later in the thesis.

1.1 Objectives.

The main objectives of the thesis are the following:

1. Develop an efficient and accurate numerical integration technique for the solution of Itô SPDEs. The motivation for the development of the numerical method comes from the work in [18], where a deterministic numerical method called the exponential time differing **(ETD)** scheme was derived. This scheme has been shown to be very promising for semi-linear problems, see for example, the deterministic work done for example in [18, 47]. As a result, we seek stochastic variants of this scheme, which we call the stochastic exponential time differencing schemes **(SETD0)** and **(SETD1)**. Since these numerical schemes are to serve as an alternative numerical method for the solution of SDEs, we carry out numerical experiments on these schemes and compare against some existing standard numerical methods.

2. Study the theoretical convergence of the numerical method developed. In particular, we wish to study convergence in time for the **SETD0** scheme in the strong sense and obtain strong error estimates for SPDEs forced with additive and multiplicative noise. The style of analysis we use in this work is based on the work in [55].

3. Develop a new numerical scheme for the solution of SPDEs interpreted in the

Stratonovich sense which we call the exponential Stratonovich integrator **(ESI)**. We compare numerically the accuracy and efficiency of the **ESI** with an existing numerical method known as the **Heun** scheme which is a natural method used for discretizing SDEs with Stratonovich noise.

4. Study the effects of spatially correlated and uncorrelated noise on bifurcation for the SPDE known as the Swift-Hohenberg equation. The motivation for carrying out this study comes from the work in [11, 12], in which they present a bifurcation diagram for the deterministic Swift-Hohenberg equation. In their work, the bifurcation diagram displays a pinning region, in which stable spatially localized states are contained. Thus, in this thesis, we wish to explore the effects of noise on the pinning/snaking region by allowing the control parameter to fluctuate. In particular, we wish to examine the dynamics of the snaking region when noise is taken into account.
   Indeed the studies and analysis of snaking region in the Swift-Hohenberg equation and the Complex Ginzburg-Laudau equation is currently an active area of research, see the recent work by [62] and [64].

1.2 Thesis outline

In Chapter 2, we give background material on SODEs and SPDEs and present some standard numerical integration techniques.
In Chapter 3, we review the subject of deterministic **ETD** schemes and show the derivation of three stochastic **ETD**. We then carry out numerical experiments on four examples of SODEs using these numerical schemes. These SODEs were interpreted both in the Itô and Stratonovich sense. We apply six numerical methods, namely the **Heun** method, the exponential Stratonovich integrator **(ESI)**, the Lord-Rougemont **(LR)** scheme, the Euler-Maruyama **(EM)** scheme, the stochastic exponential time differencing schemes **(SETD0)** and **(SETD1)**, to obtain approximate solutions. For simulations of SODEs with Stratonovich noise, the **Heun** and **ESI** schemes were used, while for the simulations of SODEs with Itô noise, the **SETD0**, **SETD1**, **LR** and

EM methods were applied. The drift correction formula was used to convert from one stochastic calculus to the other. Numerical experiments were performed to obtain the strong and weak order of convergence for all the numerical methods. We also study briefly SDEs with small noise.

In Chapter 4, we study the theoretical strong convergence of the **SETD0** scheme for SPDEs with additive and multiplicative noise subject to periodic boundary conditions. We only consider convergence in time and not convergence in space. For SPDEs with additive noise, we consider the infinite dimensional Wiener process and for the SPDEs with multiplicative noise, we consider a one dimensional Brownian motion. We prove strong error estimates for second order and fourth-order SPDEs. For the case of **SETD1** scheme, we will only study numerically the strong convergence of this scheme in Chapter 5.

In Chapter 5, we numerically investigate the strong convergence of the three numerical schemes developed in this thesis, that is, the **SETD0** and **SETD1** schemes for the direct simulations of Itô SODEs and the **ESI** scheme for the direct simulations of Stratonovich SODEs.

The Allen-Cahn equation (second-order SPDE) and the Swift-Hohenberg equation (fourth-order SPDE) were used as numerical examples in the experiments. These SPDE examples which are interpreted in the Itô sense were discretized in space by a Fourier spectral method, this procedure gives rise to a system of Itô SODEs, in which we then apply the **SETD0** and **SETD1** schemes to perform the numerical integration. We also compare the numerical results with the **LR** scheme and semi-implicit **EM** scheme.

On the other hand, in order to use the **ESI** scheme for numerical integration, we perform an Itô-Stratonovich correction, so that the resulting Stratonovich SPDEs gives rise to Stratonovich SODEs upon discretizing the spatial variable first. The **ESI** scheme is compared against the standard **Heun** scheme.

In Chapter 6, we study the effects of stochastic forcing on the Swift-Hohenberg (SH) equation forced with Itô and Stratonovich noise. In particular we consider noise white in time and spatially correlated/uncorrelated noise. We allow the control parameter in

the underlying system to fluctuate and perform direct simulations on the SH equation using the new numerical method we propose in this thesis called the exponential Stratonovich Integrator **ESI** scheme. This scheme is also compared against standard numerical method for the direct simulation of Stratonovich SDEs, called the **Heun** method. We also perform a drift correction on the SH equation with Stratonovich noise, in order to allow us have an Itô equation. This form of equation provides the framework to allow us take out the systematic contribution of noise by using the small noise expansion idea in [27]. The resulting ODE system is then examined using AUTO to obtain bifurcation diagrams displaying the snaking region for the spatially localized states.

We give concluding discussions on the findings in this thesis in Chapter 7.

Chapter 2

Background for SODEs & SPDEs.

In this chapter, we give some background material used in this thesis for the numerical approximation of SODEs and SPDEs.

2.1 Background for SODEs.

A **stochastic ordinary differential equation (SODE)** is an equation that incorporates time dependent random elements in the differential equation system, see for example [50, 70]. Equations with noise have been shown to play important modelling role in many areas such as population dynamics [50], filtering [70], investment finance [40], biology [50], chemistry [28], circuit simulation [97], wave propagation [57] to mention a few.

A general autonomous Itô SODE is written in the following form

$$dX(t) = f(X(t))dt + g(X(t))dW(t), \quad t \in [t_0, T] \quad X(t_0) = X_0, \tag{2.1.1}$$

where $X(t) \in \mathbb{R}^d$, $f : \mathbb{R}^d \to \mathbb{R}^d$ (is known as the drift coefficient), $g : \mathbb{R}^d \to \mathbb{R}^{d\times m}$ (is known as the diffusion coefficient), and $W(t)$ is a m-dimensional Brownian motion. The integral formulation of (2.1.1) is

$$X(t) = X_0 + \int_{t_0}^{t} f(X(s))ds + \int_{t_0}^{t} g(X(s))dW(s), \tag{2.1.2}$$

where the first integral is understood in the sense of a Riemann-Stieltjes integral and the second integral is understood in the sense of an Itô stochastic integral [23, 50].

The stochastic integral can be interpreted in different ways. The most widely used interpretations of a stochastic integral are the Itô and Stratonovich, see [50]. It is possible to switch between one interpretation and the other. The solution to a scalar Itô-rule stochastic differential equation (2.1.1) with drift coefficient f and diffusion coefficient g is equivalent to the solution of a scalar Stratonovich-rule SDE with drift coefficient $\tilde{f}$ and diffusion coefficient $\tilde{g}$, provided $\tilde{g} = g$, and $\tilde{f} = f - \frac{1}{2}gg'$ [50]. For many SDEs of practical interest, analytic solutions are rarely available, thus numerical methods to approximate their solutions are required. A number of computational techniques have been developed to solve these kinds of equations [50]. Some of such computational techniques includes the Euler-Maruyama and the Milstein method. These methods are always derived under the rules of stochastic calculus; SDEs makes sense in the integral representation (2.1.2). This integral representation contains two integrals, the ordinary and stochastic integral. The integrand function in the ordinary integrals follows the rules of deterministic calculus, in which the integrand function in the Riemann sum approximating the Riemann integral is evaluated at any arbitrary point in a given interval, however, for the case of a stochastic integral, the integrand function needs to be evaluated at a specific point in an interval [50]. Consequently, when the stochastic integral is evaluated at the left-end point, we say such integral is an Itô stochastic integral and if the stochastic integral is evaluated at the midpoint, we say such integral is a Stratonovich stochastic integral [70].

Higher order stochastic numerical methods can also be useful in some contexts. It is usually straight forward to derive these kinds of methods, however, the problem lies in the complexities involved in the implementation of higher order stochastic integrals, in addition to the cumbersome calculations of derivatives of the coefficients of the underlying system. We do not pursue higher order methods in this thesis, as we wish to examine solutions of SPDES.

SDEs are either forced with additive or multiplicative noise. An SDE is said to have additive noise if all the entries of the diffusion co-efficient matrix are either constant or functions of time only. But if the diffusion co-efficient contains functions of the state variables, then the SDE is said to have multiplicative noise [50].

Note that in the case of additive noise, the Stratonovich system coincides with Itô system [50, 70].
In what follows, we give a quick overview on the concept of Wiener process and stochastic integrals.

Definition 2.1.1. Wiener process [50, 70].
A stochastic process $W(t), t \in [0, \infty)$, is said to be a Wiener process if

i. $W(0) = 0$ (with probability 1)

ii. For $0 \leq s < t \leq T$, the increment $W(t) - W(s) \sim \mathcal{N}(0, t - s)$ with mean 0 and variance $t - s$.

iii. For $0 \leq s < t < u < v \leq T$, the increments $W(v) - W(u)$ and $W(t) - W(s)$ are independent.

iv. $\mathbb{E}[W(t)] = 0$ and $\mathbb{E}[W(s)W(t)] = \min\{s, t\}$.

The property $\mathbb{E}[W(s)W(t)] = \min\{s, t\}$ can be used to demonstrate the independence of the Wiener increments. Suppose that $0 \leq t_0 < \cdots < t_{i-1} < t_i < \cdots < t_{j-1} < t_j < \cdots t_n$; then

$$\begin{aligned}
\mathbb{E}((W(t_i) - W(t_{i-1}))(W(t_j) - W(t_{j-1}))) &= \mathbb{E}(W(t_i)W(t_j)) - \mathbb{E}(W(t_i)W(t_{j-1})) \\
&- \mathbb{E}(W(t_{i-1})W(t_j)) + \mathbb{E}(W(t_{i-1})W(t_{j-1})) \\
&= t_i - t_i - t_{i-1} + t_{i-1} = 0,
\end{aligned}$$

and hence the increments $W(t_i) - W(t_{i-1})$ and $W(t_j) - W(t_{j-1})$ are independent.
The sample paths of the Wiener process $W(t)$ are continuous, but nowhere differentiable and not of bounded variation on any finite time interval [50].
The standard Wiener process is also known as Brownian motion. Brownian motion is a stochastic process which serves as the basis for the theory of stochastic differential equations. The term "Brownian" was coined from the name of a Scottish botanist,

Robert Brown, who first reported in 1827 experimental observations involving the erratic behaviour of pollen grains that were bombarded by water molecules.

Itô stochastic integral.

A Japanese mathematician Koisy Itô [45] in the 1950's, introduced the Itô stochastic integral. Consider a partition $0 = t_0 < t_1 < \cdots < t_M = T$ with time step size $\Delta t = (T - t_0)/M$, the Itô integral is defined as the mean-square limit of the sum in (2.1.3), whereby the integrand is evaluated at the left-hand endpoint $t_k = k\Delta t$ of the subinterval $[t_k, t_{k+1}]$, that is,

$$\int_0^T g(X(t))\, dW(t) := \text{ms}- \lim_{M\to\infty} \sum_{k=0}^{M-1} g(X(t_k))\, [W(t_{k+1}) - W(t_k)]\,. \tag{2.1.3}$$

Here ms- lim denotes the limit in the mean square sense. Evaluating the function $g(X(t))$ at the beginning of the subinterval $[t_k, t_{k+1}]$ renders $g(X(t_k))$ statistically independent of $[W(t_k), W(t_{k+1})]$ and thus ensuring that the Itô integral has zero mean [50, 70].

Let $|\cdot|$ denote the standard Euclidean norm on $\mathbb{R}^d$ and $|\cdot|_F$ denote the Frobenius norm on $\mathbb{R}^{d\times m}$.

Existence and uniqueness of strong solutions of Itô SODEs.

Theorem 2.1.1. *[50, 13, 48, 23]. Let the functions f and g in (2.1.1) be measurable on the interval $[t_0, T]$ and suppose for some positive constants $c \in \mathbb{R}$ and for all $x, y \in \mathbb{R}^d$, the following conditions are satisfied*

1. *Coefficients f and g satisfy the Lipschitz conditions*

$$|f(x) - f(y)| \le c|x - y| \quad \text{and} \quad |g(x) - g(y)|_F \le c|x - y| \tag{2.1.4}$$

2. *Coefficients f and g satisfy the linear growth conditions*

$$|f(x)|^2 \le c^2(1 + |x|^2) \quad \text{and} \quad |g(x)|_F^2 \le c^2(1 + |x|^2) \tag{2.1.5}$$

3. $X(t_0)$ *is independent of* $W(t), t_0 \leq t \leq T$, *and* $\mathbb{E}\left[X^2(t_0)\right] < \infty$.

Then there exists a pathwise unique strong solution $X(t)$ *of the SDE (2.1.1) with initial condition* X_0 *on* $[t_0, T]$ *with*

$$\sup_{t\in[t_0,T]} \mathbb{E}\left[X^2(t)\right] < \infty. \tag{2.1.6}$$

The uniqueness of the solution is pathwise uniqueness, if $X(t)$ *and* $\overline{X}(t)$ *are two solutions of the SDE, then*

$$\mathbb{P}\left(\sup_{[t_0,T]} |X(t) - \overline{X}(t)| = 0\right) = 1. \tag{2.1.7}$$

Stratonovich stochastic integral.

A Russian physicist R. L. Stratonovich [88] proposed in the 1960s an alternative stochastic integral, which is widely known as the Stratonovich stochastic integral. The Stratonovich integral is defined as the mean-square limit of the sum in (2.1.8), whereby the integrand is evaluated at the mid-point $\frac{1}{2}(t_k + t_{k+1})$ of each partition subinterval, that is,

$$\int_0^T g(X(t)) \circ dW(t) = \text{ms}- \lim_{M\to\infty} \sum_{k=0}^{M-1} g\left(X\left(\frac{t_k + t_{k+1}}{2}\right)\right)\Big[W(t_{k+1}) - W(t_k)\Big], \tag{2.1.8}$$

where the symbol $\circ$ is employed to distinguish the Stratonovich integral from the Itô integral.

Modelling issue: Itô or Stratonovich

The question as to which of these stochastic integrals to use has been asked in the literature. While both approaches are correct, the choice of which to use depends on the modelling process that leads to the SDE formulation. Both of the approaches has particular features which one can take advantage of.

For instance, Itô stochastic calculus has direct connection with diffusion processes and martingale theory [40, 70] in which the random variable $X(t)$ is non-anticipating, so that information about $X(t)$ at time t does not depend on events occurring after time

t. It also allows easy calculations of moments of the solution of an SDE, which offers many theoretical advantages.
From an application point of view, Itô SDEs are often considered when large number of independent entities, for example, the sales of shares in finance and bacteria in biology, while Stratonovich SDE is better considered when the white noise is meant to be a suitable approximation of a smoother but less tractable noise [40].

In any case, once a particular form of stochastic forcing has been chosen, it is possible to switch between the two stochastic calculi.
For example, in the scalar case, consider the Itô SDE given in (2.1.1). The equivalent Stratonovich SDE is given by

$$dX(t) = \tilde{f}(X(t))dt + g(X(t)) \circ dW(t), \tag{2.1.9}$$

where

$$\tilde{f}(X(t)) = f(X(t)) - \frac{1}{2}\frac{\partial g}{\partial x}(X(t))\, g(X(t)). \tag{2.1.10}$$

The two equations (2.1.1) and (2.1.9), though under different rules of calculus, have the same solution [70, 50]. Examples of these equations and numerical experiments carried out on them are presented in chapters 3 and 5.

2.2 Numerical methods for SODEs.

In this section, we outline standard numerical methods for SODEs. We will also be investigating the convergence of these numerical methods later in the thesis.
There are many definitions of convergence for sequences of random variables. However, the two most common ways of measuring the accuracy of a numerical solution of SDEs are strong convergence (which is for problems involving direct simulation, where it is important that the trajectories of the numerical solution are close to the exact solution) and weak convergence (where for example, only certain moments of the solution are of interest).
It has been established that strong convergence implies weak convergence, however

the reverse is not the case [50].

We now give the definitions of strong and weak convergence of a numerical method for SODEs.
Let $[t_0, T]$ denote the time interval with grid $\mathcal{J}_{\Delta t}^{M} = \{t_0, t_1, \cdots, t_k, \cdots, t_M = T\}$ such that the time grid is equidistant with the time step size $\Delta t = \frac{T-t_0}{M}$ and $t_k = k\Delta t$, for $k = 0, 1, \cdots, M$.

Strong convergence [51].

Let X_M and $X(t_M)$ denote the numerical solution and exact solution of (2.1.1) respectively at step point t_M. Then X_M is said to converges strongly to $X(t_M)$ if

$$\lim_{\Delta t \to 0} \mathbb{E}\left[|X_M - X(t_M)|\right] = 0. \tag{2.2.1}$$

The numerical solution X_M converges strongly with order $\gamma > 0$ if there exists a positive constant C which does not depend on Δt such that

$$\mathbb{E}\left[|X_M - X(t_M)|\right] \leq C\Delta t^{\gamma}.$$

Weak convergence [50, 51].

Let X_M and $X(t_M)$ denote the numerical solution and exact solution of (2.1.1) respectively at step point t_M, and let $\mathcal{C}_P^m(\mathbb{R}^d, \mathbb{R})$ denote the space of m times continuously differentiable functions $\rho : \mathbb{R}^d \to \mathbb{R}$ such that ρ and all its partial derivatives of orders up to and including order m, have polynomial growth. Then for this class of test functions $\rho : \mathbb{R}^d \to \mathbb{R}$, X_M is said to converges weakly to $X(t_M)$ if

$$\lim_{\Delta t \to 0} \left|\mathbb{E}\left[\rho(X_M)\right] - \mathbb{E}\left[\rho(X(t_M))\right]\right| = 0. \tag{2.2.2}$$

The numerical solution X_M converges weakly with order $\beta > 0$ if for each $\rho \in \mathcal{C}_P^{2(\beta+1)}(\mathbb{R}^d, \mathbb{R})$ there exists a positive constant C which does not depend on Δt such that

$$\left|\mathbb{E}\left[\rho(X_M)\right] - \mathbb{E}\left[\rho(X(t_M))\right]\right| \leq C\Delta t^{\beta}.$$

We recall that $|\cdot|$ denotes the Euclidean norm in $\mathbb{R}^d$.

We now present two schemes in the literature for Itô SDEs and one scheme for Stratonovich SDEs. For clarity, we outline the schemes for one-dimensional SDEs.

Euler Maruyama method.

The Euler Maruyama method [50] is the simplest stochastic numerical method constructed from the stochastic Itô Taylor expansion. The Euler-Maruyama method for (2.1.1) is defined by

$$\widehat{X}_{k+1} = \widehat{X}_k + f(\hat{X}_k)\Delta t + g(\widehat{X}_k)\Delta W_k, \quad n = 0, 1, \cdots, M-1, \tag{2.2.3}$$

where $\widehat{X}_k$ is an approximation to the solution X at t_k and the noise increment $\Delta W_k = W(t_{k+1}) - W(t_k)$ is a $\mathcal{N}(0, \Delta t)$ distributed random variable. The Euler-Maruyama (**EM**) method has strong order of convergence 0.5. However, for SDEs with additive noise, the strong order of convergence of the Euler-Maruyama method is 1 and weak order of convergence 1 [50].
If only weak convergence is required, the noise increments can be replaced by simpler two-point distributed random variables $\Delta\widehat{W}_k$ with

$$P\Big(\Delta\widehat{W}_k = \pm\sqrt{\Delta t}\Big) = \frac{1}{2}.$$

Lord-Rougemont method.

Consider the following semi-linear SODE with additive noise

$$dX(t) = \Big[LX(t) + f(X(t))\Big]dt + dW(t), \tag{2.2.4}$$

where $L \in \mathbb{R}^{d\times d}$ is a linear (matrix) operator and $f : \mathbb{R}^d \to \mathbb{R}^d$ is in general nonlinear. The Lord-Rougemont (**LR**) method [54] for equation (2.2.4) is given as

$$\widehat{X}_{k+1} = e^{\Delta t L}\Big(\widehat{X}_k + \Delta t f(\widehat{X}_k) + \Delta W_k\Big), \tag{2.2.5}$$

$\Delta W_k = W(t_{k+1}) - W(t_k)$ is an independent and identically distributed normal random variable.

Heun method.

The stochastic **Heun** method [50] for (2.1.9) is written as

$$\widehat{X}_{k+1} = \widehat{X}_k + \frac{1}{2}\Big(f(\widehat{X}_k) + f(\widetilde{X}_{k+1})\Big)\Delta t + \frac{1}{2}\Big(g(X_k) + g(\widetilde{X}_{k+1})\Big)\Delta W_k, \tag{2.2.6}$$

where $\widetilde{X}_{k+1}$ is an Euler- predictor update for the corrector (2.2.6) given by

$$\widetilde{X}_{k+1} = \widehat{X}_k + f(\widehat{X}_k)\Delta t + g(\widehat{X}_k)\Delta W_k. \tag{2.2.7}$$

We develop three other numerical schemes later in the thesis and examine the Lord-Rougemont method with multiplicative noise.

Simulating the Wiener process in MATLAB.

In order to simulate numerically the Wiener process $W(t)$ for $0 \leq t \leq T$, we discretize the time interval into M segments with partitions $0 = t_0, t_1, t_2, \cdots, t_k = T$, where $\Delta t = t_{k+1} - t_k$, $k = 0, 1, 2, \cdots, M-1$. It is well known that $W(t)$ is Gaussian with $\mathbb{E}[W(t)] = 0$ and $\mathbb{E}[(W(t))^2] = \Delta t$. The random variable $\Delta W(t_k) = W(t_{k+1}) - W(t_k)$ is then normally distributed with mean zero and variance Δt, that is, $\Delta W(t_k) \sim \mathcal{N}(0, \Delta t)$. Then $\Delta W(t_k)$ can be generated as

$$\Delta W(t_k) = \sqrt{\Delta t}\,\beta_k, \tag{2.2.8}$$

where β_k is an independent and identically distributed standard normal random variable with mean 0 and variance 1. Hence, for a given initial condition $W_0 = W(0)$, a realization of the standard Wiener process $W(t)$ at discretization times t_k is given by

$$W(t_{k+1}) = W(t_k) + \Delta W(t_k), \quad k = 0, 1, 2, \cdots, M-1. \tag{2.2.9}$$

The Wiener increments which appear in the numerical schemes will be generated using the built-in random number generator in MATLAB. A single discretized Wiener path over $[0, 1]$ with number of time subinterval, $M = 1000$ is displayed in Figure 2.1.

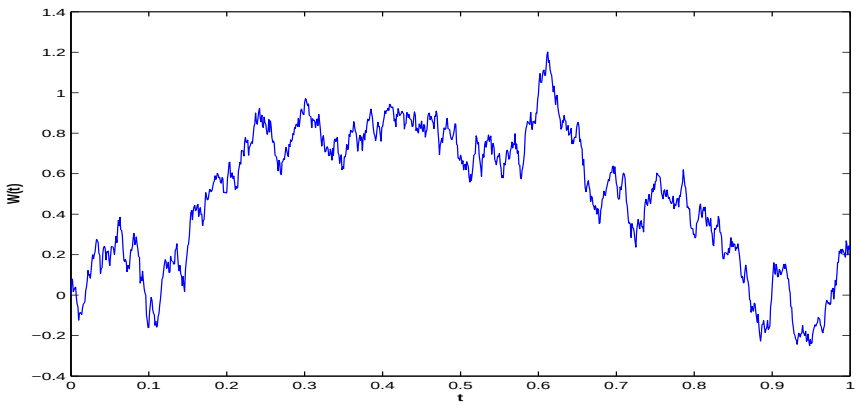

Figure 2.1: A single discretized Wiener path over $[0, 1]$ with number of time subintervals $M = 1000$.

2.3 Background for SPDEs.

In this section, we give some background material on SPDEs and present briefly the definitions, notations for the norms and function spaces and standard results used in this thesis.

Preliminaries.

Definition 2.3.1. Spatial domain [71].
A domain $\mathbb{D}$ is a non-trivial, connected, open subset of $\mathbb{R}^d$ and a domain is bounded if $\mathbb{D} \subset \{x \in \mathbb{R}^d : |x| \leq K\}$ for some $K > 0$. Here $|\cdot|$ denotes the Euclidean norm in $\mathbb{R}^d$.

Definition 2.3.2. Lebesgue space [77, 19].
A Lebesgue space L^p is the space of measurable functions $u(x)$ whose absolute value to the pth power is integrable, provided $p \in [1, \infty)$:

$$\int_{\mathbb{D}} |u(x)|^p dx < \infty.$$

This space is endowed with the norm

$$||u||_{L^p} = \left(\int_{\mathbb{D}} |u(x)|^p dx \right)^{1/p}.$$

The L^2 space is a particular case of the L^p space. It is a Hilbert space with inner product $(u, v) := \int_{\mathbb{D}} u\bar{v}dx$ and norm

$$||u||_{L^2} = \left(\int_{\mathbb{D}} |u(x)|^2 dx\right)^{1/2} = \sqrt{(u,u)_{L^2}}.$$

Definition 2.3.3. Sobolev spaces [19, 77, 76].

Sobolev spaces provide the natural setting in which to analyze PDEs. These spaces give us information about how smooth the functions are.

The Sobolev space $H^m(\mathbb{D})$ is defined through (distributional) derivatives as

$$H^m(\mathbb{D}) = \{u : D^\alpha u \in L^2(\mathbb{D}), \quad \text{for all} \quad 0 \leq |\alpha|_k \leq m\} \tag{2.3.1}$$

with norm

$$||u||_m = \Big\{ \sum_{0\leq|\alpha|_k\leq m} ||D^\alpha u||^2_{L^2} \Big\}^{1/2}, \tag{2.3.2}$$

where $\alpha = (\alpha_1, \alpha_2, \cdots \alpha_m)$ is a standard multi-index notation such that $|\alpha|_k = \alpha_1 + \alpha_2 + \cdots + \alpha_m$ and $D^\alpha u$ denotes the partial derivative

$$D^\alpha u = \frac{\partial^{|\alpha|_k} u}{\partial x_1^{\alpha_1} \partial x_2^{\alpha_2} \cdots \partial x_m^{\alpha_m}}. \tag{2.3.3}$$

When considering Sobolev spaces of periodic functions, carrying out analysis is significantly more straight forward than for those spaces on bounded domains, since one is not faced with the issues of boundary. Thus because of this simplification, we shall use this tool in our error analysis in Chapter 4 where we carry out the strong convergence analysis of SPDE. In our work, we shall represent the function $u(t)$ as a Fourier series. With this in mind, we give the definitions of Sobolev spaces for periodic functions.

Let $m \in \mathbb{R}$. Then by $H^m([0, 2\pi])$, we denote

$$H^m([0,2\pi]) = \left\{ u \in L^2([0,2\pi]) : \sum_{n\in\mathbb{Z}} (1+n^2)^m |u_n|^2 < \infty \right\}, \tag{2.3.4}$$

where u_n are the Fourier coefficients of u. The norm is given by

$$||u||_m = \left(\sum_{n\in\mathbb{Z}} (1+n^2)^m |u_n|^2 \right)^{1/2}, \tag{2.3.5}$$

where the symbol $|\cdot|$ here denotes the absolute value.

Note that the norm equivalence of (2.3.2) and (2.3.5) is shown in [77].

Remark:

Note that Sobolev spaces with negative exponent are allowed, that is, $H^{-\gamma}([0,2\pi])$ with $\gamma \in \mathbb{R}^+$. Sobolev space with negative exponent allows us to study functions which are less smooth than L^2 functions [96].

The $\mathbb{Q}$-Wiener process [19].

Let H be a Hilbert space with inner product $(\cdot,\cdot)$ and norm $||\cdot||$ and let $(\Omega, \mathcal{F}, \mathbb{P})$ be a probability space.

Let $\mathbb{Q}$ be the covariance operator of the Wiener process $W(t), t \in [0,T]$, with eigenvalues λ_n and corresponding eigenfunctions ψ_n, then the trace of $\mathbb{Q}$ is defined as follows:

$$Tr(\mathbb{Q}) = \sum_{n=1}^{\infty} \lambda_n. \tag{2.3.6}$$

If $\mathbb{Q} \equiv I$, then $Tr(\mathbb{Q}) = +\infty$ and the Wiener process is called a cylindrical Wiener process. If $Tr(\mathbb{Q}) < \infty$, the Wiener process is called a nuclear Wiener process or a $\mathbb{Q}$-Wiener process and $\mathbb{Q}$ is in trace class.

Definition 2.3.4. Hilbert-Schmidt operator [19].

An operator $T \in L(H) := L(H,H)$ is Hilbert-Schmidt if

$$||T||_{HS}^2 := \sum_{n\in\mathcal{I}} ||T\psi_n||^2 < \infty, \tag{2.3.7}$$

where $||\cdot||_{HS}$ denotes the Hilbert-Schmidt norm and $L(H) := L(H,H)$ is the space of bounded linear operators from H to H. We denote the space of Hilbert-Schmidt operators from $\mathbb{Q}^{1/2}(H)$ to H by $L_2^0 := HS(\mathbb{Q}^{1/2}(H), H)$ and the corresponding norm $||\cdot||_{HS}$ by

$$||\Phi||_{L_2^0} := \left|\left|\Phi\mathbb{Q}^{1/2}\right|\right|_{HS} = \left(\sum_{n\in\mathbb{N}^d} \left|\left|\Phi\mathbb{Q}^{1/2}\psi_n\right|\right|^2\right)^{1/2}, \tag{2.3.8}$$

where the space $\mathbb{Q}^{1/2}(H)$ is defined as the subspace of the space H with the norm $||u||_{\mathbb{Q}^{1/2}(H)} = \left|\left|\mathbb{Q}^{-1/2}u\right|\right|, u \in \mathbb{Q}^{1/2}(H)$.

Proposition 2.3.1. ***Representation of the $\mathbb{Q}$-Wiener process*** *[19, 73].*
Let $\psi_n, n \in \mathbb{N}$, be an orthonormal basis of H consisting of eigenvectors of $\mathbb{Q}$ with corresponding eigenvalues $\lambda_n, n \in \mathbb{N}$. Then an H-valued stochastic process $W(t), t \in [0,T]$, is a $\mathbb{Q}$-Wiener process if and only if

$$W(t) = \sum_{n=1}^{\infty} \sqrt{\lambda_n}\beta_n(t)\psi_n, \tag{2.3.9}$$

where $\beta_n(t), \{n \in \mathbb{N}|\lambda_n > 0\}, t \geq 0$ are independent and identically distributed real-valued standard Brownian motions on the probability space $(\Omega, \mathcal{F}, \mathbb{P})$.

A general Itô SPDE.

A general Itô stochastic partial differential equation is given as

$$du = \Big[Au + f(u)\Big]dt + \epsilon\Big[\mu + \phi g(u)\Big]dW(t) \tag{2.3.10}$$

where u is an H-valued random process, A is a linear operator, which is in general unbounded, acting on the Hilbert space H, defined in $\mathcal{D}(A) \subset H$, the functions $f : H \to H$ and $g : H \to L_2^0$ are in general nonlinear. $W(t)$ is a $\mathbb{Q}$-Wiener process on the probability space $(\Omega, \mathcal{F}, \mathbb{P})$ with values in H. $W(t)$ is represented in (2.3.9). The parameter ϵ allows us to control the intensity of the noise while the parameters μ and ϕ allow us to have additive or multiplicative noise SPDE.
When $\mu = 1$ and $\phi = 0$, we have the following Itô SPDE with additive noise,

$$du = \Big[Au + f(u)\Big]dt + \epsilon dW(t) \tag{2.3.11}$$

and when $\mu = 0$ and $\phi = 1$, we have the following Itô SPDE with multiplicative noise

$$du = \Big[Au + f(u)\Big]dt + \epsilon g(u)dW(t). \tag{2.3.12}$$

2.4 Existence and uniqueness of the mild solution of Itô SPDEs.

In this thesis, we consider parabolic SPDEs. We now give the assumptions needed for the existence and uniqueness of solution of the mild soluton of the Itô SPDE (2.4.8).

Assumption 2.4.1. ***Assumption on the linear operator*** *A [71].*
Assume that the linear operator A is a positive self-adjoint operator and A generates an analytic semigroup $e^{tA}, t > 0$. Then there exist sequences of negative real eigenvalues $\{\alpha_n\}_{n\in\mathbb{N}}$ and an orthonormal basis of H of eigenfunctions $\{\psi_n\}_{n\in\mathbb{N}}$ such that the linear operator $A : \mathcal{D}(A) \subset H \to H$, where $\mathcal{D}(A)$ denotes the domain of A. The operator A and the $\mathcal{D}(A)$ are represented as follows:

$$Au = \sum_{n=1}^{\infty} \alpha_n(\psi_n, u)\psi_n, \quad \forall u \in \mathcal{D}(A),$$

where

$$\mathcal{D}(A) = \{u \in H : \sum_{n=1}^{\infty} |\alpha_n|^2 |(\psi_n, u)|^2 < \infty\}. \tag{2.4.1}$$

Assumption 2.4.2. ***Assumption on the drift term*** *f [71].*
For every $u, v \in H$ and for $f : H \to H$, f continuous in H, there exists a constant $C > 0$, such that

i. Lipschitz condition on f

$$||f(u) - f(v)|| \leq C\,||u - v||\,. \tag{2.4.2}$$

ii. Growth condition on f

This condition is a consequence of the Lipschitz condition in (2.4.2)

$$||f(u)|| \leq ||f(0)|| + ||f(u) - f(0)|| \leq ||f(0)|| + C\,||u|| \leq C(1 + ||u||). \tag{2.4.3}$$

Assumption 2.4.3. ***Assumption on the diffusion term*** *g* ***for SPDEs with multiplicative noise*** *[71].*

For every $u, v \in H$ and for $g : H \to L_2^0$, g continuous in H, there exists a constant $C > 0$, such that

i. Lipschitz condition on g

$$||g(u) - g(v)||_{L_2^0} \leq C\,||u - v||\,. \tag{2.4.4}$$

ii. Growth condition on g

This condition is a consequence of the Lipschitz condition in (2.4.4)

$$||g(u)||_{L_2^0} \leq ||g(0)||_{L_2^0} + ||g(u) - g(0)||_{L_2^0} \leq ||g(0)||_{L_2^0} + C\,||u|| \leq C(1 + ||u||). \tag{2.4.5}$$

where $||\cdot||$ denotes the norm associated to the inner product of the Hilbert space H and L_2^0 is the space of Hilbert-Schmidt operators from $\mathbb{Q}^{1/2}(H)$ to H.

Assumption 2.4.4. ***Assumption on the noise for SPDEs with additive noise****[19].*
The covariance operator $\mathbb{Q}$ of the Wiener process $W(t)$ satisfies $Tr(I-\Delta)^{\gamma} < \infty$ such that

$$\sum_{n\in\mathbb{Z}} (1 + n^2)^{\gamma} \lambda_n < \infty. \tag{2.4.6}$$

where λ_n's are the eigenvalues of the covariance $\mathbb{Q}$ of $W(t)$ and the parameter $\gamma, (\gamma \geq -1/2)$ describes the regularity of the noise.

Definition 2.4.1. (Mild solution) [19].
A predictable H-valued process $u(t)$ is said to be a mild solution of (2.3.10) if

$$\mathbb{P}\left(\int_0^t ||u(s)||^2\, ds < +\infty \right) = 1, \tag{2.4.7}$$

and for any $t \in [0, T]$, we have that

$$u(t) = e^{tA}u_0 + \int_0^t e^{(t-s)A} f(u(s))ds + \epsilon \int_0^t e^{(t-s)A} \Big[\mu + \phi g(u(s)) \Big] dW(s). \tag{2.4.8}$$

Theorem 2.4.1. ***Existence, uniqueness and properties of the mild solution****[19].*
Assume that the initial solution u_0 is an $\mathcal{F}_0$-measurable H-valued random variable and Assumptions 2.4.1, 2.4.2, 2.4.3 (or 2.4.4) holds, then

i. There exist a mild solution u to (2.3.10) satisfying

$$\mathbb{P}\left(\int_0^T ||u(s)||^2 < \infty\right) = 1.$$

ii. For any $p \geq 2$, there exist a constant $C = C(p,T)$, such that

$$\sup_{0\leq t\leq T} \mathbb{E}||u(t)||^p \leq C(1 + \mathbb{E}||u_0||^p).$$

iii. For any $p > 2$, there exist a constant $C_0 = C_0(p,T)$, such that

$$\mathbb{E}\sup_{0\leq t\leq T} ||u(t)||^p \leq C_0(1 + \mathbb{E}||u_0||^p),$$

In this thesis, we use the mild solution approach [19] to study, analyze and build numerical discretization schemes for SPDEs. Other approaches for analyzing SPDEs are the variational approach, (see [73]) and the martingale approach, (see [19]).
The existence and uniqueness of the mild solution of a general SPDE is guaranteed under the assumption that the operator A is the generator of an analytic semigroup, $e^{tA}, t \geq 0$ using the fixed point method [17, 19, 73, 90].

2.5 A collection of standard results.

In this section, we collect all the results from the literature which will be needed in the convergence proof in Chapter 4.

Lemma 2.5.1. ***Cauchy-Schwarz inequality*** *[23].*
Let H be a Hilbert space. Then

$$|(u,v)| \leq ||u||\,||v|| \quad \forall u, v \in H.$$

An example of the application of the Cauchy-Schwarz inequality is given by

$$\left|\int_0^t u ds\right|^2 \leq t\int_0^t |u|^2 ds. \tag{2.5.1}$$

Lemma 2.5.2. ***Gronwall inequality*** *[23, 50, 63].*

Let y, z: $[t_0, T] \to \mathbb{R}$ be integrable with

$$0 \leq y(t) \leq z(t) + C \int_{t_0}^{t} y(s)ds \tag{2.5.2}$$

for $t \in [t_0, T]$ where $C > 0$. Then for $t \in [t_0, T]$

$$y(t) \leq z(t) + C \int_{t_0}^{t} e^{C(t-s)} z(s)ds. \tag{2.5.3}$$

Lemma 2.5.3. ***Doob martingale inequality*** *[50].*

Let $X = \{X(t), t \geq 0\}$ be a separable martingale with finite pth- moment. Then for any $p > 1$

$$\mathbb{E} \sup_{0 \leq s \leq t} |X(t)|^p \leq \Big(\frac{p}{p-1}\Big)^p \mathbb{E}(|X(t)|^p). \tag{2.5.4}$$

Lemma 2.5.4. ***Jensen's inequality*** *[50, 70].*

Let $(\Omega, \mathcal{F}, \mathbb{P})$ be a probability space and let $X : \Omega \to \mathbb{R}^n$ be a random variable. If $\mathcal{G} \subset \mathcal{F}$, $\phi : \mathbb{R} \to \mathbb{R}$ is convex and $\mathbb{E}\big[|\phi(X)|\big] < \infty$, then

$$\phi\Big(\mathbb{E}\big[X|\mathcal{G}\big]\Big) \leq \mathbb{E}\Big[\phi(X)|\mathcal{G}\Big]. \tag{2.5.5}$$

Lemma 2.5.5. ***Itô isometry*** *[19].*

Let $\phi \in L_2^0$. Then $\int_0^t \phi(s)dW(s)$ can be defined, and the following isometry property holds:

$$\mathbb{E}\left|\left|\int_0^t \phi(s)dW(s)\right|\right|^2 = \int_0^t ||\mathbb{E}\phi(s)||_{L_2^0}^2 \, ds. \tag{2.5.6}$$

Lemma 2.5.6. *[56, 71, 74, 99] [smoothing properties of the semigroup].*

Assume that the linear operator A generates an analytic semigroup $e^{tA}, t \geq 0$, with negative real eigenvalues $\{\alpha_n\}_{n \in \mathbb{N}}$, then for any $\theta \in [0, 1/2)$ and $\beta \geq 0$ there exist a constant $C > 0$ such that

$$\Big|\Big|A^{\beta} e^{tA}\Big|\Big| \leq C t^{-\beta} \quad for \quad t > 0 \tag{2.5.7}$$

$$\Big|\Big|A^{-\theta}(I - e^{tA})\Big|\Big| \leq C t^{\theta} \quad for \quad t \geq 0. \tag{2.5.8}$$

Lemma 2.5.7. *[55, 99].*

Let Assumptions 2.4.1, 2.4.2 and 2.4.4 hold, then for a mild solution $u(t)$ of a SPDE (2.3.11), for $C > 0$ and $r \leq \gamma + 1$

$$\mathbb{E} \sup_{0 \leq t \leq T} ||u(t)||_r^2 \leq C(1 + ||u_0||_r^2) \tag{2.5.9}$$

where $||\cdot||_r$ denotes the norm associated to the inner product of the Hilbert space H^r. The parameters r and γ describe the regularities of the solution and noise respectively.

Lemma 2.5.8. *[49].*

Let Assumptions 2.4.1, 2.4.2 and 2.4.4 hold, then for a mild solution $u(t)$ of a SPDE (2.3.11) and for $\theta < 1$ and $p \geq 1$

$$\sup_{0 \leq t \leq T} \mathbb{E}||A^\theta u(t)||_{L^2}^p < \infty. \tag{2.5.10}$$

Lemma 2.5.9. *[49].*

Let Assumptions 2.4.1, 2.4.2 and 2.4.4 hold, then for a mild solution $u(t)$ of a SPDE (2.3.11) and for $p \geq 1$

$$\sup_{0 \leq t \leq T} \mathbb{E}||u(t)||_{L^2}^p < \infty. \tag{2.5.11}$$

2.6 A review on numerical approximation for SPDEs.

Numerical approximation of stochastic partial differential equations has attracted much attention in recent years. In particular, strong approximation of SPDEs have been studied extensively, see for example [3, 20, 32, 33, 34, 35, 36, 37, 38, 39, 46, 54, 55, 74, 84, 99].

In this section, we give an overview of some work that has been done in line with numerical approximation techniques and convergence theory for the numerical methods for SPDEs. We begin by reviewing SPDEs with additive noise.

In [84], a nonlinear reaction diffusion equation driven by additive space-time white noise on the domain $(0, 1)$ with Dirichlet boundary conditions was considered. A finite difference approximation was then applied for the spatial discretization of the SPDE with a spectral approximation to the noise, and then the theta-method was used for

the time discretization of the resulting system of equations. A strong convergence theory was obtained and it was shown that the scheme for spatial discretization converge with order 0.5 and the scheme for the temporal discretization converges with order 0.25.

In [33, 34], the authors worked on the strong convergence of finite difference schemes for the quasi-linear parabolic SPDEs with dirichlet boundary conditions on a bounded domain in one dimension. Estimates related to the L^p convergence were obtained using implicit finite difference schemes. Almost sure convergence was shown for the case where the nonlinear terms of the SPDE are Lipschitz continuous, while convergence in probability was shown for the case where the nonlinear terms of the SPDE are not Lipschitz continuous. The authors showed that the implicit and explicit finite difference schemes converge with order 0.5 in space and 0.25 in time.

In [20], explicit finite difference approximation was applied to a parabolic SPDE with space-time white noise and a zero nonlinear term, $f = 0$, the SPDE is supplemented with periodic boundary conditions. The authors also showed that the scheme converges strongly with order 0.5 in space and order 0.25 in time. The authors show that these rates are the best attainable if only evaluation of the noise are used. However, the authors remarked that it is possible to improve this convergence rate by using suitable linear functionals of the noise.

In [39], the Galerkin methods, collocation methods and finite element method were used for the space discretization of a quasi-linear evolution equation, while the explicit Euler scheme, the implicit Euler scheme and the Crank-Nicolson method were used for the time discretization. The author obtained a strong order of 0.5 for the Implicit Euler scheme for the case where the SPDE is forced with a smoother noise.

In [55], the authors applied the Galerkin method for the spatial discretization of a parabolic SPDE, the resulting SODEs were discretized with an stochastic exponential integrator known as the Lord-Rougemont scheme. They considered a type of noise that allows one to alter the regularity of the noise, so that the higher the regularity of the noise, the smoother the solution paths, and by implication, the rate of convergence is improved. They found out that the L^2 error decays like

$N^{-1/2}, N^{-1}, N^{-3/2}, N^1, N^1$ for $H^{-1/2}, H^0, H^{-1/2}, H^1, H^2$ noise respectively, where N denotes the size of the Galerkin truncation.

Recently, in [46] the authors applied a Galerkin projection to a parabolic SPDE, and used an exponential Euler scheme for the time discretization of the finite dimensional Galerkin-SDE. The authors used the linear functional of the noise to achieve a high order of convergence, (instead of using only evaluation of noise, which can only converge with the optimum rate of 0.25). They showed numerically and proved a convergence theory to show that the exponential Euler scheme converges with order 1.

In [38], the author considered a parabolic SPDE driven by a multiplicative space-time white noise. The implicit scheme was used for the discretization and show that it converges with a temporal rate of Δt^{α} where $\alpha < 0.125$.

In [99], finite element method was considered for a linear SPDE forced by multiplicative space-time white noise in a multidimensional case. The piecewise linear finite element elements method was used for the space discretization of the SPDE, while the backward Euler method was used for the time discretization of the resulting system of SODEs.

In this thesis, our interest is to obtain strong convergence estimates for additive and multiplicative noise for the stochastic exponential time differencing scheme, see Chapter 4.

2.7 A review on noise in spatially extended systems.

There has been a great interest in the influence of noise in physical applications as fluctuation plays important roles in spatially extended systems. Noise has been found to be useful in many areas: Nucleation of waves in excitable media [86, 85], front propagation [78, 83], structure formation in excitable media [14], pattern formation in Turing systems [53], electro-convection in nematic liquid crystals [98], convective roles in the Rayleigh-Bénard instabilities [1], turbulent flows [80], chemical waves [58] and phase transitions [94] to mention a few.

The role of noise can either be constructive or destructive. For example, in statistical mechanics, the occurrence of noise-induced disordering phase transitions, indicates that the higher the intensity of noise, the larger the disorder, while on the other hand, noise induced ordering transitions produces a counterintuitive phenomenon, in which an increase in noise intensity enhances the order [94]. For example, in the field of chemical kinetics, the phenomenon in which there is an escape of a system from a metastable state cannot be possible without the presence of fluctuations [27].
Different kinds of stochastic contribution can be taken into account for the forcing of spatially extended systems, this could be additive or multiplicative. As we have seen in [50], additive noise term is a random term that does not depend on the state of the system, whereas for multiplicative noise, the random term is coupled with the state of the system. In general, the effects of multiplicative noise on a system are different from the effect of additive noise [43, 26]. These stochastic contributions can either be taken in the Itô sense or Stratonovich sense when noise is multiplicative; the interpretation to consider is a modelling issue. For example, in [26], multiplicative Itô noise was used to study the Swift-Hohenberg equation and in [43], where noise-induced phase transition was studied, the multiplicative noise was interpreted in Stratonovich sense. Also in [81], multiplicative Stratonovich noise was shown to influence the velocity of kinks in stochastic reaction diffusion equations. The phenomenon of kinks and anti-kinks have been rigorously studied in [59, 61, 60].
In this thesis, we aim to study the effects of a number of different stochastic forcing on the Swift-Hohenberg (SH) equation. In what follows, we present how we discretize a SPDE.

2.8 Numerical discretization for SPDEs.

In this thesis, numerical discretization of SPDEs is carried out by the method of lines approach, that is to say, we first carry out spatial discretization of the SPDE, this procedure gives rise to an infinite system of SODEs; and secondly, we discretize the system of SODEs using time discretization techniques to obtain approximate solutions

to the SPDEs.

We use the Fourier spectral method for the spatial discretization of SPDEs in this thesis. In what follows, we briefly explain this numerical method.

2.8.1 Fourier spectral method.

The Fourier spectral method is a method which allows one to represent a given function $u(x)$ by the orthogonal eigenfunctions of a given operator A. For a detailed survey on the subject of Fourier spectral method, see [91, 31].

In simulations of SPDEs with periodic boundary conditions, the fast Fourier transform can be used for computations. However, if faced with problems that have other forms of boundary conditions, such as Neumann or Dirichlet, then the discrete cosine transform and the discrete since transform can be used respectively.

To describe a numerical scheme for (2.3.10), we consider for the purpose of illustration, an SPDE with additive noise. See Chapters 4 and 5 for the multiplicative noise case.

Consider the following SPDE

$$du(x,t) \;=\; \Big[Au(x,t) + f(u(x,t))\Big]dt + \epsilon dW(x,t), \tag{2.8.1}$$

with periodic boundary conditions $u(0,t) = u(2\pi,t)$ and a given initial condition $u(x,0)$. In order to apply the Fourier spectral method on (2.8.1), we need to represent the function $u(x,t)$ as a Fourier series as follows:

$$u(x,t) := \mathcal{F}^{-1}(u_n)(x) := \sum_{n\in\mathbb{Z}} u_n(t)e^{inx}, \tag{2.8.2}$$

where the Fourier coefficients $\hat{u}_n$ are given by

$$u_n(t) := (\mathcal{F}u)_n := \frac{1}{2\pi}\int_0^{2\pi} u(x)e^{-inx}dx. \tag{2.8.3}$$

The Fourier modes $\psi_n(x) = e^{inx}$, $n \in \mathbb{Z}$ are the eigenfunctions of A.

Therefore, for a second-order SPDE with operator $A = \Delta$, we get that

$$\Delta u(x,t) = \sum_{n\in\mathbb{Z}} \alpha_n u_n(t)\psi_n(x) = \sum_{n\in\mathbb{Z}} -n^2 u_n(t)e^{inx}, \tag{2.8.4}$$

and for a fourth-order SPDE with operator $A = -\Delta^2$, we get that

$$-\Delta^2 u(x,t) = \sum_{n\in\mathbb{Z}} \alpha_n u_n(t)\psi_n(x) = \sum_{n\in\mathbb{Z}} -n^4 u_n(t)e^{inx}. \tag{2.8.5}$$

Next, we substitute (2.3.9), (2.8.2), (2.8.4) or (2.8.5) into (2.8.1) to get

$$d\sum_{n\in\mathbb{Z}} u_n(t)\psi_n(x) = \left[\sum_{n\in\mathbb{Z}} \alpha_n u_n(t)\psi_n(x) + \sum_{n\in\mathbb{Z}} f_n(u(t))\psi_n(x)\right]dt + \epsilon\sum_{n\in\mathbb{Z}} \lambda_n^{1/2}\psi_n(x)d\beta_n(t) \tag{2.8.6}$$

where f_n is the nth component of the function f, so that $f(u(t)) = \sum_{n\in\mathbb{Z}} f_n(u(t))\psi_n$ and the last term on the LHS of (2.8.6) comes from the definition of the Wiener process (2.3.9).

Next, we take the inner product of (2.8.6), which is equivalent to multiplying both sides of (2.8.6) by $\psi_m(x)$ and then integrate over the domain, to obtain

$$d\sum_{n\in\mathbb{Z}} u_n(t)\int_0^{2\pi}\psi_n(x)\psi_m(x)dx = \sum_{n\in\mathbb{Z}} \alpha_n u_n(t)\int_0^{2\pi}\psi_n(x)\psi_m(x)dxdt +$$

$$\sum_{n\in\mathbb{Z}} f_n(u(t))\int_0^{2\pi}\psi_n(x)\psi_m(x)dxdt + \epsilon\sum_{n\in\mathbb{Z}}\lambda_n^{1/2}\int_0^{2\pi}\psi_n(x)\psi_m(x)dxd\beta_n(t). \tag{2.8.7}$$

Using the orthonormality condition, we end up with the following infinite system of SODEs

$$u_n(t) = e^{t\alpha_n}u_n(0) + \int_0^t e^{(t-s)\alpha_n}f_n(u(s))ds + \epsilon\int_0^t e^{(t-s)\alpha_n}\lambda_n^{1/2}d\beta_n(t), \quad \forall n\in\mathbb{Z}. \tag{2.8.8}$$

A numerical discretization of (2.8.1) requires that we consider a truncation of the Fourier modes, n in (2.8.8). Thus, if we apply a Galerkin truncation to (2.8.1), and define finite dimensional subspaces H_N of H by $H_N := \text{span}(\psi_1, \psi_2, \cdots, \psi_N)$ and denote by $P_N : H \to H_N$, the orthogonal projection of H to the subspace generated by $\{\psi_n : |n| \le N\}$, i.e.

$$P_N u = \sum_{n=1}^{N}(\psi_n, u)\psi_n, \tag{2.8.9}$$

for $u \in H$ and $N \in \mathbb{N}$.

Then we can truncate the initial data u_0, the functions f and the Wiener process

$W(t)$ by

$$u^N(0) := P_N u(0),\ \ f(u^N) := P_N f(u^N),\ \ W^N(t) = P_N W(t) = \sum_{n=1}^{N} \sqrt{\lambda_n}\,\psi_n \beta_n(t),$$

for all $u \in H$ and $N \geq 1$.

Hence, the infinite system of SODEs (2.8.8) becomes

$$u_n^N(t) = e^{t\alpha_n} u_n^N(0) + \int_0^t e^{(t-s)\alpha_n} f_n(u^N(s))ds + \epsilon \int_0^t e^{(t-s)\alpha_n} \lambda_n^{1/2} d\beta_n(t), \quad \forall |n| \leq N. \tag{2.8.10}$$

We remark at this point, that the time discretization of the system of SODEs (2.8.10) is one of the objectives of this PhD work. We therefore presented in the following chapters standard numerical techniques for the integration of these SODEs and also propose new numerical methods for the solution of SODEs .

Applying Fourier spectral method for the space discretization of the SPDE gives spectral accuracy in space [6, 91]. The nonlinear terms of the SPDE are evaluated in physical space, but the time stepping is carried out in Fourier space. Doing this can give rise to aliasing problems, and so one has to take care to filter out high frequencies appropriately [24, 91] and we also took account of dealiasing using the 2/3 rule.
Aliasing errors are a source of concern with spectral methods since the high wave number components interact during the calculation of the nonlinear term giving rise to wave numbers that are not resolved [6, 15, 30, 91]. These can then reflect back and corrupt/pollute wave numbers that are carried by the computations [82]. Without using any de-aliasing technique, the spectral method may suffer from some mild numerical instability [29]. To filter out these aliasing errors, we use the 2/3 de-aliasing rule [15], whereby, one sets to zero 1/3 of the high frequency modes and keeps 2/3 of the Fourier modes unchanged [44].

2.8.2 Discretization of the infinite-dimensional noise.

The infinite-dimensional Wiener process is given by

$$W(t) = \sum_{n=1}^{\infty} \sqrt{\lambda_n}\,\beta_n(t)\psi_n, \tag{2.8.11}$$

where $\beta_n(t), t \geq 0$ are independent and identically distributed real-valued standard Brownian motions, $\psi_n(x)$ and λ_n respectively denote the eigenfunctions and the eigenvalues of the $\mathbb{Q}$-Wiener process (2.3).

When considering the discretization of a SPDE, we need to truncate (2.8.11) in our numerical computations for practical purposes. Thus for a given number of spatial grid points N, we can write the truncated Wiener process as follows:

$$W^N(t) = \sum_{n=1}^{N} \sqrt{\lambda_n}\beta_n(t)\psi_n. \tag{2.8.12}$$

In this thesis we have shown how to discretize a SPDE using the Fourier spectral method in Section 2.8.1. Thus when we represent the functions in the SPDE as a Fourier series, knowing also that the Wiener process (2.8.11) can be likened to a Fourier series, we get at the end of the spatial discretization, a system of infinite-dimensional system of SODEs in time such that a time discretization scheme will be needed to finally obtain the solution of the SPDE. To use the noise in (2.8.12) in a time discretization scheme at times $t_k = k\Delta t$ on the time interval $[0, T]$ for $k = 0, 1, \cdots, M$, we take the Wiener increment $\Delta W^N(t_k)$ as a vector in space, such that $\Delta W^N(t_k)$ can be generated as

$$\Delta W^N(t_k) = W^N(t_{k+1}) - W^N(t_k) = \sqrt{\Delta t}\sum_{n=1}^{N} \sqrt{\lambda_n}\beta_{k,n}\psi_n, \tag{2.8.13}$$

where $\Delta t = T/M$ denotes the time step size , where $M \in \mathbb{N}$ denotes the number of time grid points and $\beta_{k,n}$ are independent and identically distributed standard normal random variables.

The eigenvalues λ_n of $\mathbb{Q}$ needs to be determined. The choice of the co-efficients λ_n will determine the correlation of the path of noise in space. Thus in the numerical discretization of SPDEs in thesis, we take noise white in time and consider two forms of spatial regularity/correlation. Firstly, we consider noise in H^γ space and secondly, we consider noise with exponential decaying correlations. The following sections show how we construct these two forms of noise.

2.8.3 Construction of H^γ noise.

Let us assume that the covariance operator $\mathbb{Q}$ of the Wiener process $W(t)$ satisfies the following

$$\sum_{n\in\mathbb{Z}}(1+n^2)^\gamma\lambda_n<\infty. \tag{2.8.14}$$

Then by (2.3.1), $W(t)\in H^\gamma$ in space, where λ_n's are the eigenvalues of the covariance $\mathbb{Q}$ of $W(t)$, which needs to be determined. To determine these eigenvalues, we equate the left hand side of (2.8.14) to a convergent series in the right hand side of (2.8.15), where ε is a small positive parameter which ensures convergence of the series $\sum_{n=1}^{\infty}\frac{1}{n^r}$, $r>1$, as follows:

$$\sum_{n\in\mathbb{Z}}(1+n^2)^\gamma\lambda_n=\sum_{n\in\mathbb{Z}}\frac{1}{n^{1+\varepsilon}}. \tag{2.8.15}$$

Then for each n, but $n\neq 0$,

$$\lambda_n=(1+n^2)^{-\gamma}|n|^{-(1+\varepsilon)},\quad n\neq 0,\quad \lambda_0=0, \tag{2.8.16}$$

These eigenvalues will be used in the Wiener process representation in (2.3.9) and this ensures that the noise is in H^γ space, where γ denotes the spatial regularity of the noise. This form of noise will be used to carry out numerical simulations in Chapter 5.

2.8.4 Construction of exponentially correlated Wiener processes.

The spatial regularity of noise in SPDEs can be related to the spatial correlation and eigenvalues $\lambda_n, n=1,2,3,\cdots$ of the covariance operator $\mathbb{Q}$ which can be seen in the representation (2.3.9). In this section, we seek to determine the eigenvalues for the $\mathbb{Q}-$Wiener process of an SPDE for the case where the boundary condition is periodic. See [57, 86, 90] for the case where the boundary condition is Dirichlet or Neumann. Consider the Wiener process representation in (2.3.9) and recall the assumption that the eigenfunctions of the $\mathbb{Q}-$Wiener process are the same with the eigenfunctions of the linear operator A of the SPDE. Then for a given spatial correlation $C(x)$ in

(2.8.18), the eigenvalues λ_n need to be determined. These coefficients will be derived in such a way that

$$\mathbb{E}\Big[W(t,x)W(t',x')\Big] \approx C(x-x')\min\{t,t'\}, \tag{2.8.17}$$

where the function $C(x)$ accounts for the spatial correlations of the noise [27] and is given as

$$C(x) = \frac{1}{2\xi}\exp\left(\frac{-\pi x^2}{4\xi^2}\right), \tag{2.8.18}$$

where ξ denotes the correlation length.

We remark that the correlation function $C(x)$ approaches the δ function as $\xi \to 0$, which means that the noise approaches the space-time white noise, in which there is no correlation between distinct points.

Lemma 2.8.1. *Assume that* $\mathbb{E}\Big[W(t,x)W(t',x')\Big] \approx C(x-x')\min\{t,t'\}$, *then*

$$\sqrt{\lambda_n} = \exp\left(\frac{-n^2\xi^2\pi}{2L^2}\right). \tag{2.8.19}$$

To prove Lemma 2.8.1, we will start by proving two preliminary Lemmas.

Lemma 2.8.2. *For* $d \in \mathbb{R}$,

$$\int_{-a}^{a} e^{-x^2}dx = \int_{-a}^{a} e^{-(x+id)^2}dx. \tag{2.8.20}$$

Proof. For any contour C in the complex plane, the following result holds.

$$\oint_C \exp(-z^2)dz = 0.$$

To prove the Lemma 2.8.2, we take C to be a rectangle with vertexes in the complex plane.

The vertices are $-a, a, a+id$ and $-a+id$.

Let $z = x+iy$, then $dz = dx+idy$ and $z^2 = (x+iy)^2 = x^2+i2xy-y^2$.

$$\begin{aligned}\oint_C e^{-z^2}dz &= \int_{-a}^{a} e^{-x^2}dx + i\int_0^d e^{-(a+iy)^2}dy + \int_a^{-a} e^{-(x+id)^2}dx + i\int_d^0 e^{-(-a+iy)^2}dy \\ &= \int_{-a}^{a} e^{-x^2}dx - \int_{-a}^{a} e^{-(x+id)^2}dx + i\int_0^d e^{-(a+iy)^2}dy - i\int_0^d e^{-(-a+iy)^2}dy.\end{aligned}$$

Next, we show that

$$\int_0^d e^{-(\pm a+iy)^2} dy \to 0 \quad \text{as} \quad a \to +\infty$$

$$\int_0^d e^{(\pm a+iy)^2} dy = \int_0^d e^{-a^2+i2ay+y^2} dy \leq \int_0^d e^{-a^2+y^2} dy = e^{-a^2} \int_0^d e^{y^2} dy$$

as $a \to \infty$, the integral tends to zero.

Since,

$$\int_0^d e^{\pm(a+iy)^2} dy \to 0 \quad \text{as} \quad a \to +\infty.$$

Thus,

$$\oint_C e^{-z^2} = \int_{-a}^{a} e^{-x^2} dx - \int_{-a}^{a} e^{-(x+id)^2} dx + i \times 0 - i \times 0$$

$$0 = \int_{-a}^{a} e^{-x^2} dx - \int_{-a}^{a} e^{-(x+id)^2} dx.$$

Hence,

$$\int_{-a}^{a} e^{-x^2} dx = \int_{-a}^{a} e^{-(x+id)^2} dx \quad \forall d \in \mathbb{R}.$$

□

Lemma 2.8.3. *For $a \in \mathbb{R}$,*

$$\int_{-\infty}^{\infty} e^{-ax^2} dx = \sqrt{\frac{\pi}{a}}. \tag{2.8.21}$$

Proof. In order to prove (2.8.21), we let

$$I = \int_0^{\infty} e^{-ax^2} dx$$

so that

$$I^2 = \int_0^{\infty} \int_0^{\infty} e^{-a(x^2+y^2)} dx dy.$$

The equation in polar form is obtained as

$$I^2 = \lim_{R\to\infty} \int_0^{\pi/2} \int_0^{R} e^{-ar^2} r dr d\theta = \lim_{R\to\infty} \int_0^{\pi/2} \left[\int_0^{R} e^{-ar^2} r dr \right] d\theta.$$

Let $x = ar^2$, so that $dx/dr = 2ar$ and $dr = dx/2ar$.

If $r = 0$, then $x = 0$ and if $r = R$ then $x = aR^2$. Now, I^2 reduces to

$$\begin{aligned} I^2 &= \lim_{R\to\infty}\int_0^{\pi/2}\left[\int_0^{aR^2} e^{-x} r\frac{dx}{2ar}\right]d\theta = \lim_{R\to\infty}\int_0^{\pi/2}\left[\frac{1}{2a}\int_0^{aR^2} e^{-x}dx\right]d\theta \\ &= \lim_{R\to\infty}\int_0^{\pi/2}\left[\frac{1}{2a}\left(-e^{-x}\Big|_{x=0}^{x=aR^2}\right)\right]d\theta = \lim_{R\to\infty}\int_0^{\pi/2}\left[-\frac{1}{2a}\left(e^{-aR^2} - e^{-0}\right)\right]d\theta \end{aligned}$$

as $R \to \infty$ we get that

$$I^2 = \int_0^{\pi/2}\left[-\frac{1}{2a}\Big(0-1\Big)\right]d\theta = \int_0^{\pi/2}\frac{1}{2a}d\theta = \frac{1}{2a}\theta\Big|_{\theta=0}^{\theta=\pi/2} = \frac{1}{2a}\left[\frac{\pi}{2} - 0\right] = \frac{\pi}{4a}.$$

Finally, we have shown that $I^2 = \frac{\pi}{4a}$, this implies that

$$I = \sqrt{\frac{\pi}{4a}} = \frac{1}{2}\sqrt{\frac{\pi}{a}}.$$

Therefore,

$$\int_0^{\infty} e^{-ax^2}dx = \frac{1}{2}\sqrt{\frac{\pi}{a}},$$

and so

$$2\int_0^{\infty} e^{-ax^2}dx = \sqrt{\frac{\pi}{a}},$$

hence the result. □

Proof of Lemma 2.8.1.

Proof. To begin with, we start with the assumption that the Gaussian noise has some correlation in space with white character in time. Note that

$$\mathbb{E}\Big[W(t,x)W(t',x')\Big] = \sum_{n\geq 1}\sqrt{\lambda_n}\sqrt{\lambda_n}\psi_n(x)\psi_n(x')\min\{t,t'\} \approx C(x-x')\min\{t,t'\}. \tag{2.8.22}$$

To get an expression for λ_n, we set $x' = 0$ and $t = t'$ [86], so that (2.8.22) becomes

$$\sum_{n\geq 1}\lambda_n\psi_n(x)\psi_n(0) \approx C(x). \tag{2.8.23}$$

Next, we take the inner product of (2.8.23) and get that

$$\lambda_n \psi_n(0) \approx \int_{\mathbb{R}} C(x)\psi_n(x)dx. \tag{2.8.24}$$

Next, we substitute the definitions of $\psi_n(0)$, $\psi_n(x)$, and $C(x)$ into (2.8.24) to obtain

$$\frac{\lambda_n}{\sqrt{L}} = \frac{1}{\sqrt{L}} \int_{\mathbb{R}} \frac{1}{2\xi} \exp\left(\frac{-\pi x^2}{4\xi^2}\right) \exp\left(\frac{in\pi x}{L}\right) dx. \tag{2.8.25}$$

Next, cancelling out $1/\sqrt{L}$ from both sides and rearranging the equation yields

$$\begin{aligned} \lambda_n &= \frac{1}{2\xi} \int_{\mathbb{R}} \exp\left(\frac{-\pi x^2}{4\xi^2}\right) \exp\left(\frac{in\pi x}{L}\right) dx \\ &= \frac{1}{2\xi} \int_{\mathbb{R}} \exp\left(\frac{-\pi x^2}{4\xi^2} + \frac{in\pi x}{L}\right) dx. \end{aligned} \tag{2.8.26}$$

Now, let $A = \frac{\pi}{4\xi^2}$ and $B = \frac{in\pi}{L}$, so that (2.8.26) reduces to the following equation,

$$\lambda_n = \frac{1}{2\xi} \int_{\mathbb{R}} \exp\Big(-Ax^2 + Bx\Big) dx. \tag{2.8.27}$$

Next, we appeal to the following standard result using a binomial formula

$$-Ax^2 + Bx = -\left(\sqrt{A}\,x - \frac{B\sqrt{A}}{2A}\right)^2 + \frac{B^2}{4A}. \tag{2.8.28}$$

Substitute (2.8.28) into (2.8.27) to get

$$\begin{aligned} \lambda_n &= \frac{1}{2\xi} \int_{\mathbb{R}} \exp\left(-\left(\sqrt{A}\,x - \frac{B\sqrt{A}}{2A}\right)^2 + \frac{B^2}{4A}\right) dx \\ &= \frac{1}{2\xi} \exp\left(\frac{B^2}{4A}\right) \int_{\mathbb{R}} \exp\left(-\left(\sqrt{A}\,x - \frac{B\sqrt{A}}{2A}\right)^2\right) dx. \end{aligned} \tag{2.8.29}$$

Next, we substitute back what A and B stands for into (2.8.27) to get

$$\lambda_n = \frac{1}{2\xi} \exp\left(\frac{-k^2\xi^2\pi}{L^2}\right) \int_{\mathbb{R}} \exp\left(-\left(\frac{\sqrt{\pi}}{2\xi}x - \frac{in\sqrt{\pi}\,\xi}{L}\right)^2\right) dx. \tag{2.8.30}$$

Then using Lemma 2.8.2, get that

$$\lambda_n = \frac{1}{2\xi} \exp\left(\frac{-n^2\xi^2\pi}{L^2}\right) \int_{\mathbb{R}} \exp\left(-\left(\frac{\sqrt{\pi}}{2\xi}x\right)^2\right) dx \tag{2.8.31}$$

and using Lemma 2.8.3, we get that the integral in (2.8.31)

$$\int_{\mathbb{R}} \exp\Big(-\frac{\pi}{4\xi^2}x^2\Big)dx = 2\xi. \tag{2.8.32}$$

Equation (2.8.31) finally becomes

$$\lambda_n = \frac{1}{2\xi} \times 2\xi \exp\bigg(\frac{-n^2\xi^2\pi}{L^2}\bigg) = \exp\bigg(\frac{-n^2\xi^2\pi}{L^2}\bigg). \tag{2.8.33}$$

Hence, the eigenvalues of the $\mathbb{Q}-$Wiener process are obtained as

$$\sqrt{\lambda_n} = \exp\bigg(\frac{-n^2\xi^2\pi}{2L^2}\bigg). \tag{2.8.34}$$

□

The derived eigenvalues (2.8.34) will be used in the Wiener process representation in (2.3.9), so that the noise is exponentially correlated in space. This noise is taken white in time. This form of noise will be used to carry out simulations in Chapter 6.

Chapter 3

Numerics for SODEs.

In this chapter, we develop and propose three stochastic time discretization techniques for the solution of SODEs with an aim to applying these for SPDEs. The derivation of the schemes is based on the exponential time differencing scheme [18]. Two of the stochastic integrators can be used for the simulation of Itô SODEs and the other can be used for the simulation of Stratonovich SODEs. We then numerically investigate the strong and weak convergence of these stochastic integrators and compare these schemes against three other standard numerical methods. We consider three examples of SODEs interpreted in the Itô and Stratonovich sense. Finally, we consider briefly SODEs with small noise.

3.1 Review on deterministic exponential integrators.

Exponential time differencing (**ETD**) schemes are numerical integration techniques that have been successful for the solution of semi-linear differential equations. In particular, they have been found to be most effective for the solutions of time dependent PDEs, see [21, 47] for example. This is because time dependent spatially discretized PDEs are in most cases discretized first in the spatial variables using spectral methods, finite difference and finite element methods, for example. This spatial discretization

often leads to a system of stiff ordinary differential equations in time. Therefore, the need to have effective and stable integration techniques.
A number of methods have been studied and used in the literature to solve these stiff systems. For example, the integrating factor method [52], linearly-implicit method also known as the semi-implicit or implicit-explicit method [2, 91, 6] and the exponential time differencing **ETD** scheme [18].

The **ETD** schemes were originally discovered in the early 60's in the area of computational electrodynamics, however they did not gain much popularity and were not in use because of the need to compute these exponential function and the functions which are closely related to the exponential function. Today, there are efficient ways to compute a matrix exponential. In [68], it was stated that matrix exponential times a vector can be computed efficiently by the use of Krylov approximations with Lanczos process or by using a scaling and squaring method, and this is what the MATLAB routine *expm* is actually based on. Other references where the computation of matrix exponential have been considered are [42, 4, 67].
Basically, the **ETD** schemes works on a nonlinear time dependent equation by solving the linear part of an equation exactly, and then treat the nonlinear part explicitly, while maintaining good stability and high accuracy [75]. The idea of solving exactly the linear part of the equation, which is usually stiff in nature is clearly an advantage of the **ETD** scheme. Other merits include the fact that the exponential function damps out the behaviour of the linear part of the equation, thereby removing the stiffness or highly oscillatory nature of the problem. The stability of the **ETD** scheme has been studied in [18, 75].

The standard **ETD** methods are derived as follows.
Consider the following semi-linear ODE

$$\frac{du(t)}{dt} = Lu + N(u(t)), \quad u(0) = u_0, \tag{3.1.1}$$

where $u : \mathbb{R} \to \mathbb{R}^d$, $L \in \mathbb{R}^{d\times d}$, $N : \mathbb{R}^d \to \mathbb{R}^d$ and d is the dimensionality of the problem.

The **ETD** scheme can be derived using the variation of constant formula as follows: Pre-multiply both sides of (3.1.1) with the integrating factor e^{-tL}.

$$e^{-tL}\frac{du}{dt} = e^{-tL}Lu + e^{-tL}N(u,t). \tag{3.1.2}$$

Re-arranging yields

$$\frac{d}{dt}e^{-tL}u = e^{-tL}N(u,t). \tag{3.1.3}$$

Next, we integrate (3.1.3) over a single time step from $t = t_k$ to $t = t_k + \Delta t$

$$\int_{t_k}^{t_k+\Delta t} \frac{d}{d\tau}e^{-\tau L}u(\tau)d\tau = \int_{t_k}^{t_k+\Delta t} e^{-\tau L}N(u,\tau)d\tau,$$

$$e^{-(t_k+\Delta t)L}u(t_k+\Delta t) - e^{-t_kL}u(t_k) = \int_{t_k}^{t_k+\Delta t} e^{-\tau L}N(u,\tau)d\tau,$$

$$u(t_k+\Delta t) = e^{\Delta tL}u(t_k) + e^{(t_k+\Delta t)L}\int_{t_k}^{t_k+\Delta t} e^{-\tau L}N(u,\tau)d\tau, \tag{3.1.4}$$

substitute $\tau = t_k + \theta\Delta t$ in the integral to get

$$u(t_k+\Delta t) = e^{\Delta tL}u(t_k) + \Delta t\int_0^1 e^{(1-\theta)\Delta tL}N(u(t_k+\theta\Delta t))d\theta. \tag{3.1.5}$$

Equation 3.1.5 is still an exact representation of the solution. Exponential time differencing schemes now arise from how we choose to approximate the nonlinear term $N(u(\tau),\tau)$ by a polynomial $p(\theta)$. The simplest choice of approximating the nonlinear tern is by a constant at $\theta = 0$.

$$u_{k+1} = e^{\Delta tL}u_k + L^{-1}\Big(e^{\Delta tL} - I\Big)N(u(t_k),t_k). \tag{3.1.6}$$

Higher order based **ETD** schemes has been developed, for example the fourth-order exponential time differencing Runge-Kutta (**ETDRK4**) method [18, 47].

3.2 Derivation of the Stochastic ETD schemes.

Our aim in this section is to derive three new stochastic versions of the **ETD** scheme. Two based on Itô interpretation and the other based on Stratonovich interpretation.

3.2.1 Itô scheme:

Consider the following semi-linear SODE

$$du(t) = (Lu(t) + N(u(t)))dt + G(u(t))dW(t), \quad u(0) = u_0, \tag{3.2.1}$$

where $u : \mathbb{R} \to \mathbb{R}^d$, $L \in \mathbb{R}^{d\times d}$, $N : \mathbb{R}^d \to \mathbb{R}^d$, $G : \mathbb{R}^d \to \mathbb{R}^{d\times m}$ and $W(t)$ is an m-dimensional Wiener process.

By the variation of constant formula for SODEs,

$$u(t) = e^{tL}u(0) + \int_0^t e^{(t-s)L}N(u(s))ds + \int_0^t e^{(t-s)L}G(u(s))dW(s). \tag{3.2.2}$$

If we consider the approximation of the functions N and G at the left-end point over a single time step, from t_k to t_{k+1}, we get that

$$u(t_{k+1}) \approx e^{L\Delta t}\left(u(t_k) + N(u(t_k))\int_{t_k}^{t_{k+1}} e^{-Ls}ds + G(u(t_k))\int_{t_k}^{t_{k+1}} e^{-Ls}dW(s)\right).$$

Working out the first integral, and letting u_k denote the approximation of u at time step t_k, and using $t_{k+1} - t_k = \Delta t$, we get that

$$u_{k+1} = e^{L\Delta t}\left(u_k + N(u_k)\int_0^{\Delta t} e^{-Ls}ds + G(u_k)\int_0^{\Delta t} e^{-Ls}dW(s)\right) \tag{3.2.3}$$

$$= e^{L\Delta t}u_k + L^{-1}\Big(e^{L\Delta t} - I\Big)N(u_k) + G(u_k)\int_0^{\Delta t} e^{L(\Delta t-s)}dW(s). \tag{3.2.4}$$

It turns out that the first two terms on the RHS of equation (3.2.4) is exactly the same as what we obtained in the deterministic **ETD** scheme. We are then left with the calculation of the third term.

There are indeed two ways we can approximate this stochastic integral, so that we obtain two variants of the SETD scheme.

3.2.2 First variant of the SETD scheme: SETD0.

To obtain the first variant of the **SETD** scheme, we approximate the integrand in the stochastic part of (3.2.4) at the left end point as follows:

$$G(u_k)\int_0^{\Delta t} e^{L(\Delta t-s)}dW(s) \approx e^{L\Delta t}e^{-L\cdot 0}G(u_k)\int_0^{\Delta t} dW(s) \tag{3.2.5}$$

$$= e^{L\Delta t}G(u_k)\Delta W_k, \tag{3.2.6}$$

where ΔW_k is given by (2.2.8).

Finally, from (3.2.4) we obtain the following numerical scheme

$$u_{k+1} = e^{L\Delta t}u_k + L^{-1}\Big(e^{L\Delta t}-I\Big)N(u_k) + e^{L\Delta t}G(u_k)\Delta W_k, \quad k = 0, 1, \cdots, M-1. \tag{3.2.7}$$

We call this scheme the **SETD0** scheme.

3.2.3 Second variant of the SETD scheme: SETD1.

In the derivation of the **SETD0** scheme, the integrand in (3.2.5) was approximated at the left end point. However, to derive the **SETD1** scheme, we seek the statistical information of the integral in (3.2.5) as a whole. The integral is a Gaussian random variable with mean 0 and the variance we calculate as follows. We know that

$$Var[X] = \mathbb{E}[X^2] - \Big(\mathbb{E}[X]\Big)^2, \tag{3.2.8}$$

therefore by using this definition and the property of Itô- isometry [50, 70], we get that

$$Var\left[\int_0^{\Delta t} e^{L(\Delta t-s)}dW(s)\right] = \mathbb{E}\left[\Big(\int_0^{\Delta t} e^{L(\Delta t-s)}dW(s)\Big)^2\right] - \left(\mathbb{E}\left[\int_0^{\Delta t} e^{L(\Delta t-s)}dW(s)\right]\right)^2 \tag{3.2.9}$$

$$= \mathbb{E}\left[\int_0^{\Delta t} e^{2L(\Delta t-s)}ds\right] - 0$$

$$= \int_0^{\Delta t} e^{2L(\Delta t-s)}ds$$

$$= L^{-1}\left(\frac{e^{2L\Delta t}-I}{2}\right). \tag{3.2.10}$$

Hence, the scheme (3.2.4) now becomes

$$u_{k+1} = e^{L\Delta t}u_k + L^{-1}\Big(e^{L\Delta t}-I\Big)N(u_k) + L^{-1/2}\Big(\frac{e^{2L\Delta t}-I}{2}\Big)^{1/2}G(u_k)\beta_k, \tag{3.2.11}$$

where β_k is an independent and identically distributed standard normal random variable with mean 0 and variance 1. We call this scheme the **SETD1** scheme.

We remark that the **SETD1** scheme uses the idea of the linear functional of the noise as presented in the work by Kloeden & Jentzen in which they derived the scheme which they call the exponential Euler scheme [46] for additive noise. However, the difference between the **SETD1** scheme and the scheme by Kloeden & Jentzen lies in the fact that the **SETD1** scheme was obtained from a multiplicative SDE while the exponential Euler scheme was obtained from an additive SDE.

3.2.4 Stratonovich scheme: ESI.

Consider the following SDE interpreted in the Stratonovich sense

$$du(t) = (Lu(t) + N(u(t)))dt + G(u(t)) \circ dW(t). \tag{3.2.12}$$

The variation of constants formula gives

$$u(t) = e^{tL}u(0) + \int_0^t e^{(t-s)L}N(u(s))ds + \int_0^t e^{(t-s)L}G(u(s)) \circ dW(s). \tag{3.2.13}$$

We recall that an approximation for the deterministic part of (3.2.13) has been obtained in (3.2.4). Thus an approximation for (3.2.13) over a single time step from t_k to t_{k+1} is now given by

$$u_{k+1} = e^{L\Delta t}u_k + L^{-1}\Big(e^{L\Delta t}-I\Big)N(u_k) + \int_{t_k}^{t_{k+1}} e^{(t_{k+1}-s)L}G(u(s)) \circ dW(s). \tag{3.2.14}$$

In order to obtain an approximation for the Stratonovich stochastic integral in (3.2.14), we approximate the integrand using the midpoint rule rather than approximating the stochastic integral at the left end point of the interval. Thus the integrand in (3.2.14) is evaluated at the discrete time $\frac{t_k+t_{k+1}}{2}$ as follows:

$$\begin{aligned}\int_{t_k}^{t_{k+1}} e^{(t_{k+1}-s)L}G(u(s))\circ dW(s) &\approx e^{\left(t_{k+1}-\frac{t_k+t_{k+1}}{2}\right)L}G\left(u(\frac{t_k+t_{k+1}}{2})\right)\Big(W(t_{k+1})-W(t_k)\Big)\\ &= \frac{1}{2}e^{\left(\frac{t_{k+1}-t_k}{2}\right)L}\Big(G(u(t_k))+G(u(t_{k+1}))\Big)\Big(W(t_{k+1})-W(t_k)\Big)\\ &= \frac{1}{2}e^{\Delta tL/2}\Big(G(u(t_k))+G(u(t_{k+1}))\Big)\Delta W_k. \qquad (3.2.15)\end{aligned}$$

Observe that the formula on the right hand side of (3.2.15) involves the $u(t_{k+1})$ term, which needs to be determined. Thus, to proceed in writing down the approximation scheme for (3.2.12), we use the Euler-Maruyama solution $u(t_{k+1})$ which we will denote as $\tilde{u}_{k+1}$ (given in (2.2.3)) as an estimate for the $u(t_{k+1})$ term in (3.2.15). Hence, we obtain the following numerical scheme for (3.2.12) as:

$$u_{k+1} = e^{L\Delta t}u_k + L^{-1}\Big(e^{L\Delta t}-I\Big)N(u_k) + \frac{1}{2}e^{\Delta tL/2}\Big(G(u_k)+G(\tilde{u}_{k+1})\Big)\Delta W_k. \qquad (3.2.16)$$

where $\tilde{u}_{k+1}$ is an Euler-Maruyama scheme used as predictor term, u_k is an approximation to the solution u at t_k and ΔW_k is given by (2.2.8). We call this scheme the exponential Stratonovich Integrator **ESI** scheme. We propose this new scheme for the numerical approximation of Stratonovich SDEs. In this thesis, we use the **ESI** to simulate SDEs interpreted in the Stratonovich sense and compare the scheme against the standard **Heun** scheme.

3.3 Numerical investigation of strong convergence.

We carry out numerical experiments on four examples of SODEs interpreted in both the Itô and Stratonovich sense. We examine the strong convergence for the **ESI**, **Heun**, **LR**, **SETD0**, **SETD1** and **EM** schemes, and also obtain their orders of convergence numerically. The **Heun** and **ESI** methods are applied directly to solve the

SDEs in the Stratonovich form and the **SETD0**, **SETD1**, **LR** and the semi-implicit **EM** methods are used to solve the SDEs in the Itô form.

In order to investigate strong convergence numerically, we consider the strong error in (2.2.1) at final time T given as $\varepsilon(\Delta t) := \mathbb{E}\left[\left|X_M - \hat{X}(t_M)\right|\right]$. We investigate how the error depends on the time step size Δt. Thus, for a choice of Δt, we calculate R simulations, such that for each realization, the values of X_M and $\hat{X}(t_M)$ becomes X_M^r and $\hat{X}^r(t_M)$ for $r = 1, \cdots, R$.
The estimate of the strong error $\varepsilon(\Delta t)$ which we denote by $\hat{\varepsilon}(\Delta t)$ is calculated as follows:

$$\hat{\varepsilon}(\Delta t) := \frac{1}{R}\sum_{r=1}^{R}\left|X_M^r - \hat{X}^r(t_M)\right|. \tag{3.3.1}$$

Equation (3.3.1) gives the numerical strong error estimated from $\varepsilon(\Delta t)$.
Strong convergence requires that the solution paths are followed exactly. To ensure that we follow the path exactly we make use of the same Wiener process used in the exact solution. The numerical experiments are then performed over a time interval $t \in [0, 1]$, with nine values of Δt. The following time step sizes were used to obtain approximate solutions: $\Delta t_1 = 1/4000$, $\Delta t_2 = 1/2000$, $\Delta t_3 = 1/1000$, $\Delta t_4 = 1/800$, $\Delta t_5 = 1/500$, $\Delta t_6 = 1/400$, $\Delta t_7 = 1/250$, $\Delta t_8 = 1/200$ and $\Delta t_9 = 1/100$.
1000 realizations of solutions were simulated and the numerical strong error (3.3.1) is obtained by averaging over these number of trajectories.

In the numerical experiments, we also compute the average computer time.
By average computer time, we mean the arithmetic mean of R independent simulations of the computer time (in seconds) it takes to obtain the rth simulation of the numerical error at time step size Δt_i, $i = 1, \cdots, 9$.

$$\text{For each } i \text{ , the average computer time} = \frac{1}{R}\sum_{r=1}^{R}\Theta_{\Delta t_i}^r, \quad i = 1, \cdots, 9, \tag{3.3.2}$$

where $\Theta_{\Delta t_i}^r$ stands for the computer time (in seconds) it takes to obtain the rth simulation of the numerical strong error at time step size Δt_i, $i = 1, \cdots, 9$ and R stands for the number of realizations.

Numerical example 1: Geometric Brownian Motion (GBM) equation [41, 50].

The following autonomous, scalar, linear Itô SDE with multiplicative noise is sometimes used to model stock price evolution:

$$dX(t) = \lambda X(t)dt + \mu X(t)dW(t), \quad X(0) = X_0, \quad t \in [0,1], \tag{3.3.3}$$

with exact solution

$$X(t) = X(0)\exp\Big((\lambda - \mu^2/2)t + \mu W(t)\Big). \tag{3.3.4}$$

In Stratonovich form, the SODE (3.3.3) becomes

$$dX(t) = \Big(\lambda - \frac{1}{2}\mu^2\Big)X(t)dt + \mu X(t) \circ dW(t). \tag{3.3.5}$$

We performed numerical experiment using the **EM** (2.2.3), **LR** (2.2.5), **SETD0** (3.2.7) and **SETD1** (3.2.11) methods to simulate the Itô SDE (3.3.3) and then use the **Heun** (2.2.6) and **ESI** (3.2.16) methods to simulate the Stratonovich SDE (3.3.5). The SDEs are numerically integrated over the time interval $t = [0, 1]$ with initial value $X(0) = 0.5$ and we take the parameters $\lambda = 0.2$ and $\mu = 0.5$.
Numerical solutions are then obtained using the 6 methods with a fixed time step $\Delta t = 1/4000$. This time step is used to generate the path for the exact solution (3.3.4).

Figure 3.1(a) graphically shows the strong convergence of the 6 numerical methods with errors at the final time, $T = 1$ computed at various time step-sizes. The slopes of the convergence for the methods applied to the SDEs (3.3.3) and (3.3.5) are displayed in Figure 3.1(a) and their respective strong orders are shown in the legend. We remark that the **LR** and **SETD0** schemes are both identical since a nonlinear term is absent in example (3.3.3).
We observe strong orders of convergence of 0.5 for the **EM**, **SETD0**, **SETD1** and **LR** methods and strong orders 1 for the **Heun** and **ESI** methods. The rates of convergence obtained for these numerical methods are indeed in good agreement with

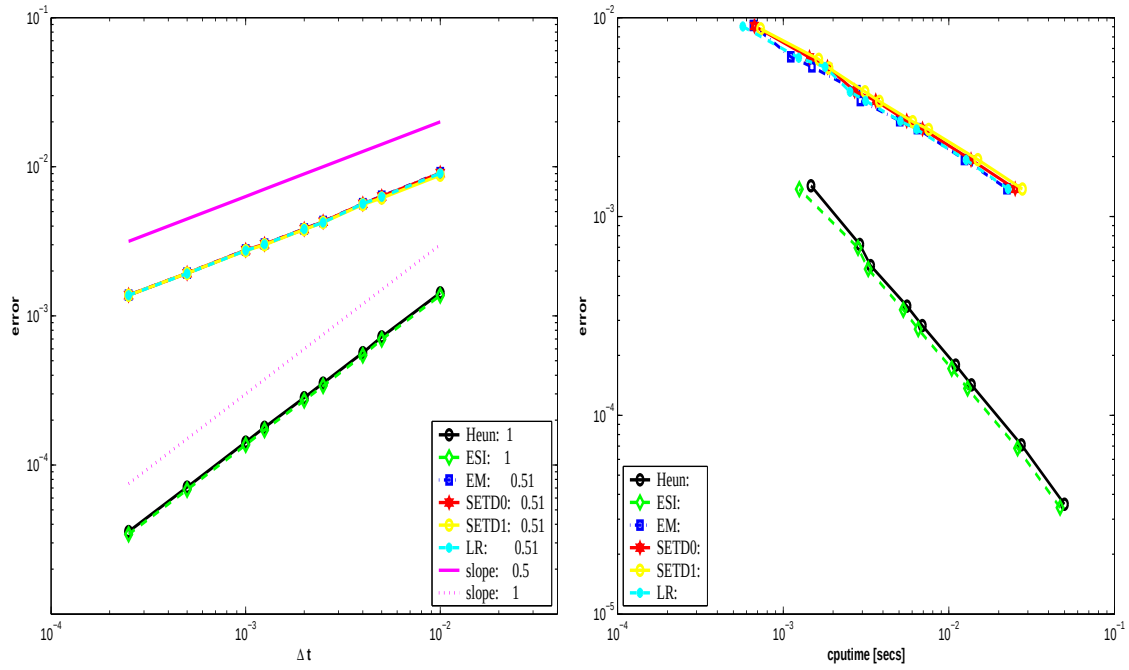

(a) (b)

Figure 3.1: Strong convergence of the **EM**, **SETD0**, **SETD1**, **LR**, **Heun** and **ESI** methods. The SDEs (3.3.3) and (3.3.5) are solved with parameters $\lambda = 0.2$, $\mu = 0.5$, $X(0) = 0.5$. (a) a log-log plot of the numerical strong error (3.3.1) versus time step-size, (b) a log-log plot of the numerical strong error (3.3.1) versus average computer time.

the theoretical results, (see for example [50]) where the **EM** method was shown to have strong order 0.5 and the **Heun** method is known to converge with strong order 1. We also add in the plot lines of slope 0.5 and 1 for reference.

We also see that the new numerical method we proposed in this thesis called the exponential Stratonovich integrator **ESI** scheme has similar accuracy as the standard **Heun** method. The **Heun** method and **ESI** scheme show great improvement over the other 4 methods in terms of accuracy. This improvement is known for Stratonovich SDEs driven by one Wiener process. In [79], the author remarks that the **Heun** scheme converging to the solution of a Stratonovich SDE has mean-square order 1 if the diffusion terms in the SDE commute, in particular, if there is only one driving Wiener process in the SDE. We will investigate the influence of two driving Wiener process on SODEs later in the Chapter.

Figure 3.1(b) illustrate the efficiency of the 6 numerical methods applied to the SDEs (3.3.3) and (3.3.5). We plot the strong error against the average computer time (in seconds) it takes for the 6 numerical methods. We observe that the **Heun** and **ESI** method are the most accurate schemes, since if we consider a fixed cputime and look at the errors obtained from the 6 methods used, we see that the **Heun** and **ESI** methods give the smallest error. In addition, if we consider a fixed error, we get that the **Heun** and **ESI** methods are computationally the fastest, thus the most efficient methods when compared to the **EM**, **LR**, **SETD0** and **SETD1** methods.

Numerical example 2:

Consider the following one-dimensional Itô SDE

$$dX(t) = -a^2X(t)(1-X(t)^2)dt + a(1-X(t)^2)dW(t), \quad X(0) = X_0, \quad t \in [0,1]. \tag{3.3.6}$$

Using $g(X(t)) = a(1-X(t)^2)$ and $g'(X(t)) = -2aX(t)$ in (2.1.9), we obtain the Stratonovich form of the SDE (3.3.6) as

$$dX(t) = \left[-a^2X(t)(1-X(t)^2) - \frac{1}{2}\Big(a(1-X(t)^2)\Big)\Big(-2aX(t)\Big)\right]dt + a(1-X(t)^2)\circ dW(t). \tag{3.3.7}$$

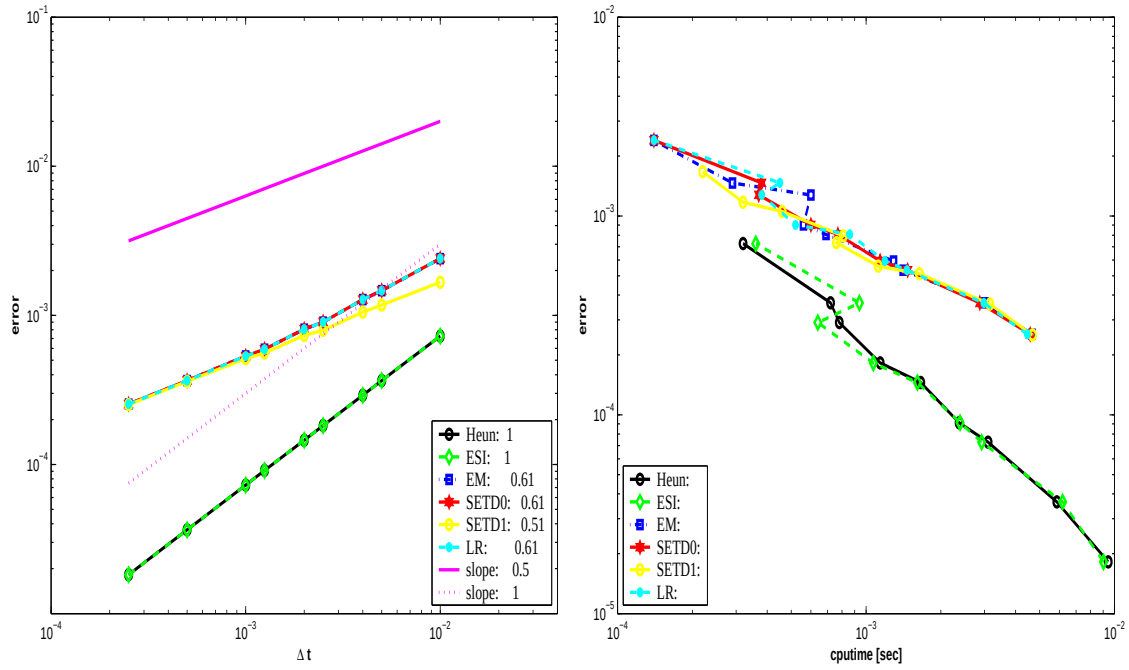

(a) (b)

Figure 3.2: Strong convergence of the **EM**, **SETD0**, **SETD1**, **LR**, **Heun** and **ESI** methods. The SDEs (3.3.6) and (3.3.8) are solved with parameters $a = 0.2$, $X(0) = 0.5$. In (a) a log-log plot of the numerical strong error (3.3.1) versus time step-size, (b) a log-log plot of the numerical strong error (3.3.1) versus average computer time.

This reduces to

$$dX(t) = a(1 - X(t)^2) \circ dW(t). \tag{3.3.8}$$

The exact solution of (3.3.8) is also a solution to (3.3.6) and it is obtained as [50]

$$X(t) = \tanh((aW(t)) + \operatorname{arctanh}(X_0)). \tag{3.3.9}$$

In Figure 3.2(a), we plot the strong error with respect to the time step-size. The legend show the strong order of 0.6 for the **EM**, **SETD0**, **SETD1** and **LR** methods and strong order 1 for **Heun** and **ESI** methods respectively. These orders obtained for this numerical example are again in good agreement with the results in theory [50]. We remark the **Heun** and **ESI** schemes are identical when applied to example (3.3.8) since a drift term is absent.
Figure 3.1(b) displays the plot of average strong error with respect to the average cputime. We see just as in numerical example 1 that the **Heun** and **ESI** method are the computationally the most accurate and fastest schemes, when compared to the **EM**, **LR**, **SETD0** and **SETD1** methods.

So far, we have considered two scalar SODEs driven by one Wiener process as test problems. The linear part of these test problems does not feature stiffness. Also the test problems are driven by a scalar Wiener process. In what follows, we consider two test problems whose linear part are stiff. The first test problem is a two-dimensional SODE driven by one Wiener process (that is, $d = 2$, $m = 1$ in Equation (2.1.1)) while the second test problem is a two-dimensional SODE driven by two Wiener processes (that is, $d = 2$, $m = 2$ in Equation (2.1.1)).

Numerical example 3:

Consider the following two-dimensional semi-linear stiff SODE driven by one Wiener process.

$$dX(t) = \Big[AX(t) + B\Big(X(t) - X(t)^3\Big)\Big]dt + CX(t)dW(t), \quad X(0) = X_0. \tag{3.3.10}$$

The Stratonovich form of (3.3.10) is obtained as

$$dX(t) = \Big[AX(t) + B\Big(X(t) - X(t)^3\Big) - \widehat{B}X(t)\Big]dt + CX(t) \circ dW(t), \quad X(0) = X_0, \tag{3.3.11}$$

where

$$A = \begin{bmatrix} -100 & 1 \\ 0 & -\frac{1}{10} \end{bmatrix}, \quad B = \begin{bmatrix} 1 & 0 \\ 0 & 1 \end{bmatrix}, \quad \widehat{B} = \frac{1}{2}\begin{bmatrix} \left(\frac{3}{4}\right)^2 & 0 \\ 0 & \left(\frac{3}{4}\right)^2 \end{bmatrix},$$

$$C = \begin{bmatrix} \frac{3}{4} & 0 \\ 0 & \frac{3}{4} \end{bmatrix}, \quad X_0 = \begin{bmatrix} \frac{2}{5} \\ \frac{3}{5} \end{bmatrix}.$$

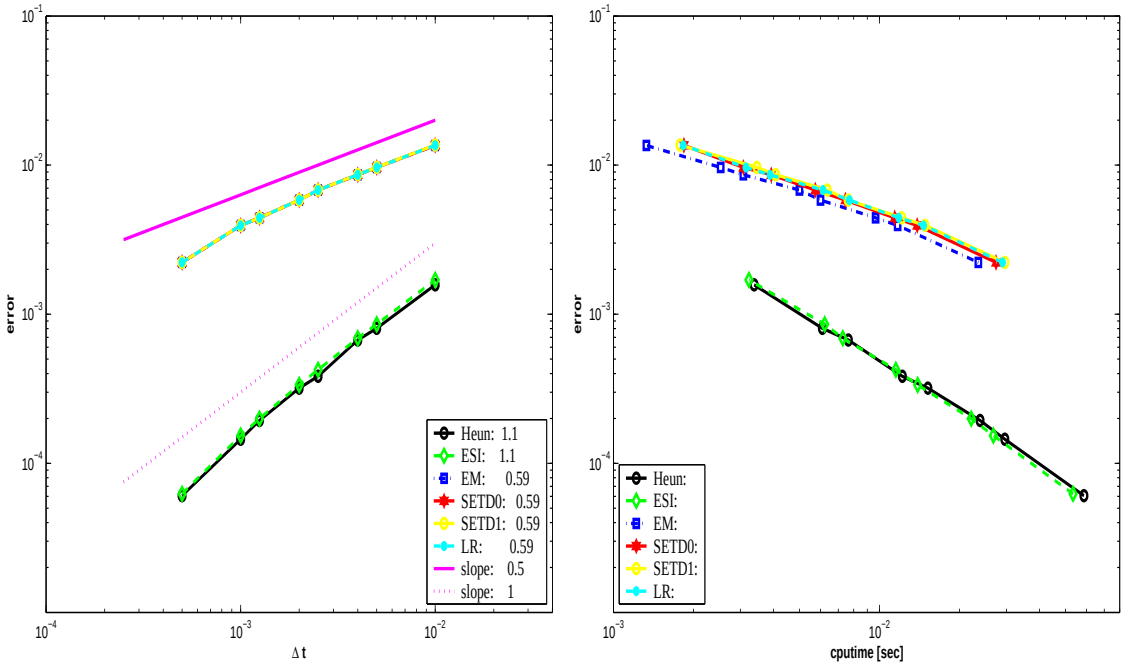

(a) (b)

Figure 3.3: Strong convergence of the **EM**, **SETD0**, **SETD1**, **LR**, **Heun** and **ESI** methods. The SDEs (3.3.10) and (3.3.11) are solved with parameters $a = 0.2$, $X(0) = 0.5$. In (a) is a log-log plot of the numerical strong error (3.3.1) versus time step-size, and in (b) is a log-log plot of the numerical strong error (3.3.1) versus average computer time.

Numerical example 4:

Consider the following two-dimensional semi-linear stiff SODE driven by two Wiener processes.

$$dX(t) = \Big[AX(t)+B\Big(X(t)-X(t)^3\Big)\Big]dt+CX(t)dW_1(t)+DX(t)dW_2(t), \quad X(0)=X_0. \tag{3.3.12}$$

The Stratonovich form of (3.3.12) is obtained as

$$\begin{aligned} dX(t) &= \Big[AX(t)+B\Big(X(t)-X(t)^3\Big)-\widehat{B}X(t)\Big]dt+CX(t)\circ dW_1(t)+DX(t)\circ dW_2(t), \\ X(0) &= X_0, \end{aligned} \tag{3.3.13}$$

where A, B, C and X_0 are given as in Numerical example 3.
The matrix D and $\widehat{B}$ for this test problem are given as:

$$D=\begin{bmatrix} 0 & -\frac{9}{10} \\ \frac{9}{10} & 0 \end{bmatrix}, \quad \widehat{B}=\frac{1}{2}\begin{bmatrix} \left(\frac{3}{4}\right)^2 & \left(\frac{9}{10}\right)^2 \\ \left(\frac{9}{10}\right)^2 & \left(\frac{3}{4}\right)^2 \end{bmatrix}.$$

Results for Numerical examples 3 and 4.

Numerical experiments were carried out to simulate the Itô SODEs (3.3.10) and (3.3.12) using the **EM** (2.2.3), **LR** (2.2.5), **SETD0** (3.2.7) and **SETD1** (3.2.11) methods while the Stratonovich SODEs (3.3.11) and (3.3.13) were simulated by using the **Heun** (2.2.6) and the **ESI** (3.2.16) methods. Figures 3.3(a) and 3.4(a) displays the strong orders of convergence of the six numerical methods applied to numerical example 3 and numerical example 4 respectively. We observe strong orders of approximately equal to 1 for the **Heun** and the **ESI** schemes when applied to SODEs driven by one Wiener process, these observed orders are two times the strong orders observed for the Itô schemes. However, when the Stratonovich schemes are applied to SODEs driven by two Wiener processes as in numerical example 4, we see that the strong orders of the **Heun** and **ESI** are approximately equal to the strong orders observed for the Itô schemes, see the legends in Figures 3.3(a) and Figure 3.4(a) for comparison. Figures 3.3(b) and (3.4(b)) displays the average computer time used to obtain the numerical strong errors of the six numerical methods. We observe that

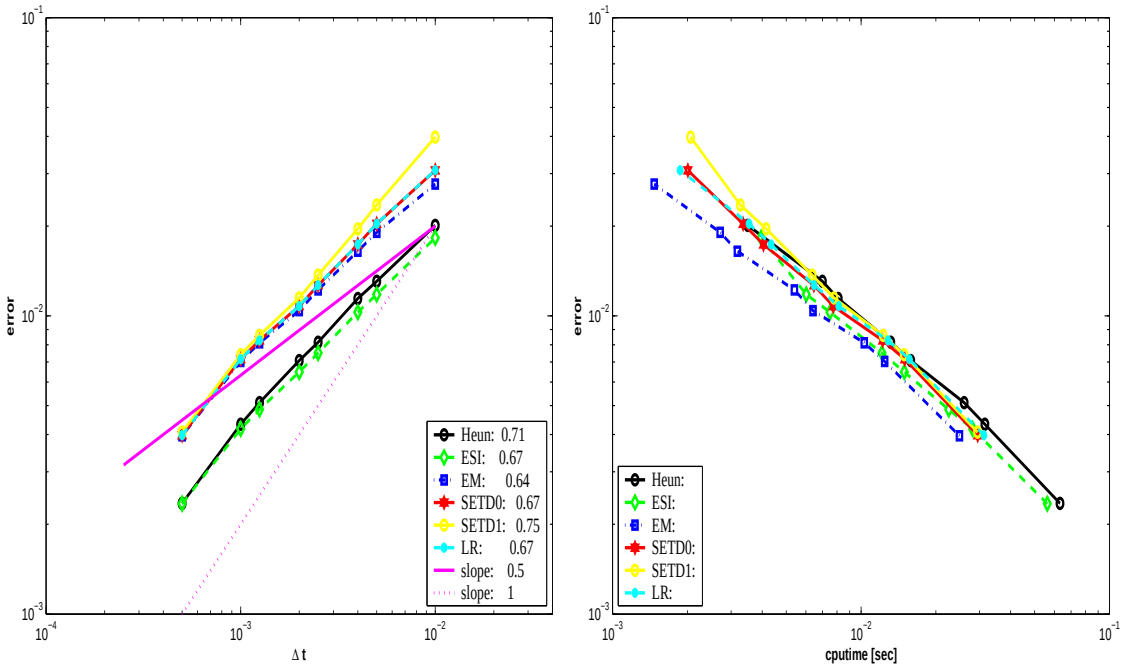

(a) (b)

Figure 3.4: Strong convergence of the **EM**, **SETD0**, **SETD1**, **LR**, **Heun** and **ESI** methods. The SDEs (3.3.12) and (3.3.13) are solved with parameters $a = 0.2$, $X(0) = 0.5$. In (a) is a log-log plot of the numerical strong error (3.3.1) versus time step-size, and (b) is a log-log plot of the numerical strong error (3.3.1) versus average computer time.

for a fixed value of the numerical strong error, the Stratonovich schemes are more efficient than the Itô schemes.

Numerical investigation of strong convergence for SODEs with small noise.

In many areas of applications in science and engineering, SDEs with small noise are of interest, as a result a number of studies have been carried out for these kinds of equation, see for example work by [7, 65]. A system of SDEs with small noise is of the form [65]:

$$dX(t) = f(t, X)dt + \beta g(t, X)dW(t), \quad X(t_0) = X_{t_0} \quad t \in [t_0, T], 0 \leq \beta \leq \beta_0, \quad (3.3.14)$$

where β is a small parameter which controls the strength of the noise in the system and β_0 is a positive number. If the parameter β is close to zero, we recover a deterministic system and there a number of effective numerical methods for the solutions of systems of this kind.

The studies of numerical methods for SODEs with small noise were carried out in [7, 8, 9, 66]. In [66], they show that for SDEs with small noise it is possible to construct special numerical methods which are more effective and easier than in the general case. Numerical integration of stochastic differential equations with small noise has been considered in the mean square sense in [65] and in the weak sense in [66].

In what follows, we perform numerical experiments to investigate the strong orders of convergence of the six previously used numerical methods applied to an example of SDE with a range of noise intensities. In particular, we are interested in observing the strong orders of convergence for the numerical methods when applied to SDE with small noise intensity.

In Chapter 5, we will also investigate the strong orders of convergence of numerical methods applied to SPDEs with small noise intensity.

Numerical experiments:

Consider the following SDE used in population dynamics [41]

$$dX(t) = rX(t)(K - X(t))dt + \beta X(t)dW(t), \quad X(0) = X_0 \tag{3.3.15}$$

where β denotes the strength of the noise.

The Stratonovich version of (3.3.15) is obtained as:

$$dX(t) = \left(rK - \frac{1}{2}\beta^2 - rX(t))\right) X(t)dt + \beta X(t) \circ dW(t). \tag{3.3.16}$$

The solution of (3.3.15) is given as (see [70])

$$X(t) = \frac{X(0)\exp\Big(\big(rK - \frac{1}{2}\beta^2\big)t + \beta W(t)\Big)}{1 + X(0)r\int_0^t \exp\Big(\big(rK - \frac{1}{2}\beta^2\big)s + \beta W(s)\Big)ds}. \tag{3.3.17}$$

In this numerical example, we perform numerical experiment to examine strong convergence of the following numerical methods; the **Heun** (2.2.6), **ESI** (3.2.16), **EM** (2.2.3), **SETD0** (3.2.7), **SETD1** (3.2.11) and **LR** (2.2.5).

Since we do not have an explicit analytic solution to (3.3.15), (Note the integral in the denominator of (3.3.17)), we take as a true solution, a solution with time step-size $\Delta t = 2^{-14}$. We then solve the SDE with following parameter values $X_0 = 0.5$, $r = 2$, $K = 1$, β ranging from 0 to 1. The subsequent coarser solutions are computed with the time step-sizes $\{2^i \Delta t\}_{i=1,\cdots,7}$, the solutions are the averaged over 1000 realizations. We see from Figure 3.5 the influence of small noise gives the effect that is observable in the deterministic setting whereby strong order of convergence is 1.

On the other hand, as noise intensity is increased, the strong order gradually reduces and approaches ≈ 0.5 for the **SETD0**, **SETD1**, **EM** and **LR**. The **Heun** and **ESI** methods are also seen to have strong order ≈ 1 for both small and large noise intensities. These results are in agreement with the theoretical results.

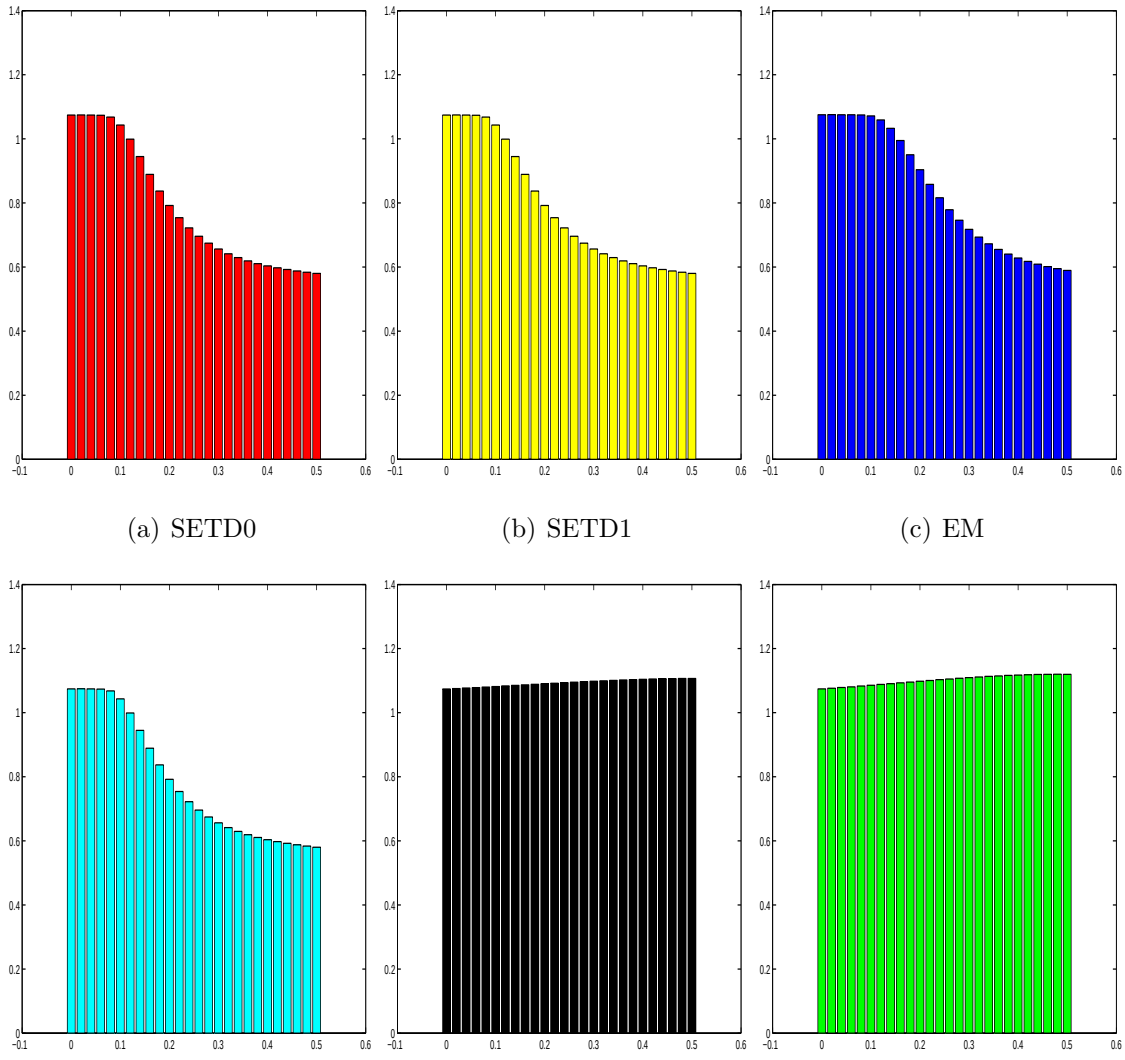

(a) SETD0 (b) SETD1 (c) EM

(d) LR (e) Heun (f) ESI

Figure 3.5: Plot of strong orders of convergence on the y-axis versus increasing noise intensities β, $\beta \in [0, 0.5]$ on the x-axis obtained using the following method, (a) **SETD0** (b) **SETD1** (c) **EM** (d) **LR** (e) **Heun** (f) **ESI** on multiplicative SDE (3.3.15).

Chapter 4

Theoretical convergence proof of SETD0 scheme.

4.1 Introduction

We study the strong numerical approximation of the following Itô parabolic SPDEs with three different forms of stochastic forcing.

SPDEs with one-dimensional multiplicative noise

$$du = \Big[Au + f(u)\Big]dt + \epsilon g(u)d\beta(t), \quad t \in [0,T], \quad u(0) = u_0, \tag{4.1.1}$$

where $\beta(t)$ is a scalar Wiener process defined in Definition 2.1.1.

SPDEs with infinite-dimensional multiplicative noise

$$du = \Big[Au + f(u)\Big]dt + \epsilon g(u)dW(t), \quad t \in [0,T], \quad u(0) = u_0, \tag{4.1.2}$$

where $W(t)$ is a $\mathbb{Q}$-Wiener process given in (2.3.9).

SPDEs with infinite-dimensional additive noise

$$du = \Big[Au + f(u)\Big]dt + \epsilon dW(t), \quad t \in [0,T], \quad u(0) = u_0, \tag{4.1.3}$$

where $W(t)$ is a $\mathbb{Q}$-Wiener process given in (2.3.9).

The function u is an H-valued random process. We take H introduced in Chapter 2 to be the Hilbert space L^2. The initial condition $u(0) = u_0 \in \mathcal{D}(A)$, where $\mathcal{D}(A)$

stands for the domain of A and it is defined in (2.4.1). A is a positive self-adjoint linear operator and it is the generator of an analytic semigroup $e^{tA}, t \geq 0$ [19], with negative real eigenvalues α_n. The functions f and g denote the drift and diffusion part of the SPDEs, and are in general nonlinear, with $f : H \to H$ and $g : H \to L_2^0$. The exact assumptions for these functions are given in Assumptions 2.4.1, 2.4.2, 2.4.3 (or 2.4.4). Finally, the SPDEs are supplemented with periodic boundary conditions on $[0, 2\pi]$.

Recall from Theorem 2.4.1 in Chapter 2, that the SPDEs (4.1.1), (4.1.2) and (4.1.3) have unique mild solutions given respectively as

$$u(t) = e^{tA}u(0) + \int_0^t e^{(t-s)A} f(u(s))ds + \epsilon \int_0^t e^{(t-s)A} g(u(s))d\beta(s), \tag{4.1.4}$$

$$u(t) = e^{tA}u(0) + \int_0^t e^{(t-s)A} f(u(s))ds + \epsilon \int_0^t e^{(t-s)A} g(u(s))dW(s), \tag{4.1.5}$$

$$u(t) = e^{tA}u(0) + \int_0^t e^{(t-s)A} f(u(s))ds + \epsilon \int_0^t e^{(t-s)A} dW(s), \tag{4.1.6}$$

where the Wiener process $\beta(t)$ in (4.1.4) is one-dimensional and the Wiener process $W(t)$ in (4.1.5) and (4.1.6) is infinite-dimensional.

4.2 Numerical methods.

We apply a Fourier-Galerkin projection to the SPDEs (4.1.1), (4.1.2) and (4.1.3) and then use the finite dimensional subspace H_N of H and the projection operator P_N introduced in Section 2.8.1, to obtain a finite dimensional SDEs in the space H_N. The SODEs corresponding to the Fourier-Galerkin projection of the SPDEs (4.1.1), (4.1.2) and (4.1.3) are given respectively by

$$du^N(t) = \Big[A_N u^N(t) + f_N(u^N(t))\Big]dt + \epsilon g_N(u^N(t))d\beta(t), \tag{4.2.1}$$

$$du^N(t) = \Big[A_N u^N(t) + f_N(u^N(t))\Big]dt + \epsilon g_N(u^N(t))dW^N(t), \tag{4.2.2}$$

$$du^N(t) = \Big[A_N u^N(t) + f_N(u^N(t))\Big]dt + \epsilon dW^N(t), \tag{4.2.3}$$

where $A_N = P_N A$, such that $A_N : H_N \to H_N$, $f_N(u) := P_N f(u)$, $g_N(u) := P_N g(u)$, $u^N(0) := P_N u(0)$ and $W^N(t) = P_N W(t) = \sum_{n=1}^{N} \sqrt{\lambda_n}\beta_n(t)\psi_n$.

The SODEs (4.2.1), (4.2.2) and (4.2.3) have unique solutions on $[0, T]$, given respectively by

$$u^N(t) = e^{A_N t}u^N(0) + \int_0^t e^{A_N(t-s)} f_N(u^N(s))ds + \epsilon \int_0^t e^{A_N(t-s)} g_N\left(u^N(s)\right) d\beta(s). \tag{4.2.4}$$

$$u^N(t) = e^{A_N t}u^N(0) + \int_0^t e^{A_N(t-s)} f_N(u^N(s))ds + \epsilon \int_0^t e^{A_N(t-s)} g_N\left(u^N(s)\right) dW^N(s), \tag{4.2.5}$$

$$u^N(t) = e^{A_N t}u^N(0) + \int_0^t e^{A_N(t-s)} f_N(u^N(s))ds + \epsilon \int_0^t e^{A_N(t-s)} dW^N(s). \tag{4.2.6}$$

We can now write down the **SETD0** approximation for (4.2.4), (4.2.5) and (4.2.6). Let $[t_0, T]$ denote the time interval with grid $\mathcal{J}_{\Delta t}^M = \{t_0, t_1, \cdots, t_M = T\}$ such that the time grid is equidistant with the time step size $\Delta t = \frac{T - t_0}{M}$ and $t_k = k\Delta t$. Then the **SETD0** approximation for (4.2.4), (4.2.5) and (4.2.6) are given respectively by

$$u^N(t_{k+1}) = e^{\Delta t A_N}u^N(t_k) + A_N^{-1}\left(e^{\Delta t A_N} - I\right) f_N(u^N(t_k)) + \epsilon e^{\Delta t A_N} g_N(u^N(t_k))\Delta\beta(t_k), \tag{4.2.7}$$

where Δt denotes the time step size and $\Delta\beta(t_k)$ is a Wiener increment given by (2.2.8).

$$u^N(t_{k+1}) = e^{\Delta t A_N}u^N(t_k) + A_N^{-1}\left(e^{\Delta t A_N} - I\right) f_N(u^N(t_k)) + \epsilon e^{\Delta t A_N} g_N(u^N(t_k))\Delta W^N(t_k), \tag{4.2.8}$$

where $\Delta W^N(t_k)$ is a Wiener increment given by (2.8.13).

$$u^N(t_{k+1}) = e^{\Delta t A_N}u^N(t_k) + A_N^{-1}\left(e^{\Delta t A_N} - I\right) f_N(u^N(t_k)) + \epsilon e^{\Delta t A_N}\Delta W^N(t_k). \tag{4.2.9}$$

Denoting the components of $u^N(t_k)$, $f_N(u^N(t_k))$, $g_N(u^N(t_k))$ and $W^N(t_k)$ by

$$u_n^N(t_k) = \Big(\psi_n, u^N(t_k)\Big), \quad f_N^n(u^N(t_k)) = \Big(\psi_n, f_N(u^N(t_k))\Big),$$

$$g_N^n(u^N(t_k)) = \Big(\psi_n, g_N(u^N(t_k))\Big) \quad W_n^N(t_k) = \Big(\psi_n, W^N(t_k)\Big), \quad |n| \leq N,$$

where ψ_n are the eigenfunctions of the linear operator A.

We assume that the linear operator A and the $\mathbb{Q}$-Wiener process have the same eigenfunctions.

The **SETD0** scheme for the SPDE (4.1.3) with infinite-dimensional additive noise denoted componentwise is given by:

$$u_n^N(t_{k+1}) = e^{\alpha_n \Delta t} u_n^N(t_k) + \frac{\left(e^{\alpha_n \Delta t} - 1\right)}{\alpha_n} f_N^n\Big(u^N(t_k)\Big) + \epsilon\sqrt{\lambda_n}\, e^{\alpha_n \Delta t} \Delta\beta_{k,n}, \quad \alpha_n \neq 0 \tag{4.2.10}$$

On the other hand, the **SETD0** for the SPDE (4.1.1) with one-dimensional multiplicative noise denoted componentwise is given by:

$$u_n^N(t_{k+1}) = e^{\alpha_n \Delta t} u_n^N(t_k) + \frac{\left(e^{\alpha_n \Delta t} - 1\right)}{\alpha_n} f_N^n\Big(u^N(t_k)\Big) + \epsilon e^{\alpha_n \Delta t} g_N^n(u^N(t_k))\Delta\beta_k \quad \alpha_n \neq 0. \tag{4.2.11}$$

where $u_n^N(t_k)$ denotes the approximation to the function u at discretization times t_k and $u_n^N(t_k)$ provides an update for $u_n^N(t_{k+1})$.

Also note that the mild solutions (4.1.6) and (4.1.4) represented component-wise are given by

$$u_n(t) = e^{\alpha_n t} u_n(0) + \int_0^t e^{(t-s)\alpha_n} f_N^n(u(s))ds + \epsilon \int_0^t e^{(t-s)\alpha_n} \sqrt{\lambda_n}\, d\beta_n(s), \quad \forall n \in \mathbb{Z} \tag{4.2.12}$$

and

$$u_n(t) = e^{\alpha_n t} u_n(0) + \int_0^t e^{(t-s)\alpha_n} f_N^n(u(s))ds + \epsilon \int_0^t e^{(t-s)\alpha_n} g_N^n(u(s))d\beta(s), \quad \forall n \in \mathbb{Z}. \tag{4.2.13}$$

Next, we iterate (4.2.10) and (4.2.11) to obtain equations which we can relate to (4.2.12) and (4.2.13) respectively; these are given as follows. For $j = 1, \cdots, M$, where M stands for the number of time discretization,

$$u_n^N(t_j) = e^{\alpha_n t_j} u_n^N(0) + \frac{\left(e^{\alpha_n \Delta t} - 1\right)}{\alpha_n} \sum_{k=0}^{j-1} e^{(t_{j-1} - t_k)\alpha_n} f_N^n\Big(u^N(t_k)\Big) + \epsilon\sqrt{\lambda_n} \sum_{k=0}^{j-1} e^{(t_j - t_k)\alpha_n} \Delta\beta_{k,n}, \tag{4.2.14}$$

and

$$u_n^N(t_j) = e^{\alpha_n t_j} u_n^N(0) \quad + \quad \frac{\left(e^{\alpha_n \Delta t} - 1\right)}{\alpha_n} \sum_{k=0}^{j-1} e^{(t_{j-1}-t_k)\alpha_n} f_N^n\Big(u^N(t_k)\Big)$$

$$+ \quad \epsilon \sum_{k=0}^{j-1} e^{(t_j - t_k)\alpha_n} g_N^n(u^N(t_k))\Delta\beta_k. \tag{4.2.15}$$

where $\Delta\beta_k$ and $\Delta\beta_{k,n}$ are independent and identically distributed normal random variables with mean 0 and variance Δt.

Equation (4.2.14) is the **SETD0** scheme for the time discretization of SPDEs forced with an infinite-dimensional additive noise and (4.2.15) is the **SETD0** scheme for the time discretization of SPDEs forced with one-dimensional multiplicative noise. In what follows, we prove convergence results for SPDEs driven by one-dimensional multiplicative noise and SPDEs driven by infinite-dimensional additive noise. We do not prove a convergence result for SPDEs driven by infinite-dimensional multiplicative noise, however we perform the numerical simulations for SPDEs with infinite-dimensional multiplicative noise in Chapters 5 and 6.

4.3 Error Analysis.

We estimate the error in the L^2 norm. Thus, we estimate

$$\big|\big|u(t_j) - u^N(t_j)\big|\big|^2 = \sum_{n\in\mathbb{Z}} |u_n(t_j) - u_n^N(t_j)|^2. \tag{4.3.1}$$

Note that in the expansion of the function $u(t)$, $n \in \mathbb{Z}$, however for practical purpose, we consider

$$u(t) = \sum_{n\in\mathbb{Z}} u_n(t)\psi_n = \sum_{|n|\leq N} u_n(t)\psi_n + \sum_{|n|>N} u_n(t)\psi_n, \tag{4.3.2}$$

and in our error analysis, we consider terms with Fourier modes $|n| \leq N$ and $|n| > N$. We refer to terms with $|n| > N$ as the tail terms.

We now state the conditions that the functions in the SPDEs (4.1.1) and (4.1.3) are required to satisfy for our convergence proofs.

Detailed assumptions on the existence and uniqueness of solution of the SPDEs are given in Chapter 2.

In the convergence analysis, we have two regularity parameters to consider r and γ; where r gives the regularity of the solution $u(t)$, see Lemma 2.5.7, and γ describes the spatial regularity of the noise, see Assumption 2.4.4.

We give the following additional assumptions on the functions f, g with the norms defined by the regularity r.

Assumption 4.3.1. *Assumptions on functions f and g;*
Consider $f : H \to H$ and $g : H \to L_2^0$, then the following conditions hold.

1. *Lipschitz condition: For $x, y \in H$, for some constant C and $r \geq 0$*

$$||f(x) - f(y)||^2 \leq C||x - y||^2, \quad ||f(x) - f(y)||_r^2 \leq C||x - y||_r^2. \tag{4.3.3}$$

$$||g(x) - g(y)||_{L_2^0}^2 \leq C||x - y||^2, \quad ||g(x) - g(y)||_{L_2^0}^2 \leq C||x - y||_r^2. \tag{4.3.4}$$

2. *Growth conditions: For $x \in H$, for some constant C_0 and $r \geq 0$*

$$||f(x)|| \leq C_0(1 + ||x||), \quad ||f(x)||_r \leq C_0(1 + ||x||_r). \tag{4.3.5}$$

$$||g(x)||_{L_2^0} \leq C_0(1 + ||x||), \quad ||g(x)||_{L_2^0} \leq C_0(1 + ||x||_r). \tag{4.3.6}$$

Note that $H^r \subseteq L^2$ is a property of the Sobolev space H^m, see (2.3.1), also note that if $x, y \in H^r$, then $x, y \in L^2$ by the definition of Sobolev space.

In what follows, we give preliminary results which will be used later in the convergence proofs.

Lemma 4.3.1. *Assume that the $u(s)$ is a mild solution for the SPDE (4.1.2), then for $0 \leq t' \leq T$,*

$$\int_0^{t'} \mathbb{E}\left[\left|\left|u(s) - u\left(\lfloor s \rfloor_{\Delta t}\right)\right|\right|^2\right] ds \leq C(\Delta t^{2\theta} + \epsilon^2 \Delta t), \tag{4.3.7}$$

where $\lfloor s \rfloor_{\Delta t} = \max_{k\in\mathbb{N}}\{t_k : t_k \leq s\}$ *and* $t_k = k\Delta t$.

Proof. We seek an estimate for the term $||u(s) - u\left(\lfloor s \rfloor_{\Delta t}\right)||^2$.

To do this, we write the solution $u(s)$ as a mild solution of the SPDE (4.1.2) as follows;

$$u(s) = e^{(s-\lfloor s \rfloor_{\Delta t})A}u(\lfloor s \rfloor_{\Delta t}) + \int_{\lfloor s \rfloor_{\Delta t}}^{s} e^{(s-\tau)A}f(u(\tau))d\tau + \epsilon\int_{\lfloor s \rfloor_{\Delta t}}^{s} e^{(s-\tau)A}g(u(\tau))dW(\tau). \tag{4.3.8}$$

This means that

$$\begin{aligned}\left|\left|u(s) - u\left(\lfloor s \rfloor_{\Delta t}\right)\right|\right|^2 &\leq \left|\left|\left(e^{(s-\lfloor s \rfloor_{\Delta t})A} - I\right)u(\lfloor s \rfloor_{\Delta t}) + \int_{\lfloor s \rfloor_{\Delta t}}^{s} e^{(s-\tau)A}f(u(\tau))d\tau\right.\right. \\ &+ \left.\left.\epsilon\int_{\lfloor s \rfloor_{\Delta t}}^{s} e^{(s-\tau)A}g(u(\tau))dW(\tau)\right|\right|^2. \end{aligned} \tag{4.3.9}$$

Next we apply the inequality $(a+b+c)^2 \leq 3(a^2+b^2+c^2)$ to get that

$$\begin{aligned}\int_0^{t'} \mathbb{E}\left[\left|\left|u(s) - u\left(\lfloor s \rfloor_{\Delta t}\right)\right|\right|^2\right]ds &\leq C\left(\int_0^{t'} \mathbb{E}\left[\left|\left|\left(e^{(s-\lfloor s \rfloor_{\Delta t})A} - I\right)u(\lfloor s \rfloor_{\Delta t})\right|\right|^2\right]ds\right. \\ &+ \left.\int_0^{t'} \mathbb{E}\left[\left|\left|\int_{\lfloor s \rfloor_{\Delta t}}^{s} e^{(s-\tau)A}f(u(\tau))d\tau\right|\right|^2\right]ds + \int_0^{t'} \mathbb{E}\left[\left|\left|\epsilon\int_{\lfloor s \rfloor_{\Delta t}}^{s} e^{(s-\tau)A}g(u(\tau))dW(\tau)\right|\right|^2\right]ds\right) \\ &\leq C(E_1 + E_2 + E_3). \end{aligned} \tag{4.3.10}$$

We now analyze each of the terms in (4.3.10). Firstly, we consider E_1.

Using Lemma 2.5.6 and Lemma 2.5.8, we get that

$$\begin{aligned} E_1 &= \int_0^{t'} \mathbb{E}\left[\left|\left|\left(e^{(s-\lfloor s \rfloor_{\Delta t})A} - I\right)u(\lfloor s \rfloor_{\Delta t})\right|\right|^2\right]ds \\ &\leq C\int_0^{t'} \left|\left|A^{-\theta}\left(I - e^{(s-\lfloor s \rfloor_{\Delta t})A}\right)\right|\right|^2 ds \underbrace{\sup_{0\leq\lfloor s \rfloor_{\Delta t}\leq t'} \mathbb{E}\left[\left|\left|A^{\theta}u(\lfloor s \rfloor_{\Delta t})\right|\right|^2\right]}_{<\infty} \\ &\leq C\int_0^{t'} \left(s - \lfloor s \rfloor_{\Delta t}\right)^{2\theta} ds \\ &\leq C\int_0^{t'} \Delta t^{2\theta} ds \leq C(T)\Delta t^{2\theta} \leq C\Delta t^{2\theta}. \end{aligned} \tag{4.3.11}$$

Next, using the Cauchy-Schwarz inequality (2.5.1), the fact that the semigroup is bounded, we get that

$$\begin{aligned} E_2 &\leq C\int_0^{t'} \mathbb{E}\left[\left|\left|\int_{\lfloor s\rfloor_{\Delta t}}^{s} e^{(s-\tau)A} f(u(\tau))d\tau\right|\right|^2\right] ds \\ &\leq C\int_0^{t'} (s-\lfloor s\rfloor_{\Delta t})\, ds \int_{\lfloor s\rfloor_{\Delta t}}^{s} \mathbb{E}\left[\left|\left|e^{(s-\tau)A} f(u(\tau))\right|\right|^2 d\tau\right] \\ &\leq C\int_0^{t'} (s-\lfloor s\rfloor_{\Delta t})\, ds \int_{\lfloor s\rfloor_{\Delta t}}^{s} \underbrace{\left|\left|e^{(s-\tau)A}\right|\right|^2}_{\leq C} d\tau \sup_{0\leq\tau\leq s} \mathbb{E}\left[||f(u(\tau))||^2\right]. \end{aligned}$$

Next, applying the growth condition in (4.3.5) and Lemma 2.5.9, we get that

$$\begin{aligned} E_2 &\leq C\int_0^{t'} (s-\lfloor s\rfloor_{\Delta t})\, ds \int_{\lfloor s\rfloor_{\Delta t}}^{s} d\tau \underbrace{\sup_{0\leq\tau\leq s} \mathbb{E}\left[1+||u(\tau)||^2\right]}_{<\infty} \\ &\leq C\int_0^{t'} (s-\lfloor s\rfloor_{\Delta t})\, ds \int_{\lfloor s\rfloor_{\Delta t}}^{s} d\tau \\ &\leq \int_0^{t'} \left(s-\lfloor s\rfloor_{\Delta t}\right)^2 ds \leq \int_0^{t'} \Delta t^2 ds \leq C(T)\Delta t^2 \leq C\Delta t^2. \end{aligned} \tag{4.3.12}$$

Applying the Itô-isometry of Lemma 2.5.5, the boundedness of exponential term, the growth condition in (4.3.6) and Lemma 2.5.9, we get that

$$\begin{aligned} E_3 &= \int_0^{t'} \mathbb{E}\left[\left|\left|\epsilon\int_{\lfloor s\rfloor_{\Delta t}}^{s} e^{(s-\tau)A} g(u(\tau))dW(\tau)\right|\right|^2\right] ds \\ &\leq C\epsilon^2 \int_0^{t'} ds \int_{\lfloor s\rfloor_{\Delta t}}^{s} \mathbb{E}\left[||g(u(\tau))||^2_{L_2^0}\, d\tau\right] \\ &\leq C(T)\epsilon^2 \int_{\lfloor s\rfloor_{\Delta t}}^{s} d\tau \underbrace{\sup_{\lfloor s\rfloor_{\Delta t}\leq\tau\leq t'} \mathbb{E}\left[1+||u(\tau)||^2\right]}_{<\infty} \\ &\leq C\epsilon^2 \int_{\lfloor s\rfloor_{\Delta t}}^{s} d\tau \leq C\epsilon^2(s-\lfloor s\rfloor_{\Delta t}) \leq C\epsilon^2\Delta t. \end{aligned} \tag{4.3.13}$$

Having worked out the estimates for the terms in (4.3.10). We get that

$$\int_0^{t'} \mathbb{E}\left[\left|\left|u(s) - u\left(\lfloor s \rfloor_{\Delta t}\right)\right|\right|^2\right] ds \leq C(\Delta t^{2\theta} + \Delta t^2 + \epsilon^2 \Delta t) \leq C(\Delta t^{2\theta} + \epsilon^2 \Delta t).$$

□

Lemma 4.3.2. *For $x, t > 0$, there exists a $C > 0$ such that*

$$\int_0^t e^{-(t-s)x} ds \;\; \leq \;\; Cx^{-1}. \tag{4.3.14}$$

Proof.

$$\int_0^t e^{-(t-s)x} ds = \frac{e^{-(t-s)x}}{x}\Bigg|_{s=0}^{s=t} = \frac{1 - e^{-tx}}{x} \leq Cx^{-1}. \tag{4.3.15}$$

□

4.4 Error estimate: multiplicative noise case.

In this section, our aim is to prove a convergence result for an SPDE with one-dimensional multiplicative noise given in Equation (4.1.1). The **SETD0** scheme given in equation (4.2.15) will be analyzed.

Theorem 4.4.1. *Assume that the initial data $u_0 \in \mathcal{D}(A) \cap H^2$, $\theta \in [0, 1/2)$ and $r \geq 0$. Consider that $\Delta t \to 0$ and $N \to \infty$ such that $\Delta t N^2 \leq \nu$, where ν is some positive parameter. Then for each $T > 0$, there exist a $C > 0$ such that*

$$\begin{aligned}\left(\mathbb{E}\left[\left|\left|u(t_j) - u^N(t_j)\right|\right|^2\right]\right)^{1/2} \;\; &\leq \;\; C\Big(N^{-2} + \Delta t^{\theta} + N^{-r}|\alpha_N^{-1}| \\ &+ \;\; \epsilon \Delta t^{\theta} + \epsilon^2 \Delta t^{1/2} + \epsilon N^{-r}|\alpha_N^{-1/2}|\Big).\end{aligned} \tag{4.4.1}$$

We prove this Theorem in §4.4.1.

In what follows, we examine two cases of the operator A, that is, $A = \Delta$ and $A = -(\Delta + 1)^2$.

Corollary 4.4.2. *Under the assumptions in Theorem 4.4.1 and for the linear operator $A = \Delta$ on $[0, 2\pi]$ with periodic boundary condition, with eigenvalue $\alpha_n = -n^2$, for each $n \in \mathbb{Z}$, we have that the strong convergence error estimate is given as*

$$\left(\mathbb{E}\left[\left|\left|u(t_j) - u^N(t_j)\right|\right|^2\right]\right)^{1/2} \leq C\Big(N^{-2} + \Delta t^{\theta} + N^{r-2} + \epsilon\Delta t^{\theta} + \epsilon^2\Delta t^{1/2} + \epsilon N^{r-1}\Big). \tag{4.4.2}$$

Proof of Corollary 4.4.2. Under the assumptions of Theorem 4.4.1, the root mean square error estimate for a linear operator with eigenvalues $\alpha_n = -n^2$ is obtained as follows.

The final estimate bounds in (4.4.53) is given as

$$\mathbb{E}\Big[\Big|\Big|u(t_j) - u^N(t_j)\Big|\Big|^2\Big] \leq C\Big(N^{2(-2)} + \Delta t^{2\theta} + \epsilon^4\Delta t^2 + N^{-2r}|\alpha_N^{-2}| + \epsilon^2\Delta t^{2\theta} + \epsilon^4\Delta t + \epsilon^2 N^{-2r}|\alpha_N^{-1}|\Big). \tag{4.4.3}$$

Substituting in the α_N's,

$$\mathbb{E}\Big[\Big|\Big|u(t_j) - u^N(t_j)\Big|\Big|^2\Big] \leq C\Big(N^{2(-2)} + \Delta t^{2\theta} + \epsilon^4\Delta t^2 + N^{2(r-2)} + \epsilon^2\Delta t^{2\theta} + \epsilon^4\Delta t + \epsilon^2 N^{-2r}N^{-2}\Big). \tag{4.4.4}$$

Simplify and write the equation in the root mean square sense as follows:

$$\left(\mathbb{E}\left[\left|\left|u(t_j) - u^N(t_j)\right|\right|^2\right]\right)^{1/2} \leq C\Big(N^{-2} + \Delta t^{\theta} + N^{r-2} + \epsilon\Delta t^{\theta} + \epsilon^2\Delta t^{1/2} + \epsilon N^{r-1}\Big). \tag{4.4.5}$$

Corollary 4.4.3. *Under the assumptions in Theorem 4.4.1 and for the linear operator $A = -(\Delta + 1)^2$ on $[0, 2\pi]$ with periodic boundary condition, with eigenvalue $\alpha_n = -n^4 + 2n^2 - 1$, for each $n \in \mathbb{Z}$, we have that the strong convergence error estimate is*

given as

$$\left(\mathbb{E}\left[\left|\left|u(t_j)-u^N(t_j)\right|\right|^2\right]\right)^{1/2} \leq C\Big(N^{-2}+\Delta t^{\theta}+\epsilon^2\Delta t+N^{r-4} + \epsilon\Delta t^{\theta}+\epsilon^2\Delta t^{1/2}+\epsilon N^{r-2}\Big). \tag{4.4.6}$$

Proof of Corollary 4.4.3. Under the assumptions of Theorem 4.4.1, the root mean square error estimate for a linear operator with eigenvalues $\alpha_n = -n^4+2n^2-1$ is obtained as follows.

The final estimate bounds in (4.4.53) is given as

$$\mathbb{E}\left[\left|\left|u(t_j)-u^N(t_j)\right|\right|^2\right] \leq C\Big(N^{2(-2)}+\Delta t^{2\theta}+\epsilon^4\Delta t^2+N^{-2r}|\alpha_N^{-2}| + \epsilon^2\Delta t^{2\theta}+\epsilon^4\Delta t+\epsilon^2N^{-2r}|\alpha_N^{-1}|\Big). \tag{4.4.7}$$

Note that $-n^4+2n^2-1<n^4$, therefore, $|\alpha_N|\leq N^4$. Substituting in the α_N, we get that

$$\mathbb{E}\left[\left|\left|u(t_j)-u^N(t_j)\right|\right|^2\right] \leq C\Big(N^{2(-2)}+\Delta t^{2\theta}+\epsilon^4\Delta t^2+N^{2(r-4)} + \epsilon^2\Delta t^{2\theta}+\epsilon^4\Delta t+\epsilon^2N^{-2r}N^{-4}\Big). \tag{4.4.8}$$

Simplify and write the equation in the root mean square sense as follows:

$$\left(\mathbb{E}\left[\left|\left|u(t_j)-u^N(t_j)\right|\right|^2\right]\right)^{1/2} \leq C\Big(N^{-2}+\Delta t^{\theta}+N^{r-4} + \epsilon\Delta t^{\theta}+\epsilon^2\Delta t^{1/2}+\epsilon N^{r-2}\Big). \tag{4.4.9}$$

Proof of Theorem 4.4.1.

The error estimate we wish to obtain bounds for is given as

$$\mathbb{E}\left[\left|\left|u(t_j)-u^N(t_j)\right|\right|^2\right] = \mathbb{E}\left[\sum_{n\in\mathbb{Z}}\left|u_n(t_j)-u_n^N(t_j)\right|^2\right]. \tag{4.4.10}$$

Note that symbol $|\cdot|$ in (4.4.10) stands for the absolute value sign.
Substituting equations (4.2.13) and (4.2.15) into (4.4.10), we get that

$$\mathbb{E}\left[\sum_{n\in\mathbb{Z}}\left|u_n(t_j)-u_n^N(t_j)\right|^2\right] \quad \leq$$

$$\mathbb{E}\left[\sum_{n\in\mathbb{Z}}\left|e^{\alpha_n tj}u_n(0)-e^{\alpha_n t_j}u_n^N(0) \quad +\right.\right.$$

$$\int_0^{t_j} e^{(t_j-s)\alpha_n}f_N^n(u(s))ds-\frac{\left(e^{\alpha_n\Delta t}-1\right)}{\alpha_n}\sum_{k=0}^{j-1}e^{(t_{j-1}-t_k)\alpha_n}f_N^n\Big(u^N(t_k)\Big) \quad +$$

$$\left.\left.\epsilon\int_0^{t_j} e^{(t_j-s)\alpha_n}g_N^n(u(s))d\beta(s)-\epsilon\sum_{k=0}^{j-1}e^{(t_j-t_k)\alpha_n}g_N^n(u^N(t_k))\Delta\beta_k\right|^2\right]. \tag{4.4.11}$$

Next, we use the following inequality

$$\Big|x+y+z\Big|^2\leq 3\Big(\big|x\big|^2+\big|y\big|^2+\big|z\big|^2\Big) \tag{4.4.12}$$

on the first term in the RHS of (4.4.11) in order to split this error term into three stand-alone parts, so that we can analyze term by term. This gives us the following estimate which we split into initial data term, non-linear term and noise term as follows:

$$\mathbb{E}\left[\sum_{n\in\mathbb{Z}}\left|u_n(t_j)-u_n^N(t_j)\right|^2\right]\leq 3\Big(\mathbf{ID}+\mathbf{NLP}+\mathbf{NoiseP}\Big) \tag{4.4.13}$$

where

$$\mathbf{ID}=\mathbb{E}\left[\sum_{n\in\mathbb{Z}}\left|e^{\alpha_n tj}u_n(0)-e^{\alpha_n t_j}u_n^N(0)\right|^2\right], \tag{4.4.14}$$

$$\mathbf{NLP}=\mathbb{E}\left[\sum_{n\in\mathbb{Z}}\left|\int_0^{t_j} e^{(t_j-s)\alpha_n}f_N^n(u(s))ds-\frac{\left(e^{\alpha_n\Delta t}-1\right)}{\alpha_n}\sum_{k=0}^{j-1}e^{(t_{j-1}-t_k)\alpha_n}f_N^n\Big(u^N(t_k)\Big)\right|^2\right], \tag{4.4.15}$$

$$\mathbf{NoiseP} = \mathbb{E}\left[\sum_{n\in\mathbb{Z}}\left|\int_0^{t_j} e^{(t_j-s)\alpha_n} g_N^n(u(s))d\beta(s) - \epsilon\sum_{k=0}^{j-1} e^{(t_j-t_k)\alpha_n} g_N^n(u^N(t_k))\Delta\beta_k\right|^2\right]. \tag{4.4.16}$$

We remark that in the process of bounding terms, the constant C changes from line to line, in some instances C may depend on the final time T, however it is always independent of Δt and N.

Initial data terms:

$$\mathbf{ID} \;=\; \mathbb{E}\left[\sum_{n\in\mathbb{Z}}\left|e^{\alpha_n t_j}u_n(0) - e^{\alpha_n t_j}u_n^N(0)\right|^2\right]. \tag{4.4.17}$$

We assumed that the initial data $u_n^N(0)$ and $u_n(0)$ coincide, therefore modes that are less that N in (4.4.17) cancel out and we are left with modes greater than N; thus, we are left to analyze the term with $|n| > N$, this term we have denoted as $\mathbf{ID_{TAIL}}$. The analysis is as follows:

By the boundedness of the exponential term and using the fact that $n^4 < 1+2n^2+n^4$, also using the definition of the H^r norm, we get that

$$\mathbf{ID_{TAIL}} = \mathbb{E}\left[\sup_{0\le t_j\le t'}\sum_{|n|>N}\left|e^{\alpha_n t_j}u_n(0)\right|^2\right] \le C\sum_{|n|>N}\left|u_n(0)\right|^2 \le \sum_{|n|>N} n^{-4}n^4\left|u_n(0)\right|^2 \le$$

$$CN^{-4}\left(\sum_{|n|>N} n^4\left|u_n(0)\right|^2\right) \le CN^{-4}\sum_{|n|>N}\left(1+2n^2+n^4\right)\left|u_n(0)\right|^2 \le$$

$$CN^{-4}\sum_{|n|>N}(1+n^2)^2\left|u_n(0)\right|^2 \le CN^{-4}\left|\left|u(0)\right|\right|_2^2 \le CN^{-4}.$$

Finally, the tail term of the initial data is bounded by CN^{-4}. Hence,

$$\mathbf{ID} \le CN^{-4}. \tag{4.4.18}$$

Nonlinear terms:

The **NLP** in (4.4.15) is given as

$$\mathbf{NLP} = \mathbb{E}\left[\sum_{n\in\mathbb{Z}}\left|\int_0^{t_j} e^{(t_j-s)\alpha_n} f_N^n(u(s))ds - \frac{\left(e^{\alpha_n\Delta t}-1\right)}{\alpha_n}\sum_{k=0}^{j-1} e^{(t_{j-1}-t_k)\alpha_n} f_N^n\Big(u^N(t_k)\Big)\right|^2\right]. \tag{4.4.19}$$

To obtain error estimate for this **NLP** term, we find it convenient to consider both the exact solution and the numerical solution in the same framework. That is to say, we will convert the time discrete scheme in the second term in the RHS of (4.4.19) into a time continuous version. Therefore,

$$\mathbf{NLP} = \mathbb{E}\left[\sum_{n\in\mathbb{Z}}\left|\int_0^{t_j} e^{(t_j-s)\alpha_n} f_N^n(u(s))ds - \int_0^{t_j} e^{(t_j-\lfloor s\rfloor_{\Delta t})\alpha_n} f_N^n\left(u^N(\lfloor s\rfloor_{\Delta t})\right)ds\right|^2\right] =$$

$$\mathbb{E}\left[\sum_{n\in\mathbb{Z}}\left|\int_0^{t_j}\left(e^{(t_j-s)\alpha_n} f_N^n(u(s)) - e^{(t_j-\lfloor s\rfloor_{\Delta t})\alpha_n} f_N^n\left(u^N(\lfloor s\rfloor_{\Delta t})\right)\right)ds\right|^2\right]. \tag{4.4.20}$$

Next, we use the fact that

$$e^{(t_j-s)\alpha_n} = e^{\left(t_j-\lfloor s\rfloor_{\Delta t}+\lfloor s\rfloor_{\Delta t}-s\right)\alpha_n} = e^{\left(t_j-\lfloor s\rfloor_{\Delta t}\right)\alpha_n} e^{\left(\lfloor s\rfloor_{\Delta t}-s\right)\alpha_n}. \tag{4.4.21}$$

We get that (4.4.20) becomes

$$\mathbf{NLP} = \mathbb{E}\left[\sum_{n\in\mathbb{Z}}\left|\int_0^{t_j} e^{(t_j-\lfloor s\rfloor_{\Delta t})\alpha_n}\left\{e^{(\lfloor s\rfloor_{\Delta t}-s)\alpha_n} f_N^n(u(s)) - f_N^n\left(u^N(\lfloor s\rfloor_{\Delta t})\right)\right\}ds\right|^2\right]. \tag{4.4.22}$$

Next, we split into three parts the term in the curly bracket in (4.4.22) by adding in and subtracting out the following terms: $f_N^n(u(s))$ and $f_N^n\left(u\left(\lfloor s\rfloor_{\Delta t}\right)\right)$. Following this approach, (4.4.22) becomes

$$\begin{aligned}\mathbf{NLP} \;\leq\; \mathbb{E}\Bigg[\sum_{n\in\mathbb{Z}}\Bigg|\int_0^{t_j} e^{(t_j-\lfloor s\rfloor_{\Delta t})\alpha_n}\Big(& f_N^n(u(s)) - f_N^n\left(u\left(\lfloor s\rfloor_{\Delta t}\right)\right) + \\ & f_N^n\left(u\left(\lfloor s\rfloor_{\Delta t}\right)\right) - f_N^n\left(u^N\left(\lfloor s\rfloor_{\Delta t}\right)\right) + \left(e^{(\lfloor s\rfloor_{\Delta t}-s)\alpha_n}-1\right) f_N^n(u(s))\Big)ds\Bigg|^2\Bigg].\end{aligned} \tag{4.4.23}$$

Applying the inequality (4.4.12) and the expression in (4.3.2) to (4.4.23), we get that $\mathbf{NLP} \leq C\Big(\mathbf{NLP}_1 + \mathbf{NLP}_2 + \mathbf{NLP}_3 + \mathbf{NLP}_{Tail}\Big)$, where

$$\mathbf{NLP}_1 = \mathbb{E}\left[\sum_{|n|\leq N}\left|\int_0^{t_j} e^{(t_j-\lfloor s\rfloor_{\Delta t})\alpha_n}\Big(f_N^n(u(s)) - f_N^n\left(u\left(\lfloor s\rfloor_{\Delta t}\right)\right)\Big)ds\right|^2\right], \tag{4.4.24}$$

$$\mathbf{NLP}_2 = \mathbb{E}\left[\sum_{|n|\leq N}\left|\int_0^{t_j} e^{(t_j-\lfloor s\rfloor_{\Delta t})\alpha_n}\Big(f_N^n\left(u\left(\lfloor s\rfloor_{\Delta t}\right)\right) - f_N^n\left(u^N\left(\lfloor s\rfloor_{\Delta t}\right)\right)\Big)ds\right|^2\right], \tag{4.4.25}$$

$$\mathbf{NLP}_3 = \mathbb{E}\left[\sum_{|n|\leq N}\left|\int_0^{t_j} e^{(t_j-\lfloor s\rfloor_{\Delta t})\alpha_n}\left(e^{(\lfloor s\rfloor_{\Delta t}-s)\alpha_n}-1\right)f_N^n(u(s))ds\right|^2\right], \tag{4.4.26}$$

and

$$\mathbf{NLP}_{Tail} = \mathbb{E}\left[\sum_{|n|>N}\left|\int_0^{t_j} e^{(t_j-s)\alpha_n} f_N^n(u(s))ds\right|^2\right]. \tag{4.4.27}$$

We now wish to obtain estimates for (4.4.24), (4.4.25), (4.4.26) and (4.4.27) .

We start by working out $\mathbf{NLP}_1$.

Using the projection operator (2.8.9), the Jensen's inequality (Lemma 2.5.4), the boundedness of the exponential term, and the Lipschitz condition in (4.3.3), the $\mathbf{NLP}_1$ (4.4.24) becomes

$$\begin{aligned}
\mathbf{NLP}_1 &\leq \mathbb{E}\left[\sum_{|n|\leq N}\left|\int_0^{t_j} e^{(t_j-\lfloor s\rfloor_{\Delta t})\alpha_n}\Big(f_N^n(u(s)) - f_N^n\left(u\left(\lfloor s\rfloor_{\Delta t}\right)\right)\Big)ds\right|^2\right] \\
&\leq C\mathbb{E}\left[\int_0^{t_j}\left|\left|P_N e^{(t_j-\lfloor s\rfloor_{\Delta t})A}\Big(f(u(s)) - f\left(u\left(\lfloor s\rfloor_{\Delta t}\right)\right)\Big)\right|\right|^2 ds\right] \\
&\leq C\int_0^{t_j}\mathbb{E}\left[\left|\left|u(s) - u\left(\lfloor s\rfloor_{\Delta t}\right)\right|\right|^2\right] ds \\
&\leq C\int_0^{t'}\mathbb{E}\left[\left|\left|u(s) - u\left(\lfloor s\rfloor_{\Delta t}\right)\right|\right|^2\right] ds.
\end{aligned} \tag{4.4.28}$$

Next using Lemma 4.3.1 we get that $\mathbf{NLP}_1 \leq C\Delta t^{2\theta} + C\epsilon^2\Delta t$.

Next, we work out the $\mathbf{NLP}_2$.

Applying the projection operator (2.8.9), the Jensen's inequality and the Lipschitz condition (4.3.3), in addition to the boundedness of the exponential term, the $\mathbf{NLP}_2$ (4.4.25) becomes

$$\begin{aligned}
\mathbf{NLP}_2 &\leq \mathbb{E}\left[\sum_{|n|\leq N}\left|\int_0^{t_j} e^{(t_j-\lfloor s\rfloor_{\Delta t})\alpha_n}\Big(f_N^n\left(u\left(\lfloor s\rfloor_{\Delta t}\right)\right)-f_N^n\left(u^N\left(\lfloor s\rfloor_{\Delta t}\right)\right)\Big)ds\right|^2\right] \\
&\leq \mathbb{E}\left[\left|\left|P_N\int_0^{t_j} e^{(t_j-\lfloor s\rfloor_{\Delta t})A}\Big(f\left(u\left(\lfloor s\rfloor_{\Delta t}\right)\right)-f\left(u^N\left(\lfloor s\rfloor_{\Delta t}\right)\right)\Big)ds\right|\right|^2\right] \\
&\leq C\mathbb{E}\left[\int_0^{t_j}\left|\left|u\left(\lfloor s\rfloor_{\Delta t}\right)-u^N\left(\lfloor s\rfloor_{\Delta t}\right)\right|\right|^2 ds\right] \\
&\leq C\int_0^{t'}\mathbb{E}\left[\left|\left|u(s)-u^N(s)\right|\right|^2 ds\right]. \qquad (4.4.29)
\end{aligned}$$

Note that we will incorporate this term into the error estimate in the statement of the theorem by applying the Gronwall's Lemma, see Lemma 2.5.2.

Next, we work out the $\mathbf{NLP}_3$.

Using the projection operator (2.8.9), Jensen's inequality (Lemma 2.5.4), in addition to using the fact that A and e^{tA} commute, we get that the $\mathbf{NLP}_3$ (4.4.26) becomes

$$\begin{aligned}
\mathbf{NLP}_3 &\leq \mathbb{E}\left[\sum_{|n|\leq N}\left|\int_0^{t_j} e^{(t_j-\lfloor s\rfloor_{\Delta t})\alpha_n}\left(e^{(\lfloor s\rfloor_{\Delta t}-s)\alpha_n}-1\right)f_N^n(u(s))ds\right|^2\right] \\
&\leq \mathbb{E}\left[\left|\left|P_N e^{(t_j-\lfloor s\rfloor_{\Delta t})A}\Big(e^{(\lfloor s\rfloor_{\Delta t}-s)A}-I\Big)f(u(s))ds\right|\right|^2\right] \\
&\leq \mathbb{E}\left[\int_0^{t_j}\left|\left|A^\theta e^{(t_j-\lfloor s\rfloor_{\Delta t})A}A^{-\theta}\Big(e^{(\lfloor s\rfloor_{\Delta t}-s)A}-I\Big)f(u(s))\right|\right|^2 ds\right] \\
&\leq C\int_0^{t'}\left|\left|A^\theta e^{(t'-\lfloor s\rfloor_{\Delta t})A}\right|\right|^2\left|\left|A^{-\theta}\Big(e^{(\lfloor s\rfloor_{\Delta t}-s)A}-I\Big)\right|\right|^2 ds\sup_{0\leq s\leq t'}\mathbb{E}\left[\left|\left|f(u(s))\right|\right|^2\right] \\
&\leq C\int_0^{t'}\left|\left|A^\theta e^{(t'-\lfloor s\rfloor_{\Delta t})A}\right|\right|^2\left|\left|A^{-\theta}\Big(I-e^{(\lfloor s\rfloor_{\Delta t}-s)A}\Big)\right|\right|^2 ds\sup_{0\leq s\leq t'}\mathbb{E}\left[\left|\left|f(u(s))\right|\right|^2\right]. \qquad (4.4.30)
\end{aligned}$$

Next, according to Lemma 2.5.6, the growth condition on function f in (4.3.5) and also the result in Lemma 2.5.9, the $\mathbf{NLP}_3$ (4.4.30) reduces to

$$\begin{aligned}
\mathbf{NLP}_3 &\leq C\int_0^{t'} (t' - \lfloor s \rfloor_{\Delta t})^{-2\theta}\, \Delta t^{2\theta} ds \sup_{0\leq s\leq t'} \mathbb{E}\left[\left|\left| f(u(s)) \right|\right|^2\right] \\
&\leq C\Delta t^{2\theta}\int_0^{t'} (t' - \lfloor s \rfloor_{\Delta t})^{-2\theta}\, ds \underbrace{\sup_{0\leq s\leq t'} \mathbb{E}\left[\left(1 + ||u(s)||^2\right)\right]}_{<\infty} \\
&\leq C\Delta t^{2\theta}\underbrace{\int_0^{t'} (t' - \lfloor s \rfloor_{\Delta t})^{-2\theta}\, ds}_{\leq C} \\
&\leq C\Delta t^{2\theta}. \qquad (4.4.31)
\end{aligned}$$

So far, in the estimation of the non-linear terms, we have been estimating terms with modes $|n| < N$, we now wish to find estimates for the tail terms of the non-linear term, that is, error with modes $|n| > N$.

$$\mathbf{NLP}_{Tail} \leq \mathbb{E}\left[\sum_{|n|>N} \left| \int_0^{t_j} e^{(t_j - s)\alpha_n} f_N^n(u(s)) ds \right|^2\right]. \qquad (4.4.32)$$

Applying the definition of H^r norm (2.3.5), the growth condition (4.3.5), Lemma 2.5.7 and Lemma 4.3.2;

$$\begin{aligned}
\mathbf{NLP}_{Tail} &\leq \mathbb{E}\left[\sum_{|n|>N} (1+n^2)^{-r}(1+n^2)^r \left| \int_0^{t_j} e^{(t_j - s)\alpha_n} f_N^n(u(s)) ds \right|^2\right] \\
&\leq C(1+N^2)^{-r}\left(\int_0^{t'} e^{(t'-s)\alpha_N} ds\right)^2 \mathbb{E}\left[\sup_{0\leq s\leq t'} \sum_{|n|>N} (1+n^2)^r \left| f_N^n(u(s)) \right|^2\right] \\
&\leq C(1+N^2)^{-r}\left(|\alpha_N^{-1}|\right)^2 \mathbb{E}\left[\sup_{0\leq s\leq t'} \left|\left| f(u(s)) \right|\right|_r^2\right] \\
&\leq C(1+N^2)^{-r}|\alpha_N^{-2}| \underbrace{\mathbb{E}\sup_{0\leq s\leq t'} \left(1 + ||u(s)||_r^2\right)}_{<\infty} \\
&\leq CN^{-2r}|\alpha_N^{-2}|. \qquad (4.4.33)
\end{aligned}$$

Putting all the estimates bounds for the nonlinear part together, we get that

$$\mathbf{NLP} \;\leq\; C\Big(\mathbf{NLP}_1 + \mathbf{NLP}_2 + \mathbf{NLP}_3 + \mathbf{NLP}_{Tail}\Big)$$

$$\leq C\Big(\Delta t^{2\theta} + \epsilon^2\Delta t + \int_0^{t'} \mathbb{E}\left[\big|\big|u(s) - u^N(s)\big|\big|^2\right] ds + \Delta t^{2\theta} + N^{-2r}|\alpha_N^{-2}|\Big)$$

$$\leq C\Big(\Delta t^{2\theta} + \epsilon^2\Delta t + +N^{2(m-r)}|\alpha_N^{-2}|\Big) + C\int_0^{t'} \mathbb{E}\left[\big|\big|u(s) - u^N(s)\big|\big|^2\right] ds. \tag{4.4.34}$$

Noise terms:

The noise term is given as

$$\mathbf{NoiseP} = \mathbb{E}\left[\sum_{n\in\mathbb{Z}}\left|\epsilon\int_0^{t_j} e^{(t_j-s)\alpha_n} g_N^n(u(s))d\beta(s) - \epsilon\sum_{k=0}^{j-1} e^{(t_j-t_k)\alpha_n} g_N^n\left(u^N(t_k)\right)\Delta\beta_k\right|^2\right]. \tag{4.4.35}$$

In order to analyse (4.4.35), we change the second term, that is, the discrete term in (4.4.35) into a time continuous version for convenience of analysis as follows:

$$\mathbf{NoiseP} \;=\; \epsilon^2\mathbb{E}\left[\sum_{n\in\mathbb{Z}}\left|\int_0^{t_j} e^{(t_j-s)\alpha_n} g_N^n(u(s))d\beta(s) - \right.\right.$$

$$\left.\left.\int_0^{t_j} e^{(t_j-\lfloor s\rfloor_{\Delta t})\alpha_n} g_N^n\left(u^N(\lfloor s\rfloor_{\Delta t})\right)d\beta(s)\right|^2\right]. \tag{4.4.36}$$

Following the same approach as in the nonlinear term estimate, we use the identity in (4.4.21), and get that

$$\mathbf{NoiseP} \leq \epsilon^2\mathbb{E}\left[\sum_{n\in\mathbb{Z}}\left|\int_0^{t_j} e^{(t_j-\lfloor s\rfloor_{\Delta t})\alpha_n}\Big\{e^{(\lfloor s\rfloor_{\Delta t}-s)\alpha_n} g_N^n(u(s)) - g_N^n\left(u^N(\lfloor s\rfloor_{\Delta t})\right)\Big\}d\beta(s)\right|^2\right]. \tag{4.4.37}$$

Next, the quantity in the curly bracket of (4.4.37) is split up into 3 parts by adding in and subtracting out the following terms: $g_N^n(u(s))$ and $g_N^n\left(u\left(\lfloor s\rfloor_{\Delta t}\right)\right)$; so that

$$\begin{aligned}\mathbf{NoiseP} \;\leq\; \epsilon^2\mathbb{E}\Bigg[\int_0^{t_j}\sum_{n\in\mathbb{Z}}\Bigg|e^{(t_j-\lfloor s\rfloor_{\Delta t})\alpha_n}\Bigg\{g_N^n(u(s))-g_N^n\left(u\left(\lfloor s\rfloor_{\Delta t}\right)\right)+\\ g_N^n\left(u\left(\lfloor s\rfloor_{\Delta t}\right)\right)-g_N^n\left(u^N\left(\lfloor s\rfloor_{\Delta t}\right)\right)+\left(e^{(\lfloor s\rfloor_{\Delta t}-s)\alpha_n}-1\right)g_N^n(u(s))\Bigg\}d\beta(s)\Bigg|^2\Bigg].\end{aligned} \tag{4.4.38}$$

By the inequality (4.4.12) and (4.3.2),

$$\mathbf{NoiseP}\leq\epsilon^2C\{\mathbf{NoiseP}_1+\mathbf{NoiseP}_2+\mathbf{NoiseP}_3+\mathbf{NoiseP}_{Tail}\}, \tag{4.4.39}$$

where

$$\mathbf{NoiseP}_1=\mathbb{E}\left[\int_0^{t_j}\sum_{|n|\leq N}\left|e^{(t_j-\lfloor s\rfloor_{\Delta t})\alpha_n}\left(g_N^n(u(s))-g_N^n\left(u\left(\lfloor s\rfloor_{\Delta t}\right)\right)\right)d\beta(s)\right|^2\right], \tag{4.4.40}$$

$$\mathbf{NoiseP}_2=\mathbb{E}\left[\int_0^{t_j}\sum_{|n|\leq N}\left|e^{(t_j-\lfloor s\rfloor_{\Delta t})\alpha_n}\left(g_N^n\left(u\left(\lfloor s\rfloor_{\Delta t}\right)\right)-g_N^n\left(u^N\left(\lfloor s\rfloor_{\Delta t}\right)\right)\right)d\beta(s)\right|^2\right], \tag{4.4.41}$$

$$\mathbf{NoiseP}_3=\mathbb{E}\left[\int_0^{t_j}\sum_{|n|\leq N}\left|e^{(t_j-\lfloor s\rfloor_{\Delta t})\alpha_n}\left(\left(e^{(\lfloor s\rfloor_{\Delta t}-s)\alpha_n}-1\right)g_N^n(u(s))\right)d\beta(s)\right|^2\right], \tag{4.4.42}$$

and

$$\mathbf{NoiseP}_{Tail}=\mathbb{E}\left[\int_0^{t_j}\sum_{|n|>N}\left|\left(e^{(t_j-s)\alpha_n}g_N^n(u(s))\right)d\beta(s)\right|^2\right]. \tag{4.4.43}$$

We now analyze each of these noise terms. We start by working out $\mathbf{NoiseP}_1$. Applying the projection operator (2.8.9) and the Itô-isometry (2.5.6) to (4.4.40), we obtain that

$$\begin{aligned}\mathbf{NoiseP}_1 \;&\leq\; \mathbb{E}\left[\int_0^{t_j}\left|\left|P_Ne^{(t_j-\lfloor s\rfloor_{\Delta t})A}\left(g(u(s))-g\left(u\left(\lfloor s\rfloor_{\Delta t}\right)\right)\right)d\beta(s)\right|\right|^2\right]\\ &\leq\; \mathbb{E}\left[\int_0^{t_j}\left|\left|e^{(t_j-\lfloor s\rfloor_{\Delta t})A}\left(g(u(s))-g\left(u\left(\lfloor s\rfloor_{\Delta t}\right)\right)\right)\right|\right|_{L_2^0}^2ds\right].\end{aligned}$$

Since the exponential term is bounded, and also by using the Lipschitz condition (4.3.4), we get that

$$\begin{aligned}\mathbf{NoiseP}_1 &\leq \mathbb{E}\left[\int_0^{t_j}\left|\left|u(s)-u\left(\lfloor s\rfloor_{\Delta t}\right)\right|\right|^2 ds\right]\\ &\leq \int_0^{t'}\mathbb{E}\left[\left|\left|u(s)-u\left(\lfloor s\rfloor_{\Delta t}\right)\right|\right|^2\right] ds.\end{aligned}$$

Applying Lemma 4.3.1, we get that

$$\mathbf{NoiseP}_1 \leq C(\Delta t^{2\theta}+\epsilon^2\Delta t). \tag{4.4.44}$$

Next, we work out $\mathbf{NoiseP}_2$.

Applying the projection operator (2.8.9), the Itô-isometry (2.5.6), the boundedness of the exponential term and the Lipschitz continuity of the function g (4.3.4), we get that the $\mathbf{NoiseP}_2$ in (4.4.41) is

$$\begin{aligned}\mathbf{NoiseP}_2 &\leq C\mathbb{E}\left[\int_0^{t_j}\left|\left|P_N e^{(t_j-\lfloor s\rfloor_{\Delta t})A}\Big(g\left(u\left(\lfloor s\rfloor_{\Delta t}\right)\right)-g\left(u^N\left(\lfloor s\rfloor_{\Delta t}\right)\right)\Big)d\beta(s)\right|\right|^2\right]\\ &\leq C\mathbb{E}\left[\int_0^{t_j}\left|\left|e^{(t_j-\lfloor s\rfloor_{\Delta t})A}\Big(g\left(u\left(\lfloor s\rfloor_{\Delta t}\right)\right)-g\left(u^N\left(\lfloor s\rfloor_{\Delta t}\right)\right)\Big)\right|\right|_{L_2^0}^2 ds\right]\\ &\leq C\int_0^{t'}\mathbb{E}\left[\left|\left|u\left(s\right)-u^N\left(s\right)\right|\right|^2\right] ds.\end{aligned} \tag{4.4.45}$$

Next, we work out $\mathbf{NoiseP}_3$.

Using the projection operator (2.8.9), the Itô-isometry (2.5.6) and Lemma 2.5.6, the $\mathbf{NoiseP}_3$ (4.4.42) becomes

$$\begin{aligned}\mathbf{NoiseP}_3 &\leq \mathbb{E}\left[\int_0^{t_j}\left|\left|P_N e^{(t_j-\lfloor s\rfloor_{\Delta t})A}\left(e^{(\lfloor s\rfloor_{\Delta t}-s)A}-I\right)g(u(s))d\beta(s)\right|\right|^2\right]\\ &\leq \mathbb{E}\left[\int_0^{t_j}\left|\left|e^{(t_j-\lfloor s\rfloor_{\Delta t})A}\left(e^{(\lfloor s\rfloor_{\Delta t}-s)A}-I\right)g(u(s))\right|\right|_{L_2^0}^2 ds\right]\\ &\leq \mathbb{E}\left[\int_0^{t_j}\left|\left|A^\theta e^{(t_j-\lfloor s\rfloor_{\Delta t})A}A^{-\theta}\left(e^{(\lfloor s\rfloor_{\Delta t}-s)A}-I\right)g(u(s))\right|\right|_{L_2^0}^2 ds\right].\end{aligned} \tag{4.4.46}$$

Using Lemma 2.5.6 and Lemma 2.5.9, (4.4.46) reduces to

$$\begin{aligned}
\mathbf{NoiseP}_3 &\leq C \underbrace{\left(\int_0^{t'} (t' - \lfloor s \rfloor_{\Delta t})^{-2\theta} \, ds \right)}_{\leq C} \Delta t^{2\theta} \sup_{0 \leq s \leq t'} \mathbb{E}\Big[\Big|\Big| g(u(s)) \Big|\Big|_{L_2^0}^2 \Big] \\
&\leq C\Delta t^{2\theta} \underbrace{\sup_{0 \leq s \leq t'} \mathbb{E}\Big[\big(1 + ||u(s)||^2\big) \Big]}_{<\infty} \\
&\leq C\Delta t^{2\theta}. \qquad (4.4.47)
\end{aligned}$$

So far, in the estimation of the noise terms, we have been estimating terms with modes $|n| \leq N$, we now wish to find estimates for the tail terms of the noise term, that is, error with modes $|n| > N$.

Applying the Itô-isometry (2.5.6) to (4.4.49), we get

$$\mathbf{NoiseP}_{Tail} \leq \mathbb{E}\left[\int_0^{t_j} \sum_{|n|>N} \Big| e^{(t_j - s)\alpha_n} g_N^n(u(s)) \Big|^2 ds \right]. \qquad (4.4.48)$$

Applying the definition of H^r norm, the assumption in (4.3.4), Lemma 2.5.7 and Lemma 4.3.2.

$$\begin{aligned}
\mathbf{NoiseP}_{Tail} &\leq \mathbb{E}\left[\int_0^{t_j} \sum_{|n|>N} (1+n^2)^{-r} (1+n^2)^r \Big| e^{(t_j - s)\alpha_N} g_N^n(u(s)) \Big|^2 ds \right] \\
&\leq C\mathbb{E}\left[\int_0^{t'} (1+N^2)^{-r} e^{2(t'-s)\alpha_N} \sum_{|n|>N} (1+n^2)^r \Big| g_N^n(u(s)) \Big|^2 ds \right] \\
&\leq C\mathbb{E}\left[\int_0^{t'} (1+N^2)^{-r} e^{2(t'-s)\alpha_N} \Big|\Big| g(u(s)) \Big|\Big|_r^2 ds \right] \\
&\leq CN^{-2r} \int_0^{t'} e^{2(t'-s)\alpha_N} ds \mathbb{E}\left[\sup_{0 \leq s \leq t'} \Big|\Big| g(u(s)) \Big|\Big|_r^2 \right]
\end{aligned}$$

$$\leq CN^{-2r}\int_0^{t'} e^{2(t'-s)\alpha_N} ds \underbrace{\mathbb{E}\sup_{0\leq s\leq t'}\Big[1+||u(s)||_r^2\Big]}_{<\infty}$$

$$\leq CN^{-2r}\int_0^{t'} e^{2(t'-s)\alpha_N} ds$$

$$\leq CN^{-2r}|\alpha_N^{-1}|. \tag{4.4.49}$$

We now collect all the estimates bounds for the **NoiseP** together as follows:

$$\mathbf{NoiseP} \leq \epsilon^2 C\{\mathbf{NoiseP}_1 + \mathbf{NoiseP}_2 + \mathbf{NoiseP}_3 + \mathbf{NoiseP}_{Tail}\} \tag{4.4.50}$$

$$\leq \epsilon^2 C\left(\Delta t^{2\theta} + \epsilon^2\Delta t + \int_0^{t'}\mathbb{E}\Big[\Big|\Big|u\left(s\right)-u^N\left(s\right)\Big|\Big|^2\Big]ds + \Delta t^{2\theta} + CN^{2(m-r)}|\alpha_N^{-1}|\right)$$

$$\leq C\Big(\epsilon^2\Delta t^{2\theta} + \epsilon^4\Delta t + \epsilon^2 N^{-2r}|\alpha_N^{-1}|\Big) + C\int_0^{t'}\mathbb{E}\Big[\Big|\Big|u\left(s\right)-u^N\left(s\right)\Big|\Big|^2\Big]ds. \tag{4.4.51}$$

Finally, combining the estimates (4.4.18), (4.4.34) and (4.4.51), we achieve the following inequality

$$\begin{aligned}E\Big[\Big|\Big|u(t_j)-u^N(t_j)\Big|\Big|^2\Big] \leq\ & C\Big(\Delta t^{2\theta} + \epsilon^4\Delta t^2 + N^{-2r}|\alpha_N^{-2}| + N^{-4}\\ &+ \epsilon^2\Delta t^{2\theta} + \epsilon^4\Delta t + \epsilon^2 N^{-2r}|\alpha_N^{-1}|\\ &+ \int_0^{t'}\mathbb{E}\Big[\Big|\Big|u\left(s\right)-u^N\left(s\right)\Big|\Big|^2\Big]ds\Big).\end{aligned} \tag{4.4.52}$$

and then by Gronwall's inequality in Lemma 2.5.2, we get that

$$\begin{aligned}E\Big[\Big|\Big|u(s)-u^N(s)\Big|\Big|^2\Big] \leq\ & C\Big(\Delta t^{2\theta} + \epsilon^4\Delta t^2 + N^{-2r}|\alpha_N^{-2}| + N^{-4}\\ &+ \epsilon^2\Delta t^{2\theta} + \epsilon^4\Delta t + \epsilon^2 N^{-2r}|\alpha_N^{-1}|\Big).\end{aligned} \tag{4.4.53}$$

Equation (4.4.53) completes the proof of Theorem 4.4.1.

4.5 Error estimate: additive noise case.

In this section, we examine strong convergence of numerical method **SETD0** for SPDE (4.1.3) driven by an infinite-dimensional additive noise. The error estimate we wish to obtain bounds for is given as

$$\mathbb{E}\Big[\Big|\Big|u(t_j) - u^N(t_j)\Big|\Big|^2\Big] = \mathbb{E}\Big[\sum_{n\in\mathbb{Z}}\Big|u_n(t_j) - u_n^N(t_j)\Big|^2\Big]. \tag{4.5.1}$$

Thus upon substituting equations (4.2.12) and (4.2.14) into (4.5.1),

$$\begin{aligned}\mathbb{E}\Big[\sum_{n\in\mathbb{Z}}\Big|u_n(t_j) - u_n^N(t_j)\Big|^2\Big] \;\leq\; & \mathbb{E}\Big[\sum_{n\in\mathbb{Z}}\Big|e^{\alpha_n t j}u_n(0) - e^{\alpha_n t_j}u_n^N(0) \quad + \\ \int_0^{t_j} e^{(t_j-s)\alpha_n} f_N^n(u(s))ds - \frac{\big(e^{\alpha_n\Delta t}-1\big)}{\alpha_n}\sum_{k=0}^{j-1} e^{(t_{j-1}-t_k)\alpha_n} f_N^n\Big(u^N(t_k)\Big) \quad + \\ \epsilon\sqrt{\lambda_n}\int_0^{t_j} e^{(t_j-s)\alpha_n}d\beta_n(s) - \epsilon\sqrt{\lambda_n}\sum_{k=0}^{j-1} e^{(t_j-t_k)\alpha_n}\Delta\beta_{k,n}\Big|^2\Big].\end{aligned} \tag{4.5.2}$$

Using the inequality in equation (4.4.12), we can separate (4.5.2) into initial data terms, non-linear terms and noise terms. We remark that bounds for the initial data terms and non-linear terms will be like those obtained in Section 4.4. We are just left with analyzing the noise term for an additive SPDE driven by an infinite-dimensional Wiener process.

$$\mathbf{NoiseP}_{\mathrm{a}} = \mathbb{E}\left[\sum_{n\in\mathbb{Z}}\left|\epsilon\int_0^{t_j} e^{(t_j-s)\alpha_n}\lambda_n^{1/2}d\beta_n(s) - \epsilon\sum_{k=0}^{j-1} e^{(t_j-t_k)\alpha_n}\lambda_n^{1/2}\Delta\beta_{k,n}\right|^2\right]. \tag{4.5.3}$$

First, we state the theorem for the theoretical convergence of the **SETD0** scheme for SPDEs with infinite-dimensional additive noise.

Theorem 4.5.1. *Assume that the initial data $u_0 \in \mathcal{D}(A)\cap H^2$, $\theta\in[0,1/2)$, $0\leq r\leq \gamma+1$ and $\gamma>-1$. Consider that $\Delta t\to 0$ and $N\to\infty$ such that $\Delta t N^2\leq\nu$, where ν is some positive parameter. Then for each $T>0$, there exist a $C>0$ such that*

$$\begin{aligned}\left(\mathbb{E}\Big[\Big|\Big|u(t_j) - u^N(t_j)\Big|\Big|^2\Big]\right)^{1/2} \;\leq\; & C\Big(N^{-2} + \Delta t^{\theta} + \epsilon^2\Delta t + N^{-r}|\alpha_N^{-1}| + \\ & \epsilon\Delta t N^{-\gamma}|\alpha_N^{1/2}| + \epsilon N^{-\gamma}|\alpha_N^{-1/2}|\Big).\end{aligned} \tag{4.5.4}$$

We prove this Theorem in §4.5.1.

Corollary 4.5.2. *Under the assumptions in Theorem 4.5.1 and for the linear operator $A = \Delta$ on $[0, 2\pi]$ with periodic boundary condition, with eigenvalue $\alpha_n = -n^2$, for each $n \in \mathbb{Z}$, we have that the strong convergence error estimate is given as*

$$\left(\mathbb{E}\left[\left|\left|u(t_j) - u^N(t_j)\right|\right|^2\right]\right)^{1/2} \leq C\Big(N^{-2} + \Delta t^{\theta} + \epsilon^2\Delta t + N^{-r-2} + \epsilon\Delta t N^{-\gamma+1} + \epsilon N^{-\gamma-1}\Big). \tag{4.5.5}$$

Proof of Corollary 4.5.2. Under the assumptions of Theorem 4.5.1, the root mean square error estimate for a linear operator with eigenvalues $\alpha_n = -n^2$ is obtained as follows.

The final estimate bounds in (4.5.20) is given as

$$\mathbb{E}\left[\left|\left|u(t_j) - u^N(t_j)\right|\right|^2\right] \leq C\Big(N^{2(-2)} + \Delta t^{2\theta} + \epsilon^4\Delta t^2 + N^{-2r}|\alpha_N^{-2}| + \epsilon^2\Delta t^2 N^{-2\gamma}|\alpha_N| + \epsilon^2 N^{-2\gamma}|\alpha_N^{-1}|\Big). \tag{4.5.6}$$

Substituting in the α_N's,

$$\mathbb{E}\left[\left|\left|u(t_j) - u^N(t_j)\right|\right|^2\right] \leq C\Big(N^{2(-2)} + \Delta t^{2\theta} + \epsilon^4\Delta t^2 + N^{2(r-2)} + \epsilon^2\Delta t^2 N^{-2\gamma}N^2 + \epsilon^2 N^{-2\gamma}N^{2\times-1}\Big). \tag{4.5.7}$$

Simplify and write the equation in the root mean square sense as follows:

$$\left(\mathbb{E}\left[\left|\left|u(t_j) - u^N(t_j)\right|\right|^2\right]\right)^{1/2} \leq C\Big(N^{-2} + \Delta t^{\theta} + \epsilon^2\Delta t + N^{-r-2} + \epsilon\Delta t N^{-\gamma+1} + \epsilon N^{-\gamma-1}\Big). \tag{4.5.8}$$

Corollary 4.5.3. *Under the assumptions in Theorem 4.5.1 and for the linear operator $A = -(\Delta + 1)^2$ on $[0, 2\pi]$ with periodic boundary condition, with eigenvalue $\alpha_n =$*

$-n^4+2n^2-1$, *for each* $n \in \mathbb{Z}$, *we have that the strong convergence error estimate is given as*

$$\left(\mathbb{E}\left[\left|\left|u(t_j)-u^N(t_j)\right|\right|^2\right]\right)^{1/2} \leq C\Big(N^{-2}+\Delta t^{\theta}+\epsilon^2\Delta t+N^{-r-4}+ \epsilon\Delta t N^{-\gamma+2}+\epsilon N^{-\gamma-2}\Big). \tag{4.5.9}$$

Proof of Corollary 4.5.3. Under the assumptions of Theorem 4.5.1, the root mean square error estimate for a linear operator with eigenvalues $\alpha_n = -n^4+2n^2-1$ is obtained as follows.

The final estimate bounds in (4.5.20) is given as

$$\mathbb{E}\left[\left|\left|u(t_j)-u^N(t_j)\right|\right|^2\right] \leq C\Big(N^{2(-2)}+\Delta t^{2\theta}+\epsilon^4\Delta t^2+N^{-2r}|\alpha_N^{-2}| + \epsilon^2\Delta t^2 N^{-2\gamma}|\alpha_N|+\epsilon^2 N^{-2\gamma}|\alpha_N^{-1}|\Big). \tag{4.5.10}$$

Note that $-n^4+2n^2-1 < n^4$, therefore, $|\alpha_N| \leq N^4$. Substituting in the α_N, we get that

$$\mathbb{E}\left[\left|\left|u(t_j)-u^N(t_j)\right|\right|^2\right] \leq C\Big(N^{2(-2)}+\Delta t^{2\theta}+\epsilon^4\Delta t^2+N^{2(r-4)} + \epsilon^2\Delta t^2 N^{-2\gamma}N^4+\epsilon^2 N^{-2\gamma}N^{4\times -1}\Big). \tag{4.5.11}$$

Simplify and write the equation in the root mean square sense as follows:

$$\left(\mathbb{E}\left[\left|\left|u(t_j)-u^N(t_j)\right|\right|^2\right]\right)^{1/2} \leq C\Big(N^{-2}+\Delta t^{\theta}+\epsilon^2\Delta t+N^{r-4}+ \epsilon\Delta t N^{\gamma+2}+\epsilon N^{\gamma-2}\Big). \tag{4.5.12}$$

Noise terms:

For the theoretical convergence proof of the **SETD0** scheme for SPDEs with infinite dimensional additive noise, we consider the noise term only. The other terms have

been proved in §4.4. In order to obtain bounds for (4.5.3), we consider terms $|n| \leq N$ and $|n| > N$, we then replace the discrete-time approximation with a continuous-time approximation. The additive noise term is given as follows:

$$\mathbf{NoiseP}_a = \mathbf{NoiseP}_{1a} + \mathbf{NoiseP}_{\text{Tail-a}},$$

where $\mathbf{NoiseP}_{1a}$ is analyzed as follows:

$$\begin{aligned}
\mathbf{NoiseP}_{1a} &\leq \mathbb{E}\left[\sum_{|n|\leq N}\left|\epsilon\int_0^{t_j} e^{(t_j-s)\alpha_n}\lambda_n^{1/2}d\beta_n(s) - \epsilon\int_0^{t_j} e^{(t_j-\lfloor s\rfloor_{\Delta t})\alpha_n}\lambda_n^{1/2}d\beta_n(s)\right|^2\right] \\
&\leq \epsilon^2\mathbb{E}\left[\sum_{|n|\leq N}|\lambda_n|\left|\int_0^{t_j}\left(e^{(t_j-s)\alpha_n} - e^{(t_j-\lfloor s\rfloor_{\Delta t})\alpha_n}\right)d\beta_n(s)\right|^2\right] \\
&\leq \epsilon^2\int_0^{t'}\mathbb{E}\left[\sum_{|n|\leq N}|\lambda_n|\left|\left(e^{(t'-s)\alpha_n} - e^{(t'-\lfloor s\rfloor_{\Delta t})\alpha_n}\right)d\beta_n(s)\right|^2\right].
\end{aligned}$$

By Doob's martingale inequality in Lemma 2.5.3 and the Itô-isometry, we get that

$$\begin{aligned}
\mathbf{NoiseP}_{1\text{a}} &\leq 4\epsilon^2\int_0^{t'}\sum_{|n|\leq N}|\lambda_n|\left(e^{(t'-s)\alpha_n} - e^{(t'-\lfloor s\rfloor_{\Delta t})\alpha_n}\right)ds \\
&\leq 4\epsilon^2\int_0^{t'}\sum_{|n|\leq N}|\lambda_n|e^{2(t'-s)\alpha_n}\left(1 - e^{(s-\lfloor s\rfloor_{\Delta t})\alpha_n}\right)^2 ds.
\end{aligned}$$

This comes from using the following equality,

$$(a-b)^2 = a^2(1-\frac{b}{a})^2. \tag{4.5.13}$$

Next, using the fact that $1 - e^{t\alpha_n} \leq -t\alpha_n$ for $0 \leq t \leq \Delta t$ and Lemma 4.3.2, we get that

$$\begin{aligned}
\int_0^{t'} e^{2(t'-s)\alpha_n}\left(1 - e^{(s-\lfloor s \rfloor_{\Delta t})\alpha_n}\right)ds &\leq \int_0^{t'} \left((s - \lfloor s \rfloor_{\Delta t})\alpha_n\right)^2 e^{2(t'-s)\alpha_n} ds \\
&\leq (\Delta t \alpha_n)^2 \int_0^{t'} e^{2(t'-s)\alpha_n} ds \\
&\leq \frac{1}{2}(\Delta t \alpha_n)^2 |\alpha_n^{-1}| \\
&\leq C\Delta t^2 |\alpha_n|. \qquad (4.5.14)
\end{aligned}$$

Hence, using the assumptions on noise in Assumption 2.4.4,

$$\begin{aligned}
\mathbf{NoiseP}_{1a} &\leq 4C\epsilon^2\Delta t^2 \sum_{|n|\leq N} |\lambda_n||\alpha_n| \\
&\leq C\epsilon^2\Delta t^2 \sum_{|n|\leq N} |\lambda_n|(1+n^2)^{\gamma}(1+n^2)^{-\gamma}|\alpha_n| \\
&\leq C\epsilon^2\Delta t^2 \sum_{|n|\leq N} (1+n^2)^{-\gamma}(1+n^2)^{\gamma}|\lambda_n||\alpha_n| \\
&\leq C\epsilon^2\Delta t^2 (1+N^2)^{-\gamma}|\alpha_N| \underbrace{\sum_{|n|\leq N} (1+n^2)^{\gamma}\lambda_n}_{<\infty} \\
&\leq C\epsilon^2\Delta t^2 N^{-2\gamma}|\alpha_N|. \qquad (4.5.15)
\end{aligned}$$

Next, we consider the tail term left over from the expansion of $u(t)$ for the noise part.

$$\mathbf{NoiseP}_{\text{Tail}-a} = \mathbb{E}\left[\sum_{n>N}\left|\epsilon \int_0^{t_j} e^{(t_j-s)\alpha_n}\lambda_n^{1/2} d\beta_n(s)\right|^2\right]. \qquad (4.5.16)$$

By Doob's martingale inequality in Lemma 2.5.3, the Itô-isometry and the result in (2.4.6), we get that (4.5.16) reduces to

$$\begin{aligned}
\mathbf{NoiseP}_{\text{Tail}-\text{a}} &\leq 4\epsilon^2 \sum_{n>N} \int_0^{t'} e^{2(t'-s)\alpha_n} \lambda_n ds \\
&\leq C\epsilon^2 \sum_{|n|>N} (1+n^2)^{\gamma} (1+n^2)^{-\gamma} \lambda_n \int_0^{t'} e^{2(t'-s)\alpha_n} ds \\
&\leq C\epsilon^2 (1+N^2)^{-\gamma} \int_0^{t'} e^{2(t'-s)\alpha_N} ds \sum_{|n|>N} (1+n^2)^{\gamma} \lambda_n \\
&\leq C\epsilon^2 N^{-2\gamma} |\alpha_N^{-1}| \underbrace{\sum_{|n|>N} (1+n^2)^{\gamma} \lambda_n}_{<\infty} \\
&\leq C\epsilon^2 N^{-2\gamma} |\alpha_N^{-1}|. \qquad (4.5.17)
\end{aligned}$$

The estimates for the noise term in the case of SPDE with additive noise:

$$\mathbf{NoiseP}_{\text{a}} = \mathbf{NoiseP}_{1\text{a}} + \mathbf{NoiseP}_{\text{Tail}-\text{a}} = C\epsilon^2 \Big(\Delta t^2 N^{-2\gamma} |\alpha_N| + N^{-2\gamma} |\alpha_N^{-1}| \Big). \quad (4.5.18)$$

Finally, combining (4.4.18), (4.4.34) and (4.5.18), we achieve the following inequality

$$\begin{aligned}
\mathbb{E}\Big[\Big|\Big| u(t_j) - u^N(t_j) \Big|\Big|^2 \Big] &\leq C\Big(N^{2(-2)} + \Delta t^{2\theta} + \epsilon^4 \Delta t^2 + N^{-2r} |\alpha_N^{-2}| \\
&+ \epsilon^2 \Delta t^2 N^{-2\gamma} |\alpha_N| + \epsilon^2 N^{-2\gamma} |\alpha_N^{-1}| \\
&+ \int_0^{t'} \mathbb{E} \sup_{0\leq s\leq t'} \big|\big| u(s) - u^N(s) \big|\big|^2 ds \Big). \qquad (4.5.19)
\end{aligned}$$

and then by Gronwall's Lemma (2.5.2), we get that

$$\begin{aligned}
\mathbb{E}\Big[\Big|\Big| u(t_j) - u^N(t_j) \Big|\Big|^2 \Big] &\leq C\Big(N^{2(-2)} + \epsilon^4 \Delta t^2 + \Delta t^{2\theta} + N^{-2r} |\alpha_N^{-2}| \\
&+ \epsilon^2 \Delta t^2 N^{-2\gamma} |\alpha_N| + \epsilon^2 N^{-2\gamma} |\alpha_N^{-1}| \Big). \qquad (4.5.20)
\end{aligned}$$

Equation (4.5.20) completes the proof of Theorem 4.5.1.

Chapter 5

Numerics for SPDEs.

5.1 Introduction.

In Chapter 4, we proved Theorem 4.4.1 and Theorem 4.5.1 on the strong convergence of the stochastic exponential time differencing **(SETD0)** scheme applied to SPDEs forced with one-dimensional multiplicative noise and SPDEs forced with infinite-dimensional additive noise. We examined the convergence of temporal discretization in the L^2 norm. That is, we look at the numerical convergence in Δt and not N.

Our aim in this chapter is to numerically investigate the strong convergence of the **SETD0** and **SETD1** schemes applied to SPDEs interpreted in the Itô sense and also investigate the strong convergence of the **ESI** scheme applied to SPDEs interpreted in the Stratonovich sense. In all our numerical examples, we only consider SPDEs with only one driving Wiener process. Thus, the orders of convergence reported is applicable to SPDEs with one driving Wiener process.

We compare the **SETD0** and **SETD1** schemes against two other standard Itô schemes, that is, the **LR** and the semi-implicit **EM** methods, and also compare the **ESI** scheme against the standard Stratonovich scheme, that is, the **Heun** scheme. To use the Stratonovich schemes, we need to perform a drift-correction on an Itô SPDE to obtain a Stratonovich SPDE, for which the Stratonovich schemes can then be applied directly.

We carry out numerical simulations using the above numerical schemes applied to

two examples of SPDEs; a second-order SPDE, the Allen-Cahn equation and a fourth-order SPDE, the Swift-Hohenberg equation. In each example, we consider three types of stochastic forcing. Firstly, SPDE with one-dimensional multiplicative noise, secondly, SPDE with infinite-dimensional multiplicative noise and thirdly, SPDE with infinite-dimensional additive noise. We show graphically the slopes and rates of convergence for each of the numerical schemes. We also compare the efficiency of the numerical methods. Furthermore, we examine the effects of increasing the spatial regularity of the noise in our numerical simulations.

5.2 Numerical examples

We consider the following cases. Let $\epsilon \in \mathbb{R}$.

1. Allen-Cahn SPDE driven by one-dimensional multiplicative noise, (see §5.4.1).

$$du = \Big(\Delta u + u - u^3\Big)dt + \epsilon u d\beta(t), \tag{5.2.1}$$

$$du = \Big(\Delta u + u - u^3 - \frac{\epsilon^2}{2}u\Big)dt + \epsilon u \circ d\beta(t), \tag{5.2.2}$$

   where the Wiener process $\beta(t)$ in (5.2.1) and (5.2.2) is one-dimensional.

2. Allen-Cahn SPDE driven by infinite-dimensional multiplicative noise, (see §5.4.2).

$$du = \Big(\Delta u + u - u^3\Big)dt + \epsilon u dW(t), \tag{5.2.3}$$

$$du = \Big(\Delta u + u - u^3 - \frac{\epsilon^2}{2}\mathrm{Tr}\mathbb{Q} \cdot u\Big)dt + \epsilon u \circ dW(t), \tag{5.2.4}$$

   where the Wiener process $W(t)$ in (5.2.3) and (5.2.4) is a $\mathbb{Q}$-Wiener process given by (2.3.9) and the $\mathrm{Tr}\mathbb{Q}$ stands for the trace of $\mathbb{Q}$.

3. Allen-Cahn SPDE driven by additive noise, (see §5.4.3).

$$du = \Big(\Delta u + u - u^3\Big)dt + \epsilon dW(t), \tag{5.2.5}$$

where the Wiener process $W(t)$ in (5.2.5) is a $\mathbb{Q}$-Wiener process given by (2.3.9). The Allen-Cahn equations are supplemented with periodic boundary conditions, $u(0,t) = u(2\pi,t)$, where $t \geq 0$ and initial condition $u(x,0)$. In our simulations, we take $u(x,0) = \sin(2x)\cos(x)$.

4. Swift-Hohenberg SPDE driven by one-dimensional multiplicative noise, (see §5.4.1).

$$du = \Big(ru - \Big(\Delta + q_c^2\Big)^2 u + \rho u^2 - gu^3\Big)dt + \epsilon u d\beta(t), \tag{5.2.6}$$

$$du = \Big(ru - \Big(\Delta + q_c^2\Big)^2 u + \rho u^2 - gu^3 - \frac{\epsilon^2}{2}u\Big)dt + \epsilon u \circ d\beta(t). \tag{5.2.7}$$

where the Wiener process $\beta(t)$ in (5.2.6) and (5.2.7) is one-dimensional, r stands for the control parameter of the Swift-Hohenberg equation and the parameters q_c, ρ and g are fixed. In our simulations, we take $q_c = 0.5, \rho = 0.41$ and $g = 1$.

5. Swift-Hohenberg SPDE driven by infinite-dimensional multiplicative noise, (see §5.4.2).

$$du = \Big(ru - \Big(\Delta + q_c^2\Big)^2 u + \rho u^2 - gu^3\Big)dt + \epsilon u dW(t). \tag{5.2.8}$$

$$du = \Big(ru - \Big(\Delta + q_c^2\Big)^2 u + \rho u^2 - gu^3 - \frac{\epsilon^2}{2}\mathrm{Tr}\mathbb{Q}\cdot u\Big)dt + \epsilon u \circ dW(t), \tag{5.2.9}$$

where the Wiener process $W(t)$ in (5.2.8) and (5.2.9) is a $\mathbb{Q}$-Wiener process given by (2.3.9) and $\mathrm{Tr}\mathbb{Q}$ stands for the trace of $\mathbb{Q}$.

6. Swift-Hohenberg driven by additive noise, (see §5.4.3).

$$du = \Big(ru - \Big(\Delta + q_c^2\Big)^2 u + \rho u^2 - gu^3\Big)dt + \epsilon dW(t), \tag{5.2.10}$$

where the Wiener process $W(t)$ in (5.2.10) is a $\mathbb{Q}$-Wiener process given by (2.3.9).

The Swift-Hohenberg equations above are supplemented with periodic boundary conditions, $u(0,t) = u(2\pi,t)$, where $t \geq 0$ and initial condition $u(x,0)$. In our simulations,

we take $u(x,0) = \cos(0.45x)\text{sech}\,(\exp(0.0014x^2))$. For numerical calculations, we take the following numerical parameters $r = -0.015$.

In all these numerical examples, ϵ denotes the noise intensity.

Remark: For SPDEs with additive noise, the Itô and Stratonovich interpretations are equivalent.

5.3 Numerical discretization.

For the numerical discretization of the SPDE examples (5.2.1)-(5.2.10), we consider a Fourier spectral method for the spatial discretization, see §2.8.1 for a brief introduction to this method. This procedure gives rise to an infinite system of stochastic ordinary differential equations (SODEs) which requires efficient and accurate time integration techniques in order to obtain solutions.

The SPDEs (5.2.1), (5.2.3), (5.2.5), (5.2.6), (5.2.8) and (5.2.10) are all interpreted in the Itô sense. Therefore, the Itô schemes outlined in §5.3.1 will be used for the simulations of the resulting SODEs obtained from first performing the spatial discretization. To use the Stratonovich schemes, we first perform a drift correction on the Itô SPDEs in order to obtain Stratonovich equations (5.2.2), (5.2.4), (5.2.7) and (5.2.9), such that the solutions obtained from the different interpretations all converge to the same solution. These Stratonovich schemes are outlined in §5.3.2. We now define the notations used in the numerical schemes in §5.3.1 and §5.3.2. Let $V^N t_k)$ denotes the numerical approximation of the solution $u^N(t)$ at discretization times $t_k = k\Delta t$ on the time interval $[0,T]$, for $k = 0, 1, \cdots, M$, $\Delta t = T/M$, denotes the time step-size, M stands for the number of time subintervals, while $N \in \mathbb{N}$ stands for the number of spatial grid points.

To apply the discretization schemes in §5.3.1 and §5.3.2, the linear operator for the Allen-Cahn SPDE is given by $A = \Delta$, such that $\Delta\psi_n = \alpha_n\psi_n = -n^2\psi_n, n \in \mathbb{Z}$, and the linear operator for Swift-Hohenberg SPDE is given by $A = r - (\Delta + q_c^2)^2$, such that $r - (\Delta + q_c^2)^2\psi_n = \alpha_n\psi_n = (r - n^4 + 2n^2 - q_c^4)\psi_n, n \in \mathbb{Z}$, where α_n denotes the eigenvalues of the operator A. The nonlinear drift terms for the Allen-Cahn SPDEs

and Swift-Hohenberg SPDEs are given by $f(u) = u - u^3$ and $f(u) = \rho u^2 - gu^3$ respectively. The diffusion terms for the Allen-Cahn SPDEs and Swift-Hohenberg SPDEs are both given by $g(u) = u$.

5.3.1 Itô schemes.

1. The stochastic exponential time differencing **SETD0** scheme is given by

   • *Multiplicative noise: one-dimensional case.*

   $$V^N(t_{k+1}) = e^{\Delta t A_N} V^N(t_k) + A_N^{-1} \left(e^{\Delta t A_N} - I\right) f_N(V^N(t_k)) + e^{\Delta t A_N} g_N(V^N(t_k)) \Delta\beta(t_k), \tag{5.3.1}$$

   where $\Delta\beta(t_k)$ is a Wiener increment given by (2.2.8).

   • *Multiplicative noise: infinite-dimensional case.*

   $$V^N(t_{k+1}) = e^{\Delta t A_N} V^N(t_k) + A_N^{-1} \left(e^{\Delta t A_N} - I\right) f_N(V^N(t_k)) + e^{\Delta t A_N} g_N(V^N(t_k)) \Delta W^N(t_k), \tag{5.3.2}$$

   where $\Delta W^N(t_k)$ is a Wiener increment given by (2.8.13).

   • *Additive noise: infinite-dimensional case.*

   $$V^N(t_{k+1}) = e^{\Delta t A_N} V^N(t_k) + A_N^{-1} \left(e^{\Delta t A_N} - I\right) f_N(V^N(t_k)) + e^{\Delta t A_N} \Delta W^N(t_k). \tag{5.3.3}$$

2. The stochastic exponential time differencing **SETD1** scheme is given by

   • *Multiplicative noise: one-dimensional case.*

   $$\begin{aligned} V^N(t_{k+1}) &= e^{\Delta t A_N} V^N(t_k) + A_N^{-1} \left(e^{\Delta t A_N} - I\right) f_N(V^N(t_k)) + \\ &\left(A_N^{-1} \left(\frac{e^{2\Delta t A_N} - I}{2I}\right)\right)^{1/2} g_N\left(V^N(t_k)\right) \frac{\Delta\beta(t_k)}{\sqrt{\Delta t}}, \end{aligned} \tag{5.3.4}$$

   where $\Delta\beta(t_k)$ is a Wiener increment given by (2.2.8).

   • *Multiplicative noise: infinite-dimensional case.*

   $$\begin{aligned} V^N(t_{k+1}) &= e^{\Delta t A_N} V^N(t_k) + A_N^{-1} \left(e^{\Delta t A_N} - I\right) f_N(V^N(t_k)) + \\ &\left(A_N^{-1} \left(\frac{e^{2\Delta t A_N} - I}{2I}\right)\right)^{1/2} g_N\left(V^N(t_k)\right) \frac{\Delta W^N(t_k)}{\sqrt{\Delta t}}, \end{aligned} \tag{5.3.5}$$

where $\Delta W^N(t_k)$ is a Wiener increment given by (2.8.13).

- *Additive noise: infinite-dimensional case.*

$$V^N(t_{k+1}) = e^{\Delta t A_N} V^N(t_k) + A_N^{-1}\left(e^{\Delta t A_N} - I\right) f_N(V^N(t_k)) + \left(A_N^{-1}\left(\frac{e^{2\Delta t A_N} - I}{2I}\right)\right)^{1/2} \frac{\Delta W^N(t_k)}{\sqrt{\Delta t}}. \tag{5.3.6}$$

In [46], they proved the convergence of the **SETD1** scheme in (5.3.6), that is, the additive noise case. The scheme was termed as the exponential Euler scheme in their work and they found out that it is possible to overcome the order barrier for the rate of convergence of SPDEs with additive noise by taking advantage of the linear functionals of the noise and the smoothening properties of the semigroup. They showed that the **SETD1** achieve order of convergence 1. In this thesis, we only show numerically the strong convergence for the **SETD1** applied to additive and multiplicative noise.

3. The Lord-Rougemont **LR** scheme [54] is given as

- *Multiplicative noise: one-dimensional case.*

$$V^N(t_{k+1}) = e^{\Delta t A_N}\left(V^N(t_k) + \Delta t f_N(V^N(t_k)) + g_N(V^N(t_k))\Delta\beta(t_k)\right), \tag{5.3.7}$$

where $\Delta\beta(t_k)$ is a Wiener increment given by (2.2.8).

- *Multiplicative noise: infinite-dimensional case.*

$$V^N(t_{k+1}) = e^{\Delta t A_N}\left(V^N(t_k) + \Delta t f_N(V^N(t_k)) + g_N(V^N(t_k))\Delta W^N(t_k)\right), \tag{5.3.8}$$

where $\Delta W^N(t_k)$ is a Wiener increment given by (2.8.13).

- *Additive noise: infinite-dimensional case.*

$$V^N(t_{k+1}) = e^{\Delta t A_N}\left(V^N(t_k) + \Delta t f_N(V^N(t_k)) + \Delta W^N(t_k)\right). \tag{5.3.9}$$

4. The semi-implicit Euler Maruyama **EM** scheme [50] is given by

- *Multiplicative noise: one-dimensional case.*

$$V^N(t_{k+1}) = (I - \Delta t A_N)^{-1}\left(V^N(t_k) + \Delta t f_N(V^N(t_k)) + g_N(V^N(t_k))\Delta\beta(t_k)\right), \tag{5.3.10}$$

where $\Delta\beta(t_k)$ is a Wiener increment given by (2.2.8).

- *Multiplicative noise: infinite-dimensional case.*

$$V^N(t_{k+1}) = (I - \Delta t A_N)^{-1}\Big(V^N(t_k) + \Delta t f_N(V^N(t_k)) + g_N(V^N(t_k))\Delta W^N(t_k)\Big), \tag{5.3.11}$$

where $\Delta W^N(t_k)$ is a Wiener increment given by (2.8.13).

- *Additive noise: infinite-dimensional case.*

$$V^N(t_{k+1}) = (I - \Delta t A_N)^{-1}\Big(V^N(t_k) + \Delta t f_N(V^N(t_k)) + \Delta W^N(t_k)\Big). \tag{5.3.12}$$

5.3.2 Stratonovich schemes.

1. The exponential Stratonovich integrator **ESI** scheme is given by

- *Multiplicative noise: one-dimensional case.*

$$V^N(t_{k+1}) = e^{\Delta t A_N} V^N(t_k) + A_N^{-1}\left(e^{\Delta t A_N} - 1\right) f_N\left(V^N(t_k)\right) +$$

$$\frac{1}{2} e^{\Delta t A_N/2}\Big(g_N\left(V^N(t_k)\right) + g_N\left(\widehat{V}^N(t_k)\right)\Big)\Delta\beta(t_k), \tag{5.3.13}$$

where $\Delta\beta(t_k)$ is a Wiener increment given by (2.2.8) and

$$\widehat{V}^N(t_k) = \Big(I - \Delta t A_N\Big)^{-1}\left(V^N(t_k) + \Delta t f_N\left(V^N(t_k)\right) + g_N\left(V^N(t_k)\right)\Delta W(t_k)\right).$$

- *Multiplicative noise: infinite-dimensional case.*

$$V^N(t_{k+1}) = e^{\Delta t A_N} V^N(t_k) + A_N^{-1}\left(e^{\Delta t A_N} - 1\right) f_N\left(V^N(t_k)\right) +$$

$$\frac{1}{2} e^{\Delta t A_N/2}\Big(g_N(V^N(t_k)) + g_N\left(\widehat{V}^N(t_k)\right)\Big)\Delta W^N(t_k), \tag{5.3.14}$$

where $\Delta W^N(t_k)$ is a Wiener increment given by (2.8.13) and

$$\widehat{V}^N(t_k) = \Big(I - \Delta t A_N\Big)^{-1}\left(V^N(t_k) + \Delta t f_N\left(V^N(t_k)\right) + g_N\left(V^N(t_k)\right)\Delta W^N(t_k)\right).$$

- *Additive noise: infinite-dimensional case.*

$$V^N(t_{k+1}) = e^{\Delta t A_N} V^N(t_k) + A_N^{-1}\left(e^{\Delta t A_N} - 1\right) f_N\left(V^N(t_k)\right) + e^{\Delta t A_N/2}\Delta W^N(t_k). \tag{5.3.15}$$

2. The semi-implicit **Heun** scheme [50] is given by

- *Multiplicative noise: one-dimensional case.*

$$V^N(t_{k+1}) = \Big(I - \frac{\Delta t}{2}A_N\Big)^{-1}\Bigg(V^N(t_k) + \frac{\Delta t}{2}\Big(A_N\widehat{V}^N(t_k) + f_N\left(V^N(t_k)\right) +$$

$$+ f_N\left(\widehat{V}^N(t_k)\right)\Big) + \frac{1}{2}\Big(g_N\left(V^N(t_k)\right) + g_N\left(\widehat{V}^N(t_k)\right)\Big)\Delta\beta(t_k)\Bigg), \tag{5.3.16}$$

where $\Delta\beta(t_k)$ is a Wiener increment given by (2.2.8) and

$$\widehat{V}^N(t_k) = \Big(1 - \Delta t A_N\Big)^{-1}\Bigg(V^N(t_k) + \Delta t f_N(V^N(t_k)) + g_N(V^N(t_k))\Delta\beta(t_k)\Bigg).$$

- *Multiplicative noise: infinite-dimensional case.*

$$V^N(t_{k+1}) = \Big(I - \frac{\Delta t}{2}A_N\Big)^{-1}\Bigg(V^N(t_k) + \frac{\Delta t}{2}\Big(A_N\widehat{V}^N(t_k) + f_N\left(V^N(t_k)\right) +$$

$$f_N\left(\widehat{V}^N(t_k)\right)\Big) + \frac{1}{2}\Big(g_N\Big(V^N(t_k)\Big) + g_N\Big(\widehat{V}^N(t_k)\Big)\Big)\Delta W^N(t_k)\Bigg), \tag{5.3.17}$$

where $\Delta W^N(t_k)$ is a Wiener increment given by (2.8.13) and

$$\widehat{V}^N(t_k) = \Big(1 - \Delta t A_N\Big)^{-1}\Bigg(V^N(t_k) + \Delta t f_N(V^N(t_k)) + g_N(V^N(t_k))\Delta W^N(t_k)\Bigg).$$

- *Additive noise: infinite-dimensional case.*

$$V^N(t_{k+1}) = \Big(I - \frac{\Delta t}{2}A_N\Big)^{-1}\Bigg(V^N(t_k) + \frac{\Delta t}{2}\Big(A_N\widehat{V}^N(t_k) + f_N\left(V^N(t_k)\right) +$$

$$f_N\left(\widehat{V}^N(t_k)\right)\Big) + \Delta W^N(t_k)\Bigg), \tag{5.3.18}$$

where $\Delta W^N(t_k)$ is a Wiener increment given by (2.8.13) and

$$\widehat{V}^N(t_k) = \Big(1 - \Delta t A_N\Big)^{-1}\bigg(V^N(t_k) + \Delta t f_N(V^N(t_k)) + \Delta W^N(t_k)\bigg).$$

Numerical implementation.

To test the strong convergence of the six numerical methods, that is, the **SETD0**, **SETD1**, **LR**, **EM**, **ESI** and **Heun** schemes, we take the number of spatial grid points as $N = 512$ and vary time step size, Δt. Solutions are then obtained at time step size $\Delta t = 1/\{M_i\}_{i=1,\cdots,8}$ where $M_1 = 2000$, $M_2 = 1000$, $M_3 = 500$, $M_4 = 400$, $M_5 = 250$, $M_6 = 200$, $M_7 = 125$, $M_8 = 100$ and $M_9 = 50$ for the Swift-Hohenberg and Allen-Cahn SPDEs.

Since we do not have analytical solutions for the numerical examples, we compute reference solutions for all the numerical examples (5.2.1)-(5.2.10) with their appropriate numerical schemes in (5.3.1)-(5.3.18) on the interval $[0, 1]$ with time step size $\Delta t = 1/4000$.

In our numerical calculations, we take noise that is white in time and we vary the spatial regularity, such that we get noise in $H^{-1/2}$, H^0, $H^{1/2}$ and H^1, i.e. $\gamma = -1/2, 0, 1/2, 1$ in the H^γ space. Details of how the infinite-dimensional noise is discretized is outlined in Section 2.8.2.

Figure 5.1 shows the effect of increasing the spatial regularity of the noise. We observe that the path gets smoother as the regularity γ is increased.

The accuracy of the numerical schemes is measured as the approximate L^2-norm of the global errors in the time interval $[0, 1]$.

The theoretical error $\Big(\mathbb{E}\left|\left|u(t_k) - V^N(t_k)\right|\right|^2_{L^2}\Big)^{1/2}$ is estimated by the numerical strong error which is computed as follows:

$$\text{error} \approx \left(\frac{1}{R}\sum_{r=1}^{R}\left|\left|u(t_k, r) - V_n^N(t_k, r)\right|\right|^2_{L^2}\right)^{1/2}, \tag{5.3.19}$$

where R denotes the number of computed paths, $u(t_k, r)$ denotes the solution u at time t_k at the r-th realization. Throughout this Chapter we used $R = 100$. We average over 100 realizations of solutions.

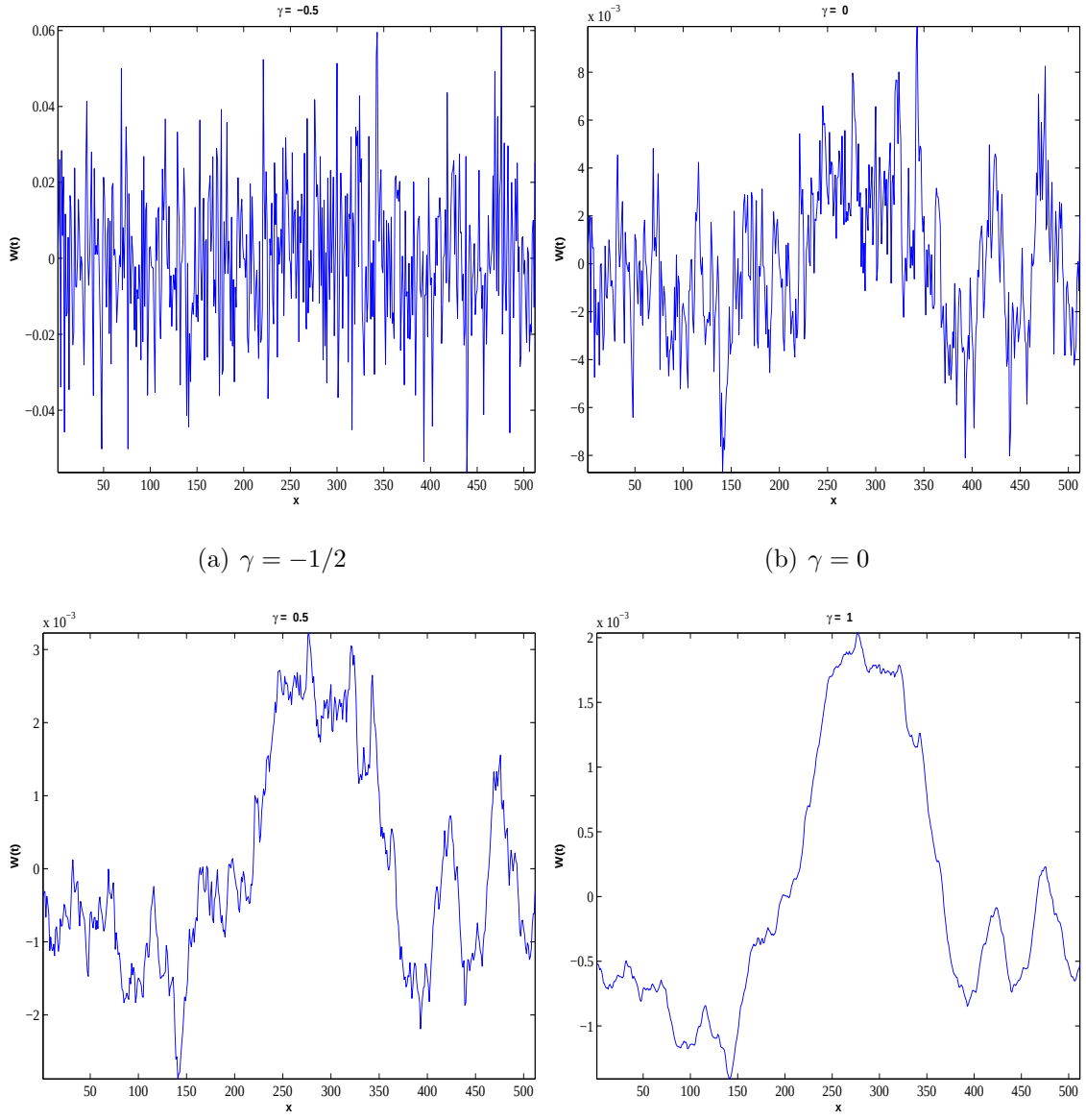

(a) $\gamma = -1/2$ (b) $\gamma = 0$

(c) $\gamma = 1/2$ (d) $\gamma = 1$

Figure 5.1: A sample path of H^γ noise used in the numerical simulations of SPDEs (5.2.1) - (5.2.10), where γ denotes the spatial regularity of the noise. In (a)$H^{-1/2}$, (b) H^0, (c) $H^{1/2}$ and (d)$= H^1$. The eigenvalues of the Wiener process used is $\lambda_n = (1+n^2)^{-\gamma}|n|^{-(1+\varepsilon)}$, where $\varepsilon \ll 1$. We see that the dynamics of the noise gets smoother as the regularity of the noise is increased.

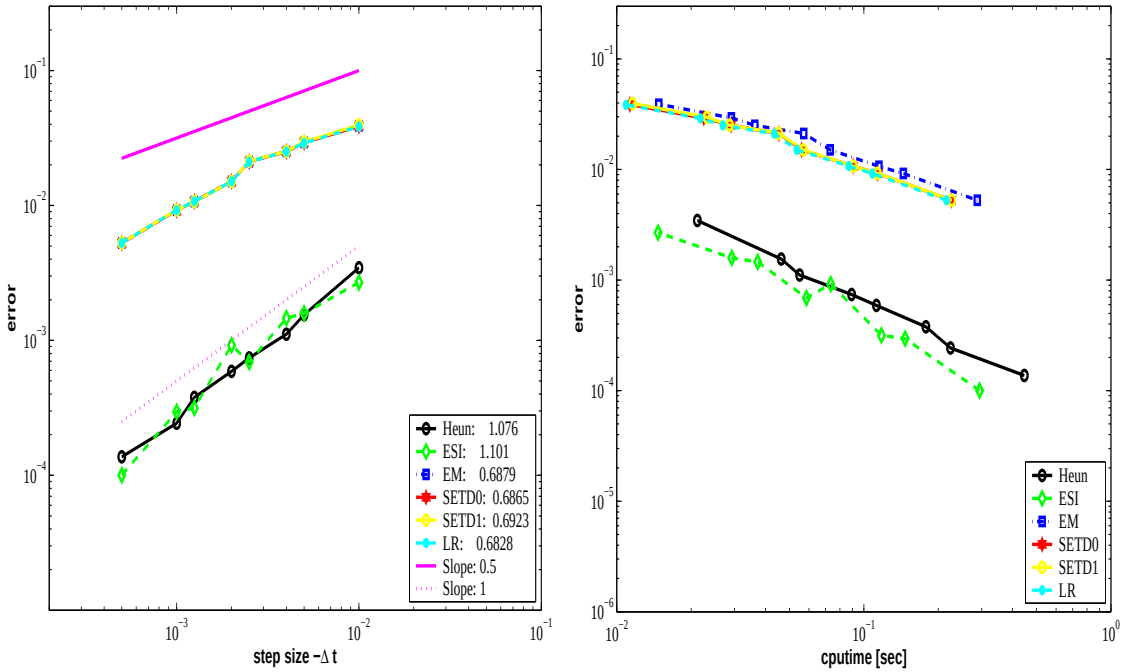

(a) (b)

Figure 5.2: Convergence in time for the **SETD0**, **SETD1**, **LR** and **EM** schemes applied to the AC equation with one-dimensional multiplicative noise (5.2.1) and the **ESI** and **Heun** schemes applied to the AC equation with one-dimensional multiplicative noise (5.2.2). The plot is a log-log plot of the numerical strong error (5.3.19) on $[0, 1]$. In (a) is the plot of the numerical strong error (5.3.19) versus time step size Δt and in (b) is the plot of the numerical strong error (5.3.19) versus cputime. We see that the numerical orders of convergence of the Itô schemes are ≈ 0.69 while the orders of convergence for the Stratonovich schemes are ≈ 1.1. We also observe that the Stratonovich schemes are more accurate than the Itô schemes. In terms of efficiency, the **ESI** scheme takes less computational time when compared to the **Heun** scheme, while the **SETD0**, **SETD1** and **LR** schemes are more efficient than the **EM** scheme. Finally, the **SETD0** scheme for which we proved a convergence result predicts an order of convergence of 0.5. This predicted order can be seen for larger time step.

5.4 Numerical convergence results.

In this section, we discuss the strong convergence, accuracy and efficiency of the numerical methods (5.3.1) - (5.3.18). We also report the strong orders of convergence as calculated numerically. All the plots in this Chapter are presented on a log-log scale.

5.4.1 One-dimensional multiplicative noise.

Figure 5.2 shows the convergence in the root mean square L^2 norm for the Itô schemes: **SETD0** (5.3.1), **SETD1** (5.3.4), **LR** (5.3.7) and **EM** (5.3.10) schemes applied to (5.2.1) and the Stratonovich schemes **ESI** (5.3.13) and **Heun** (5.3.16) schemes applied to AC equation (5.2.2) at final time $T = 1$. We observe from Figure 5.2(a) that the Itô schemes all converge with a strong order of ≈ 0.69. This rate of convergence is slightly better than the theoretically predicted rate of convergence of order 0.5 for the **SETD0** scheme, which we proved a theoretical convergence result for, in Chapter 4, see Theorem 4.4.1. We remark that the slopes of convergence computed for the Itô and Stratonovich schemes all match up, thus implying that they have approximately the same accuracy. Figure 5.2(b) shows the efficiency of the numerical methods. We plot the the numerical strong error (5.3.19) against cputime, and we observe that the **SETD0**, **SETD1** and **LR** schemes takes less computational time when compared to the **EM** scheme, which makes the **SETD0**, **SETD1** and **LR** schemes the most efficient amongst the Itô schemes. For the Stratonovich schemes, the **ESI** is the more efficient than the **Heun** scheme at all the time steps.

Figure 5.3 shows the rate of convergence in the root mean square L^2 norm for the Itô schemes: **SETD0**, **SETD1**, **LR** and **EM** methods when applied to the SH equation (5.2.6) and the Stratonovich schemes: **ESI** and **Heun** scheme when applied to the SH equation (5.2.7). We observe strong orders of convergence of 0.67 and 1 for the Itô and Stratonovich methods respectively at final time $T = 1$. We see in Figure 5.3(a) that the slopes of convergence of all the Itô schemes match up. Figure 5.3 (b) shows the efficiency of these numerical methods. We see that the **SETD0**, **SETD1** and **LR**

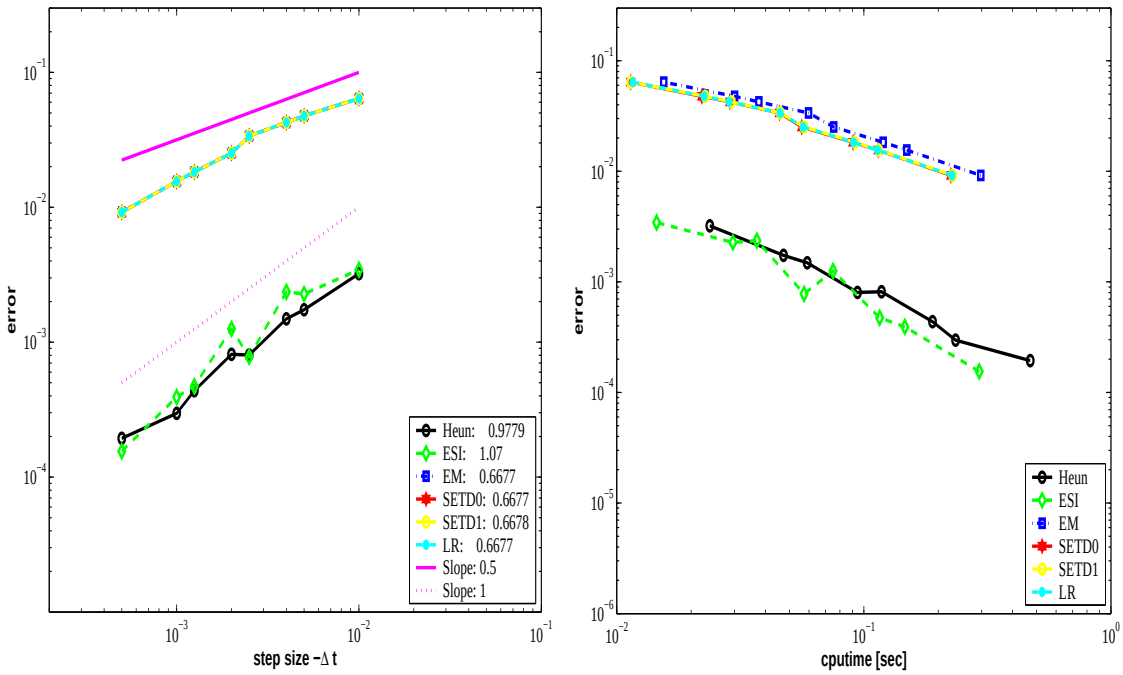

(a) (b)

Figure 5.3: Convergence in time for the **SETD0**, **SETD1**, **LR** and **EM** schemes applied to the SH equation with one-dimensional multiplicative noise (5.2.6) and the **ESI** and **Heun** schemes applied to the SH equation with one-dimensional multiplicative noise (5.2.7). The plot is a log-log plot of the numerical strong error (5.3.19) on $[0, 1]$. In (a) is the plot of the numerical strong error (5.3.19) versus time step size Δt and in (b) is the plot of the numerical strong error (5.3.19) versus cputime. We see that the numerical orders of convergence of the Itô schemes are ≈ 0.67 while the orders of convergence for the Stratonovich schemes are ≈ 1. We also observe that the Stratonovich schemes are more accurate than the Itô schemes. In terms of efficiency, the **ESI** scheme takes less computational time when compared to the **Heun** scheme, while the **SETD0**, **SETD1** and **LR** schemes are more efficient than the **EM** scheme.

schemes are more efficient than the **EM** scheme while the **ESI** scheme is again more efficient than the **Heun** method.

5.4.2 Infinite-dimensional multiplicative noise.

Here, we perform numerics on the Allen-Cahn equation and Swift-Hohenberg equation with infinite-dimensional multiplicative noise, however we do not have theoretical convergence result to compare with numerical rates of convergence.

Figure 5.4 (a - d) shows the rate of strong convergence at final time $T = 1$ for the Itô schemes: **SETD0** (5.3.2), **SETD1** (5.3.5), **LR** (5.3.8) and **EM** (5.3.11) schemes applied to Itô AC equation (5.2.3) and the Stratonovich schemes: **ESI** (5.3.14) and **Heun** (5.3.17) schemes applied to Stratonovich AC equation (5.2.4) for different spatial regularities of noise. We report in detail the strong orders for each numerical scheme in the legend of each Figure. We also add slopes of 0.5 and 1 for reference purpose.

We present simulation results for noise in H^γ, $\gamma = -1/2, 0, 1/2, 1$ for the Itô and Stratonovich schemes. We observe that for $H^{-1/2}$ noise, the order of strong convergence is ≈ 0.6 for the **SETD0**, **LR**, **EM** and **ESI** schemes and an order of ≈ 0.8 & 1 for the **SETD1** and **Heun** schemes respectively. The **EM** method appears to be the most accurate for the case where noise is in $H^{-1/2}$, however, we observe that as we increase the spatial regularity of the noise, from $\gamma = -1/2$ to $\gamma = 1$, the **ESI** scheme is the most accurate numerical method, followed by the **SETD1** scheme. For smaller Δt, the **Heun** and the **ESI** schemes have better rates of convergence when compared to the Itô schemes. We also observe that the strong orders of the numerical methods increase as we increase the spatial regularity of the noise, γ. In addition, we see that error decreases as regularity is increased.

In figure 5.5 (a-d), we display the rates of strong convergence for the **SETD0** (5.3.2), **SETD1** (5.3.5), **LR** (5.3.8) and **EM** (5.3.11) schemes applied to the Itô SH equation (5.2.8) and the **ESI** (5.3.14) and **Heun** (5.3.17) schemes applied to the Stratonovich SH equation (5.2.9). We observe in this numerical example, that when noise is in $H^{-1/2}$, the **SETD1** with strong order ≈ 0.8 and **ESI** scheme with strong order ≈ 0.7

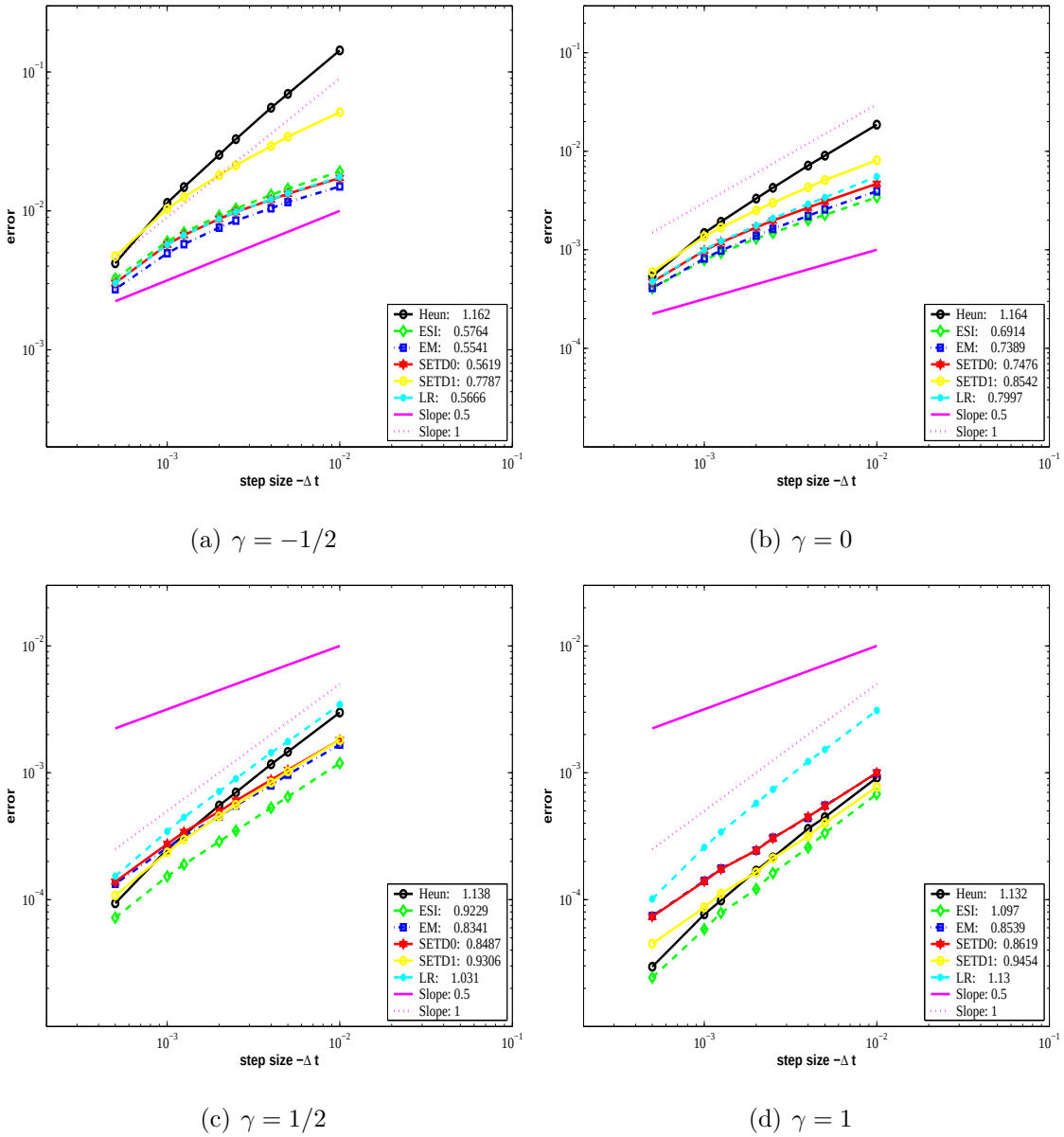

(a) $\gamma = -1/2$ (b) $\gamma = 0$

(c) $\gamma = 1/2$ (d) $\gamma = 1$

Figure 5.4: Convergence in time for the **SETD0**, **SETD1**, **LR** and **EM** schemes applied to the AC equation with multiplicative infinite-dimensional noise (5.2.3) and the **ESI** and **Heun** schemes applied to the AC equation with multiplicative infinite-dimensional noise (5.2.4). The plot is a log-log plot of the numerical strong error (5.3.19) on $[0, 1]$. From (a) - (d), is the plot of the numerical strong error (5.3.19) versus time step. In (a) $H^{-1/2}$, (b) H^0, (c) $H^{1/2}$ and (d) H^1 noise. respectively the most accurate Stratonovich and Itô schemes when noise is in H^1.

are the most accurate of the six numerical methods. In fact the **SETD1** scheme does slightly better in terms of the error constant and strong order of convergence. The **Heun** method has a strong order of ≈ 0.9; although, for the largest time step, the **Heun** method is the least accurate method, however, as the time step is decreased, the **Heun** method out performs the other three Itô schemes, that is, the **SETD0**, **LR** and **EM** method, see Figure 5.5(a).

Increasing the spatial regularity of the noise, does lead to smaller errors and we see that this increase in spatial regularity of noise favour the **Heun** method, such that it gradually get more accurate than the **SETD1** scheme. In this numerical example, we observe that increasing γ does not seem to have significant effect on the strong orders of the Itô numerical methods. Finally, when noise is in H^1, we obtain strong orders ≈ 0.5 and 1 for the Itô and Stratonovich schemes respectively. The **SETD1** is the most accurate scheme amongst the Itô schemes, while the **ESI** is the most accurate scheme amongst the Stratonovich schemes.

5.4.3 Infinite-dimensional additive noise.

So far, we have considered SPDEs with multiplicative noise. We now focus our attention on SPDEs wth additive noise. In Figure 5.7 (a-d), we show the convergence in the root mean square L^2 norm for the **SETD0** (5.3.3), **SETD1** (5.3.6) the **LR** (5.3.9), **EM** (5.3.12), **ESI** (5.3.15) and the **Heun** (5.3.18) schemes. We observe that when we take noise in $H^{-1/2}$, the Itô schemes converge with strong order of approximately 0.5; on the other hand, for the case of Stratonovich schemes, the **Heun** method has strong order ≈ 1 while the **ESI** scheme has a strong order of ≈ 0.5. This low order of convergence for the **ESI** scheme is not surprising because the **ESI** scheme is suited mainly for Stratonovich equations, and in this numerical example, we are considering SPDEs with additive noise. Nevertheless, the **ESI** scheme is more accurate than the **Heun** scheme. We also see that increasing the spatial regularity of the noise gives rise to higher orders of convergence and smaller errors. In this numerical example, the **EM** method seems to have the smallest error when compared to the the other Itô schemes for $H^{-1/2}, H^0$ and $H^{1/2}$ noise. However, **SETD1** scheme turns out to be the

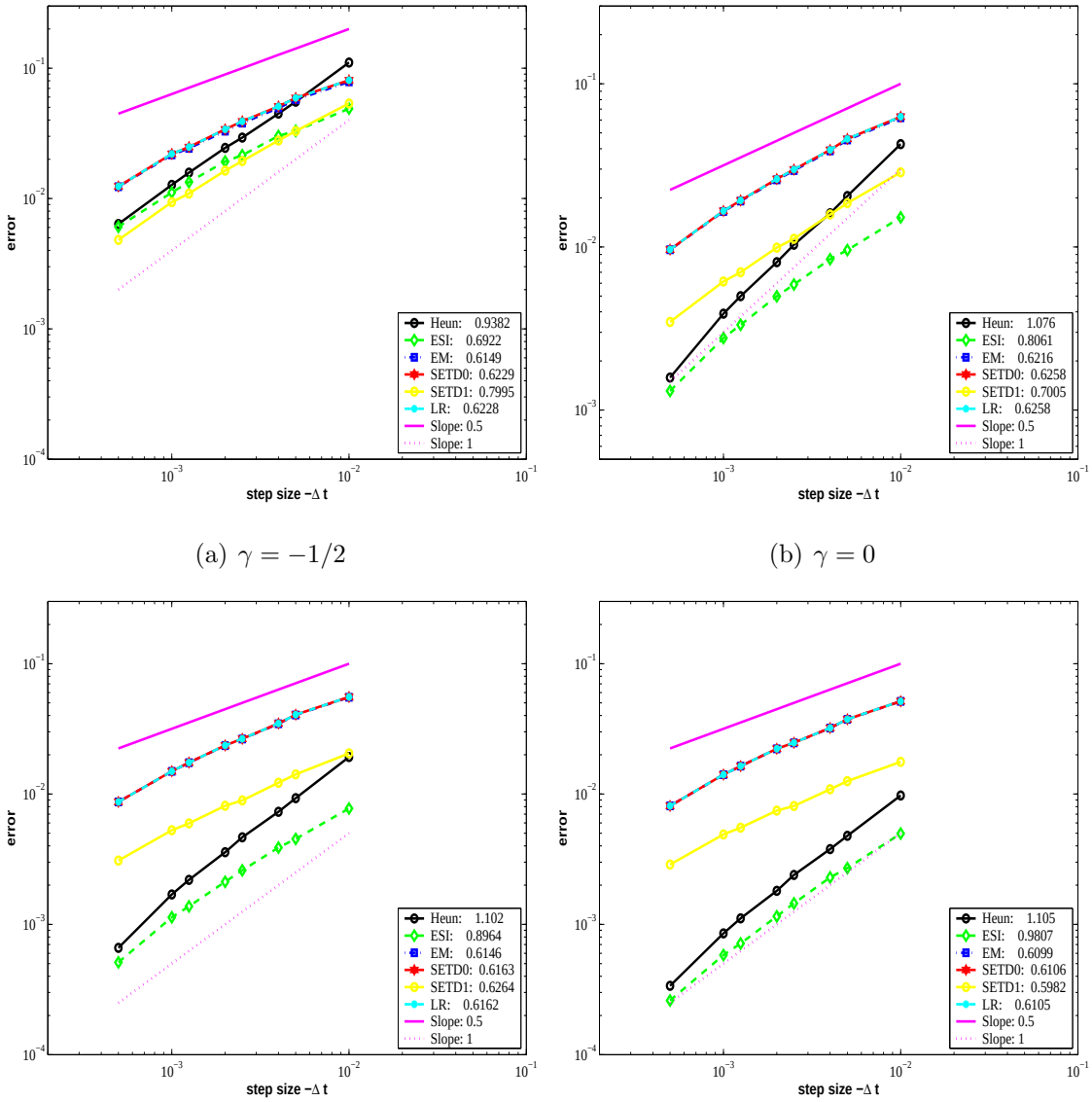

(a) $\gamma = -1/2$ (b) $\gamma = 0$

(c) $\gamma = 1/2$ (d) $\gamma = 1$

Figure 5.5: Convergence in time for the **SETD0**, **SETD1**, **LR** and **EM** schemes applied to the SH equation with multiplicative infinite-dimensional noise (5.2.8) and the **ESI** and **Heun** schemes applied to the SH equation with multiplicative infinite-dimensional noise (5.2.9). The plot is a log-log plot of the numerical strong error (5.3.19) on $[0, 1]$. From (a) - (d), is the plot of the numerical strong error (5.3.19) versus time step. In (a) $H^{-1/2}$, (b) H^0, (c) $H^{1/2}$ and (d) H^1 noise. We see that the **ESI** and **SETD1** schemes are respectively the most accurate Stratonovich and Itô schemes when noise is in H^1.

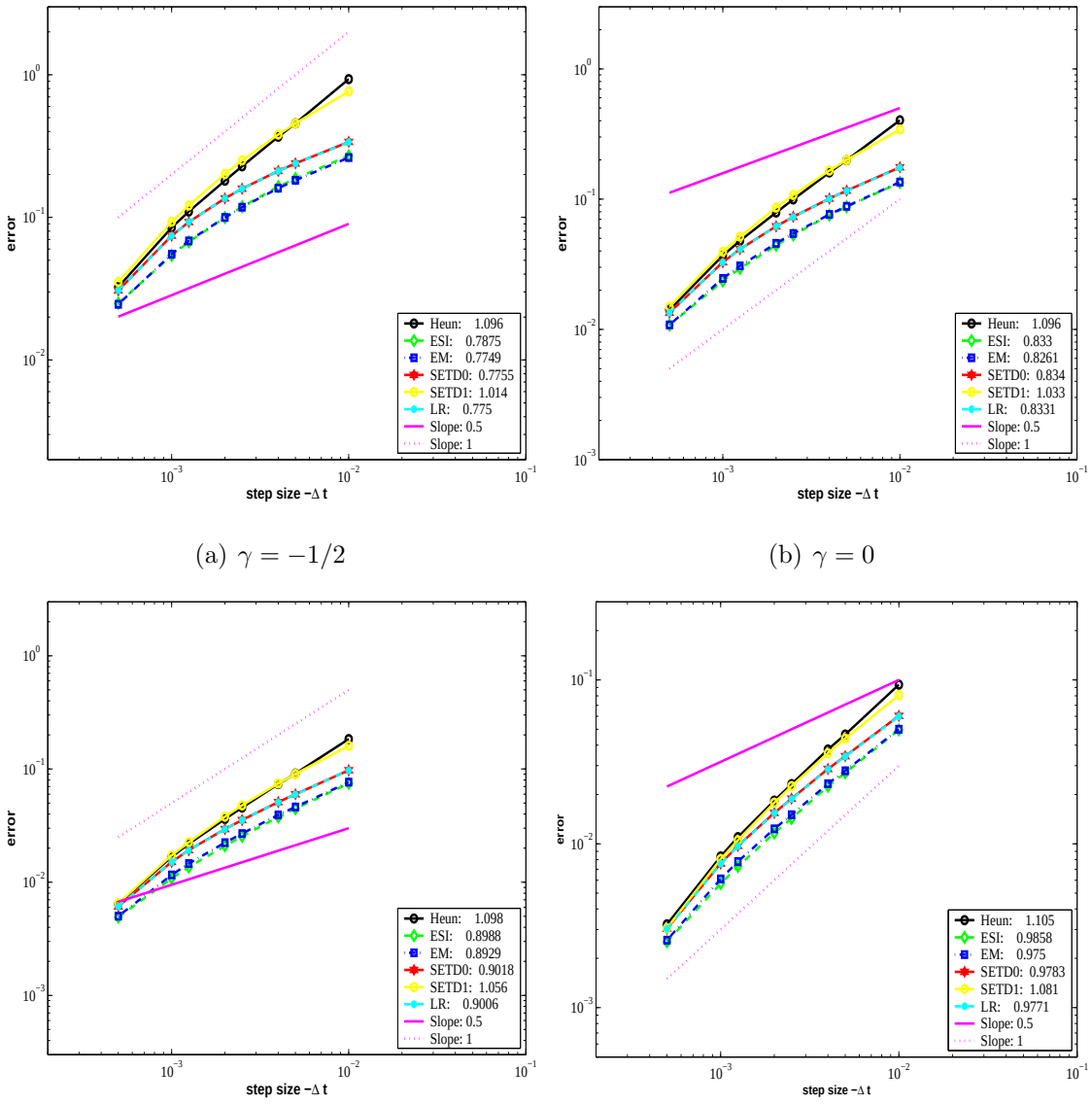

(a) $\gamma = -1/2$ (b) $\gamma = 0$

(c) $\gamma = 1/2$ (d) $\gamma = 1$

Figure 5.6: Convergence in time for the **SETD0**, **SETD1**, **LR**, **EM**, **ESI** and **Heun** schemes applied to the SH equation with additive infinite-dimensional noise (5.2.10). The plot is a log-log plot of the numerical strong error (5.3.19) on $[0, 1]$. From (a) - (d), is the plot of the numerical strong error (5.3.19) versus time step. In (a) $H^{-1/2}$, (b) H^0, (c) $H^{1/2}$ and (d) H^1 noise. We see that the numerical orders of convergence for the Itô schemes and the **ESI** scheme increase from 0.78 to 0.98 as we increase the spatial regularity of the noise. The **Heun** scheme consistently has strong order 1.

best method amongst the Itô schemes.

Figure 5.6 displays the strong order of convergence for the SH equation (5.2.10) with additive noise. Clearly, for this numerical example, the **EM** scheme behaves like the **ESI** scheme and they both have the smallest error amongst the Itô and Stratonovich schemes. The **SETD1** and **Heun** schemes though have the largest error, they both have strong order 1, which is faster than the other numerical methods. The strong order of convergence of all the numerical methods increase as the regularity of noise is increased. Although, we observe that for this fourth-order SPDE, the rate of convergence obtained from using $H^\gamma, \gamma = -1/2, 0, 1/2, 1$ noise is faster compared with the AC equation. This is because the SH equation has smoother solutions.

5.5 SPDEs with small noise:

In this section, we are interested in investigating the effects of small noise on convergence of numerical methods applied to SPDEs. We carry out experiments in exactly the same way as the sections above but now with small noise, by taking a noise intensity value of $\epsilon = 0.02$ in all the numerical simulations.

In Figure 5.8(a), we show the strong order of convergence of the Itô schemes: **SETD0** (5.3.1), **SETD1** (5.3.4), **LR** (5.3.7) and **EM** (5.3.10) schemes applied to the Itô AC equation (5.2.1) driven by a one-dimensional multiplicative noise and the Stratonovich schemes **ESI** (5.3.13) and **Heun** (5.3.16) schemes applied to Stratonovich AC equation (5.2.2) driven by a one-dimensional multiplicative noise. We obtain strong orders of convergence of ≈ 1 for all the numerical methods. The **SETD0** for which we proved a theoretical convergence result in this thesis, (see Theorem 4.4.1) indicates that the numerical result is indeed in good agreement with theory for small noise. In comparing our theory with numerical simulations, we consider that the noise intensity ϵ scales like $\Delta t^{0.5}$, in which case the term that dominates in the error estimates as obtained in the Theorem is $\epsilon\Delta t$. We see that the **LR** scheme has the largest error in this numerical example when compared to the other numerical methods. In terms of

efficiency, the **SETD0** and **SETD1** schemes are computationally the fastest followed by the **ESI** and **EM** scheme. The **Heun** method is the least efficient, see Figure 5.8(b).

In Figure 5.9(a), we present the strong convergence of the Itô and Stratonovich schemes applied to the SH equation with a one-dimensional multiplicative noise (5.2.6) and (5.2.7) respectively using a small noise intensity values of $\epsilon = 0.02$. All the numerical methods converge with strong order 1. We see that the **Heun** method behaves like the **ESI** scheme. The **SETD0** and **SETD1** schemes are the most efficient amongst the Itô schemes and just as we have seen previously the **ESI** scheme takes less computational time when compared to the **Heun** scheme, see Figure 5.9(b).

In Figure 5.10, we show for different spatial regularity of noise, the strong convergence of the **SETD0**, **SETD1**, **LR** and the **EM** schemes when applied to the Itô AC equation with infinite-dimensional multiplicative noise and the **ESI** and **Heun** schemes when applied to the Stratonovich AC equation with infinite-dimensional multiplicative noise with small noise intensity $\epsilon = 0.02$. We observe strong order ≈ 1 when we take H^γ noise with $\gamma = 0, 1/2, 1$. However, when noise is in $H^{-1/2}$, only the **LR** scheme amongst the Itô schemes achieved the strong order ≈ 1 for small noise, but with the price of larger errors at each time step when compared to the other numerical method, which are seen to produces strong order ≈ 0.8. In these cases, to achieve an order 1 rate of convergence, the noise intensity value needs to be taken much smaller. The observed trends for the AC equation with an infinite-dimensional multiplicative noise is also seen for the case of AC equation with additive noise forcing, see Figure 5.12.

Numerical simulations to test the strong orders of convergence of the Itô and Stratonoivch schemes applied to the Itô SH equation with infinite-dimensional noise (5.2.8) and Stratonovich SH equation (5.2.9) multiplicative noise using small noise intensity value $\epsilon = 0.02$ suggest strong orders ≈ 1 when noise is in H^1, see Figure 5.11. Similar trend is also observed for the numerical methods applied to the SH equation with infinite-dimensional additive noise, see Figure 5.13.

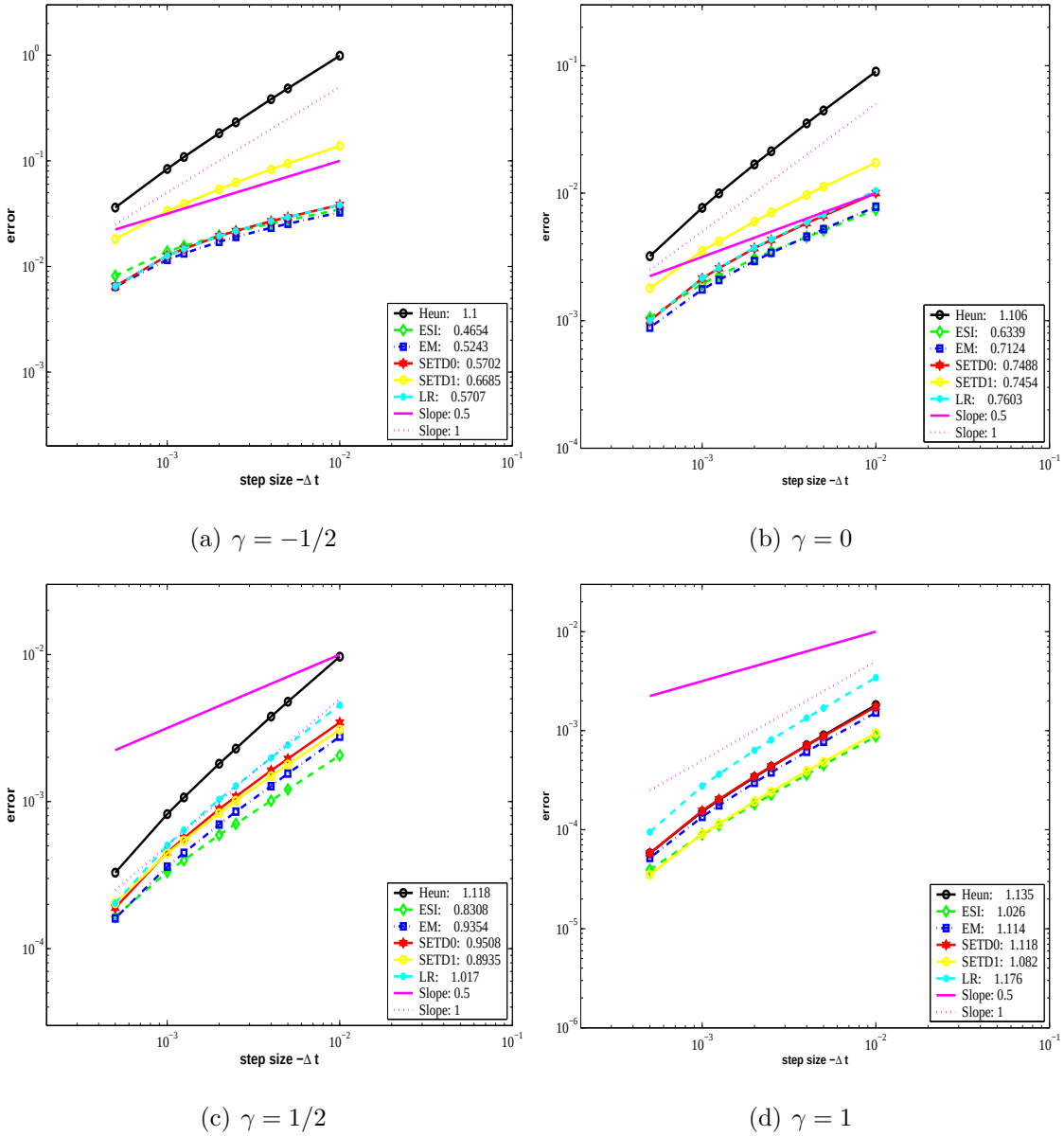

(a) $\gamma = -1/2$ (b) $\gamma = 0$

(c) $\gamma = 1/2$ (d) $\gamma = 1$

Figure 5.7: Convergence in time for the **SETD0**, **SETD1**, **LR**, **EM**, **ESI** and **Heun** schemes applied to the AC equation with additive infinite-dimensional noise (5.2.5). The plot is a log-log plot of the numerical strong error (5.3.19) on $[0, 1]$. From (a) - (d), is the plot of the numerical strong error (5.3.19) versus time step. In (a) $H^{-1/2}$, (b) H^0, (c) $H^{1/2}$ and (d) H^1 noise. We observe that the numerical orders of convergence for the Itô schemes and the **ESI** scheme increase from 0.5 to 1 as we increase the spatial regularity of the noise. The **Heun** scheme consistently has strong order 1 as expected.

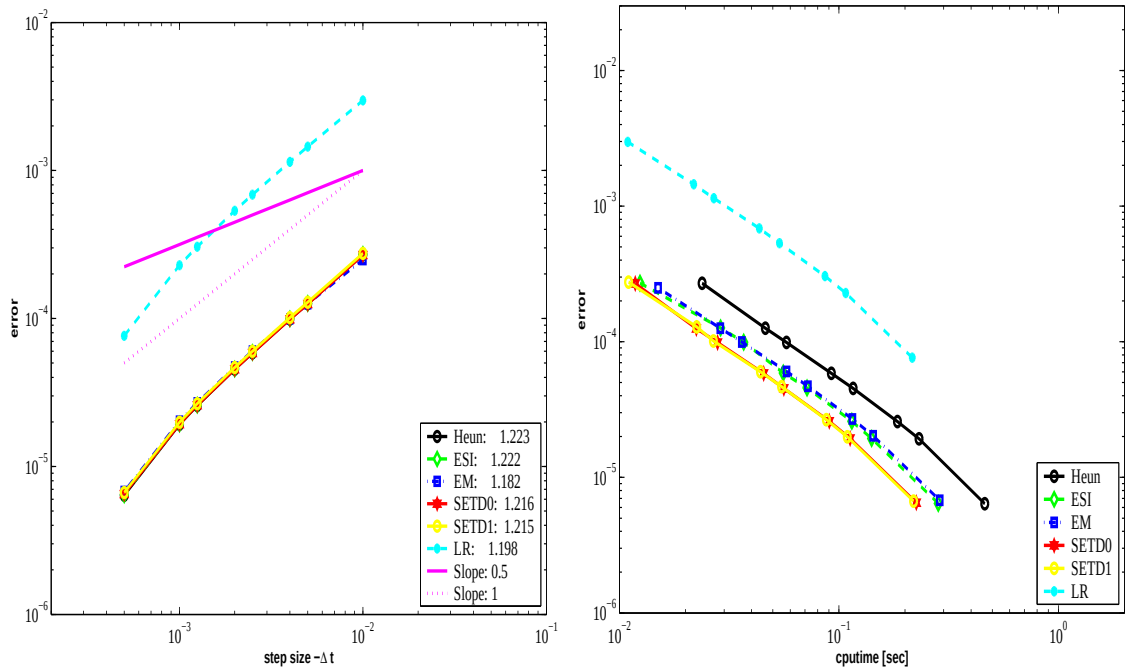

(a) (b)

Figure 5.8: Convergence in time for the **SETD0**, **SETD1**, **LR** and **EM** schemes applied to the AC equation with one-dimensional multiplicative noise (5.2.1) and the **ESI** and **Heun** schemes applied to the AC equation with one-dimensional multiplicative noise (5.2.2) with small noise intensity $\epsilon = 0.02$. The plot is a log-log plot of the numerical strong error (5.3.19) on $[0, 1]$. In (a) is the plot of the numerical strong error (5.3.19) versus time step size Δt and in (b) is the plot of the numerical error (5.3.19) versus cputime. We see that the numerical orders of convergence of the Itô schemes and the Stratonovich schemes are ≈ 1.

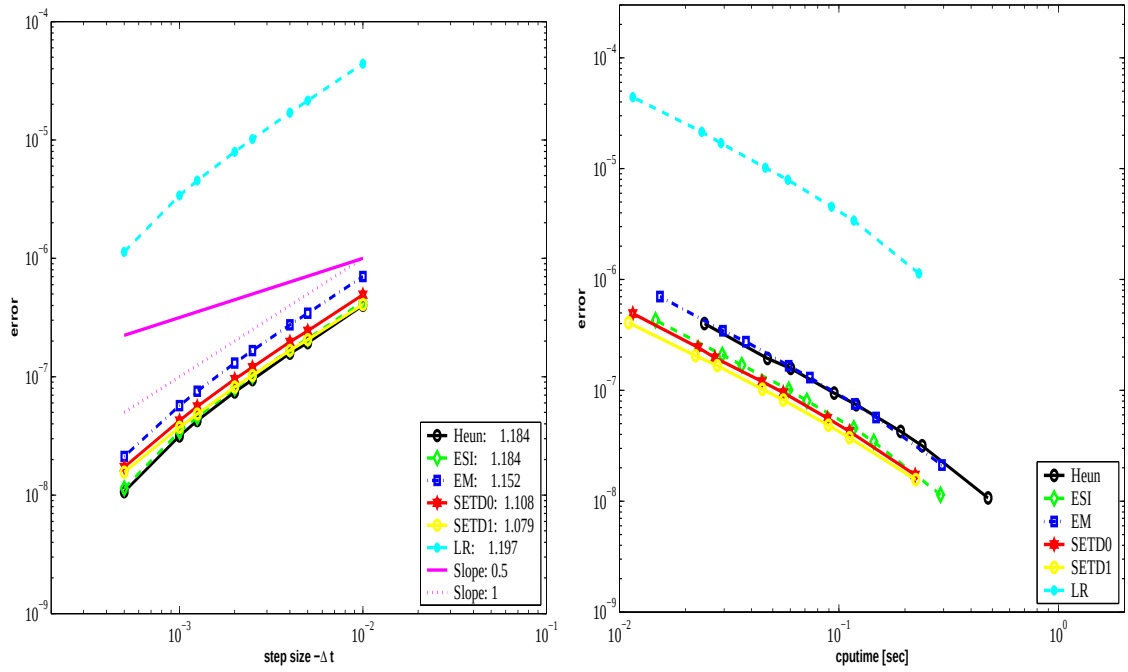

(a) error versus Δt for $\gamma = -0.5$

(b) error versus cputime $\gamma = -0.5$

Figure 5.9: Convergence in time for the Itô schemes: **SETD0**, **SETD1**, **LR** and **EM** schemes applied to the SH equation with one-dimensional multiplicative noise (5.2.1) and the **ESI** and **Heun** schemes applied to the SH equation with one-dimensional multiplicative noise (5.2.2) with small noise intensity $\epsilon = 0.02$. The plot is a log-log plot of the numerical strong error (5.3.19) on $[0, 1]$. In (a) is the plot of numerical strong error (5.3.19) versus time step size Δt and in (b) is the plot of numerical strong error (5.3.19) versus cputime. All the numerical schemes converge to a strong order of ≈ 1. The **SETD0** scheme for which we proved a convergence result suggests an order of convergence of 1 and this result is in excellent agreement with the numerical result as shown in this figure.

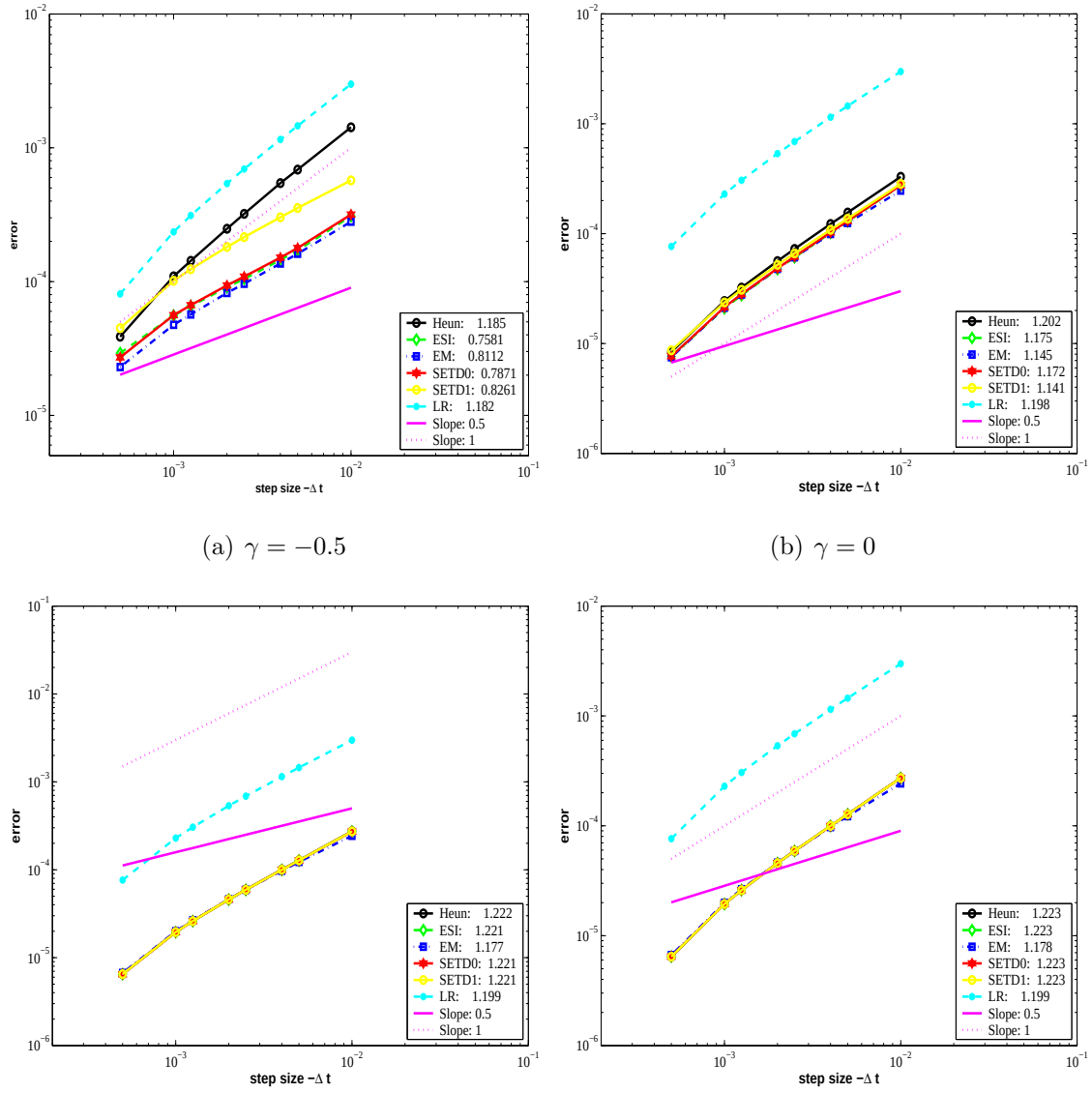

(a) $\gamma = -0.5$ (b) $\gamma = 0$

(c) $\gamma = 0.5$ (d) $\gamma = 1$

Figure 5.10: Convergence in time for the **SETD0**, **SETD1**, **LR** and **EM** schemes applied to the AC equation with multiplicative infinite-dimensional noise (5.2.3) and the **ESI** and **Heun** schemes applied to the AC equation with multiplicative infinite-dimensional noise (5.2.4) with small noise intensity $\epsilon = 0.02$. The plot is a log-log plot of the numerical strong error (5.3.19) on $[0, 1]$. From (a) - (d), is the plot of the numerical strong error (5.3.19) versus time step. In (a) $H^{-1/2}$, (b) H^0, (c) $H^{1/2}$ and (d) H^1. We see that the numerical orders of convergence for all the numerical method is ≈ 1 for $H^\gamma, \gamma = 0, 1/2, 1$. For the case of $H^{-1/2}$, only the **LR** and **Heun** schemes achieved order 1, the other numerical schemes are of orders ≈ 0.8.

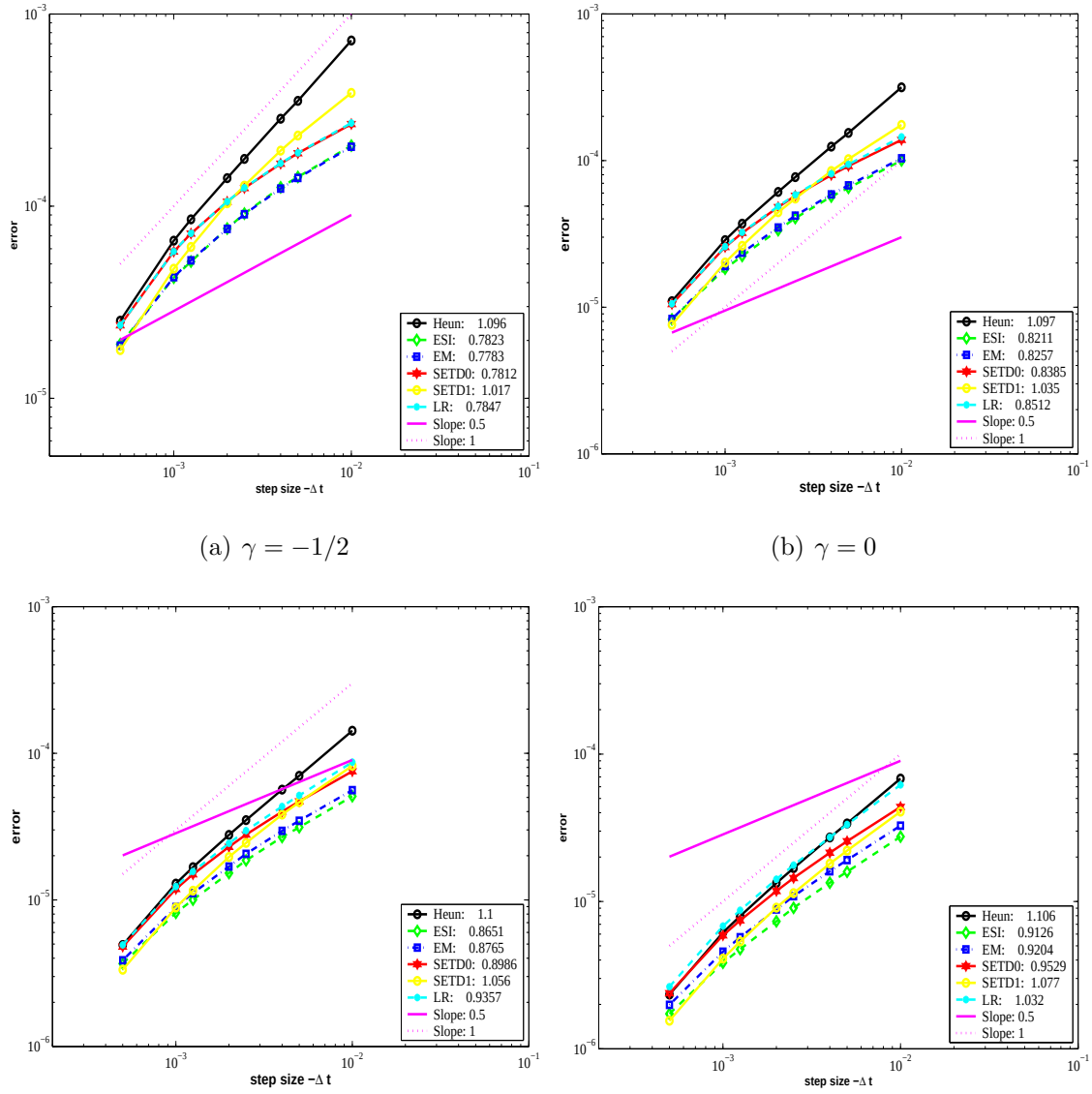

(a) $\gamma = -1/2$ (b) $\gamma = 0$

(c) $\gamma = 1/2$ (d) $\gamma = 1$

Figure 5.11: Convergence in time for the **SETD0**, **SETD1**, **LR** and **EM** schemes applied to the SH equation with multiplicative infinite-dimensional noise (5.2.8) and the **ESI** and **Heun** schemes applied to the SH equation with multiplicative infinite-dimensional noise (5.2.9) with small noise intensity $\epsilon = 0.02$. The plot is a log-log plot of the numerical error (5.3.19) on $[0, 1]$. From (a) - (d), is the plot of the numerical strong error (5.3.19) versus time step. In (a) $H^{-1/2}$, (b) H^0, (c) $H^{1/2}$ and (d) H^1 noise. We see that the order of convergence for the (5.3.2), (5.3.8), (5.3.11) and (5.3.14) is $\approx 0.8, 0.9, 1, 1$ for $H^\gamma, \gamma = -1/2, 0, 1/2, 1$ respectively. The **Heun** method has order 1 for all the different spatial regularities.

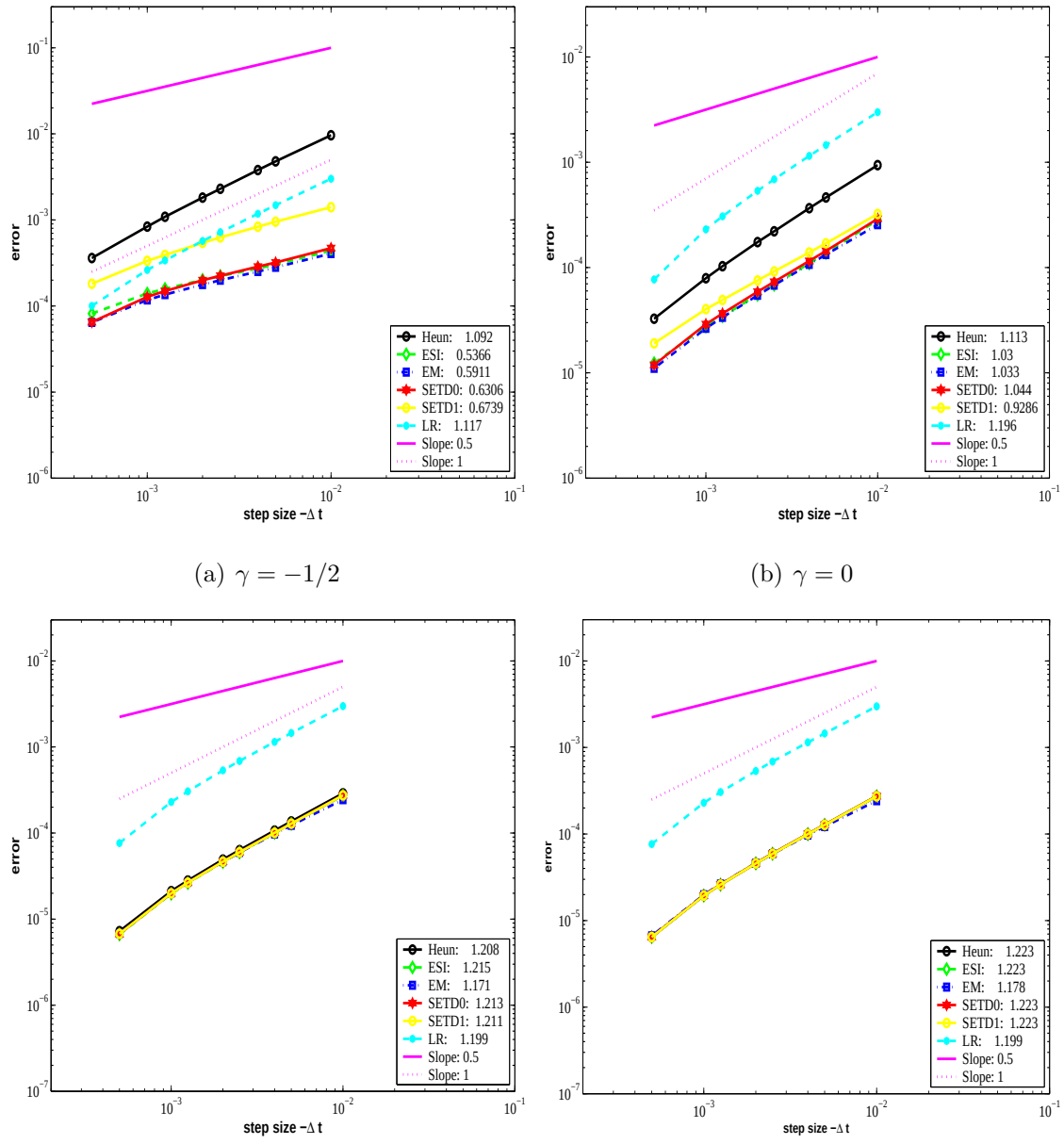

(a) $\gamma = -1/2$ (b) $\gamma = 0$

(c) $\gamma = 1/2$ (d) $\gamma = 1$

Figure 5.12: Convergence in time for the **SETD0**, **SETD1**, **LR**, **EM**, **ESI** and **Heun** schemes applied to the AC equation with additive infinite-dimensional noise (5.2.5) with small noise intensity $\epsilon = 0.02$. The plot is a log-log plot of the numerical strong error (5.3.19) on $[0, 1]$. From (a) - (d), is the plot of the numerical strong error (5.3.19) versus time step. In (a) $H^{-1/2}$, (b) H^0, (c) $H^{1/2}$ and (d) H^1 noise. We see that the numerical orders of convergence for the numerical methods are ≈ 1 for $H^\gamma, \gamma = 0, 1/2, 1$. For the case of $H^{-1/2}$, only the **LR** and the **Heun** schemes achieved order 1.

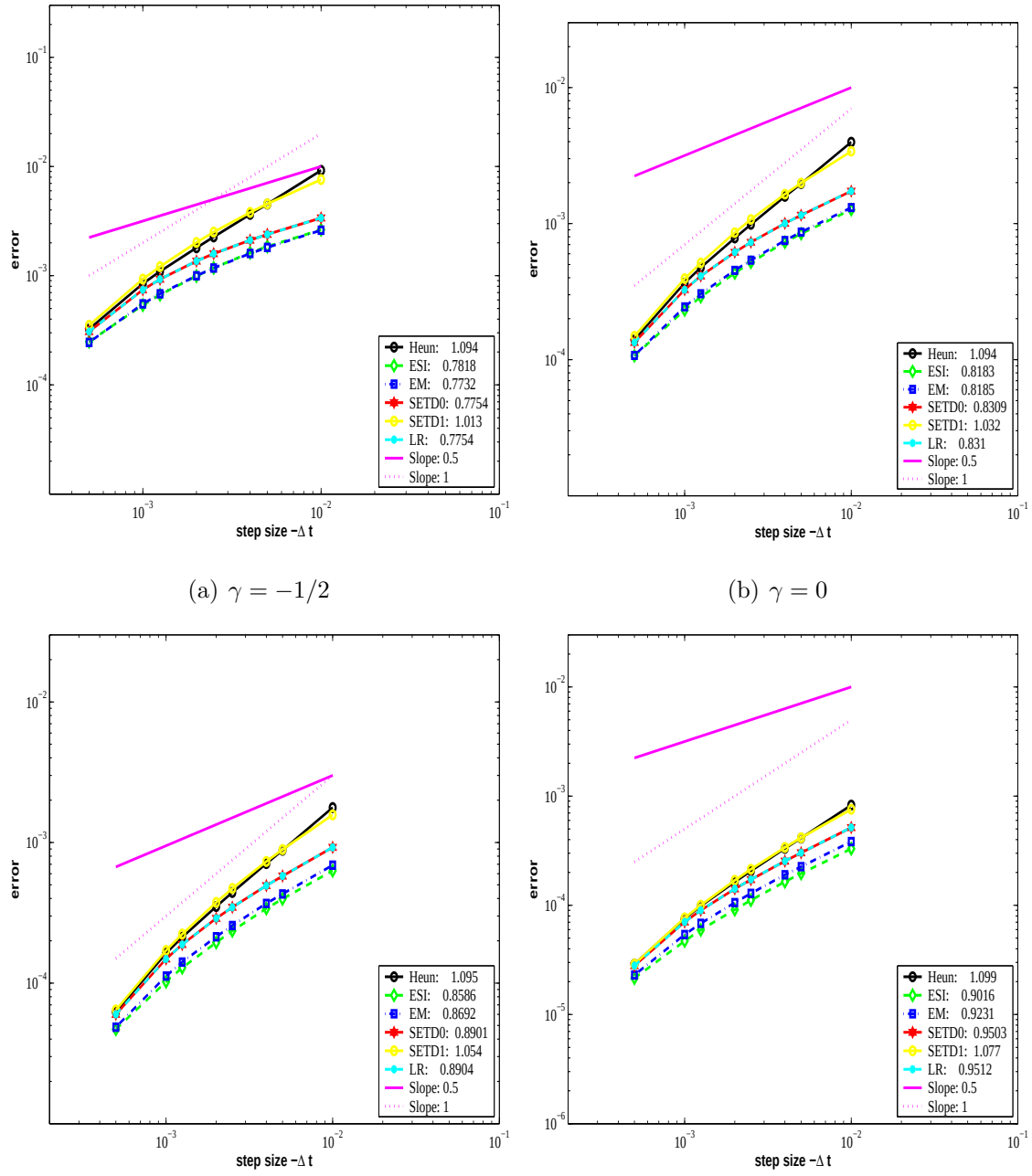

(a) $\gamma = -1/2$ (b) $\gamma = 0$

(c) $\gamma = 1/2$ (d) $\gamma = 1$

Figure 5.13: Convergence in time for the **SETD0**, **SETD1**, **LR**, **EM**, **ESI** and **Heun** schemes applied to the SH equation with additive infinite-dimensional noise (5.2.10) with small noise intensity, $\epsilon = 0.02$. The plot is a log-log plot of the numerical strong error (5.3.19) on $[0, 1]$. From (a) - (d), is the plot of the numerical strong error (5.3.19) versus time step. In (a) $H^{-1/2}$, (b) H^0, (c) $H^{1/2}$ and (d) H^1 noise.

5.6 Concluding remarks.

First, numerical simulation results for the **SETD0** scheme applied to SPDEs with one-dimensional multiplicative noise agree with the theoretical convergence results we proved in this thesis. It was shown that the **SETD0** converges with strong orders 0.5 and 1 when applied to SPDEs with large and small noise intensities respectively. We remark that the strong convergence of the **SETD0** scheme also works when applied to infinite-dimensional multiplicative noise, as we have shown through numerical experimentation.

Secondly, we observed that the higher the regularity of the noise, the higher the order of convergence of the numerical methods. We also observe that the error decreases with an increase in the regularity.

Thirdly, we obtain improved order of strong convergence for small noise SPDEs. Finally, in most of the numerical examples we carried out simulations on, the **ESI** schemes is the most accurate and efficient numerical methods amongst the Stratonovich schemes and the **SETD0** and **SETD1** schemes are the most accurate and efficient amongst the Itô schemes.

Chapter 6

Numerics for the Swift-Hohenberg SPDE.

In this chapter, we numerically investigate the influence of stochastic forcing on the Swift-Hohenberg (SH) equation. We perform experiments with three forms of forcing, that is, forcing with infinite-dimensional multiplicative Stratonovich noise, infinite-dimensional multiplicative Itô noise and infinite-dimensional additive noise. In particular, our aim in this Chapter is to examine the effects of noise on the pinning region in the bifurcation diagram of the deterministic SH equation, for specific cases of the control parameter r, see Figure 6.1(b). The numerical methods employed for the simulation of the equation is the **ESI** method introduced in section 3.2 for the case where noise is considered in the Stratonovich sense and the **SETD0** method for the case where noise is taken in the Itô sense. For the case where noise is additive, we remark that the Itô equation and Stratonovich equation are equivalent, therefore the **SETD0** and the **ESI** schemes coincides. Finally, we present numerical results for a range of noise intensities and varying spatial correlation lengths.

6.1 Introduction to the Swift-Hohenberg equation.

The Swift-Hohenberg model for hydrodynamic instability for the Rayleigh-Bérnard convection was first introduced in 1976 by Swift and Hohenberg [89]. Since then, the

model has been used for studying nonlinear phenomena in various fields: For example, pattern formation and hydro dynamical instability problems where the model describes the onset of convection in a Rayleigh-Bénard cell heated from below (see [10, 27]), hydrodynamics [89], nonlinear optics [69], elasticity and solid mechanics [16]. The Swift-Hohenberg model is a higher-order extension of the classical Fisher-Kolmogorov model [87].

The model is written as a PDE in the following form:

$$\frac{\partial u}{\partial t} = \Big(ru - \Big(\Delta + q_c^2\Big)^2 u + \rho u^2 - gu^3\Big), \tag{6.1.1}$$

where $u(0) = u_0$ is the initial data to be supplied, $x \in [-L, L]$, $r \in \mathbb{R}$ is the bifurcation or control parameter which may change the qualitative behaviour of the solutions of (6.1.1) and the parameters q_c, ρ and g are coefficients that are taken as fixed. Δ denotes the Laplace operator. The function u in (6.1.1) plays the same role as the variable for concentration in chemical reactions or temperature in convection problems. It is well known that the Swift-Hohenberg PDE exhibits multiple stable and unstable spatially localized states (see, [72, 92, 93]). The deterministic SH equation given in (6.1.1) has a quadratic and cubic nonlinearity. This form of equation was studied in [10] in which they showed the existence of these localized states, also the SH equation with cubic and quintic nonlinearities was investigated in [12] . The homoclinic snaking is illustrated graphically in the bifurcation diagram for the SH equation, see Figure 6.1(b), where the snaking is pinned in an interval $-0.01453 \leq r \leq -0.01245$.

Our main aim in this chapter is to study the effects of noise on this pinning region.

In the literature, the effects of noise have been studied on the SH equation, for example, in [95], the phenomenon of stochastic resonance in the Swift-Hohenberg equation was studied and they showed that the presence of Gaussian space time white noise in combination with periodic signal in spatial non-linear systems may give rise to ordered spatiotemporal structures which are not present in the absence of noise and also pointed out that the presence of spatiotemporal stochastic resonance arising when the

system undergoes a bifurcation is a usual mechanism for pattern formation.
It was shown in [27] that when the SH equation with a multiplicative noise term is used to model the behaviour of the onset of convection in a Rayleigh- Bénard cell, the noise can induce a shift in the change from conduction to convection, and cause convection patterns to arise, a phenomenon which will not exist in the absence of noise. In [27] also, multiplicative noise was found to have a stabilizing effect on the convective structure.

The motivation for undergoing these studies comes from the work in [10]. In their work, they investigated the localized states in the deterministic SH equation (6.1.1) and show a bifurcation diagram with four branches. Two of the branches are homoclinic, the other is flat and the last one is patterned. On one of the homoclinic branches lie four sample profiles and on the other branch lie two sample profiles. Localized states were found to lie on the two homoclinic solutions contained in a pinning interval, a result for the bifurcation of the SH equation, (see Figures 8 & 9 in [10]).
In our work, we examine the dynamical behaviour of the Swift-Hohenberg equation (6.1.1) forced with multiplicative and additive noise, in particular, we investigate the effect of noise on the pinning region containing one homoclinic branch for a sample profile. In the case of multiplicative noise, we consider the scenarios where the stochastic SH equation is interpreted in the Stratonovich and Itô sense. We perform continuation on the control parameter r for the deterministic SH equation, and obtain the bifurcation diagram in Figure 6.1(b).
In order to study the effects of noise on the SH equation (6.1.1), we fix the parameters q_c, ρ and g by taking $q_c = 0.5, \rho = 0.41$ and $g = 1$ and then allow the control parameter r to fluctuate, so that instead of having the term ru in equation (6.1.1), we will have $(r + \nu dW)u$ for the case where the stochastic forcing is interpreted in the Itô sense and $(r + \nu \circ dW)u = ru + \nu u \circ dW$ for the case where the stochastic forcing is interpreted in the Stratonovich sense. The additive noise case does not necessarily have a direct effect on the control parameter, but we shall investigate this case to see if we get any effect.

We perform simulations using the following control parameter values, $r = -0.015$, -0.01453, -0.013, -0.01245, -0.012, and then examine the dynamics of the solution from the start of the integration time $t = 0$ to $T = 8000$. The key control parameter values where we hope to see an effect of noise are the parameter values outside the pinning interval of the deterministic SH equation, $-0.01453 \leq r \leq -0.01245$, that is, the control parameters $r = -0.015$ and / or $r = -0.012$.

We now give the equations we shall be performing numerical simulations on.

We consider the following SPDEs with infinite-dimensional noise

$$\text{“Stratonovich“}: \quad du(t) = \Big[Au(t) + f(u(t))\Big]dt + \nu u(t) \circ dW(t), \tag{6.1.2}$$

$$\text{“Ito“}: \quad \Big[Au(t) + f(u(t))\Big]dt + \nu u(t) dW(t), \tag{6.1.3}$$

$$\text{“Additive“}: \quad \Big[Au(t) + f(u(t))\Big]dt + \nu dW(t), \tag{6.1.4}$$

where $A = r - \left(\Delta + q_c^2\right)^2$ and $f(u) = \rho u^2 - g u^3$. The SPDEs are supplemented with periodic boundary condition

$$u(-L, t) = u(L, t); \quad t \geq 0, \quad L = 80, \tag{6.1.5}$$

and initial condition

$$u(x, 0) = \cos(0.45x)\text{sech}\left(\exp(0.0014x^2)\right); \quad x \in [-L, L]. \tag{6.1.6}$$

Note that in Chapter 5, the domain is $[0, 2\pi]$. In this Chapter, we change the domain to $[-80, 80]$. Equation (6.1.6) is a 'three-bumps' function similar to one of the sample profiles considered in [10], see Figure 6.1(a).

Equations (6.1.2), (6.1.3) and (6.1.4) are respectively the SH equation with infinite-dimensional multiplicative Stratonovich noise, infinite-dimensional multiplicative Itô noise and infinite-dimensional additive noise. The parameter ν denotes the noise intensity and $W(t)$ is the $\mathbb{Q}$-Wiener process, see Section 2.3.

In this chapter, we take noise to be white in time and with exponential decaying correlations in space, see Section 2.8.4 in Chapter 2.

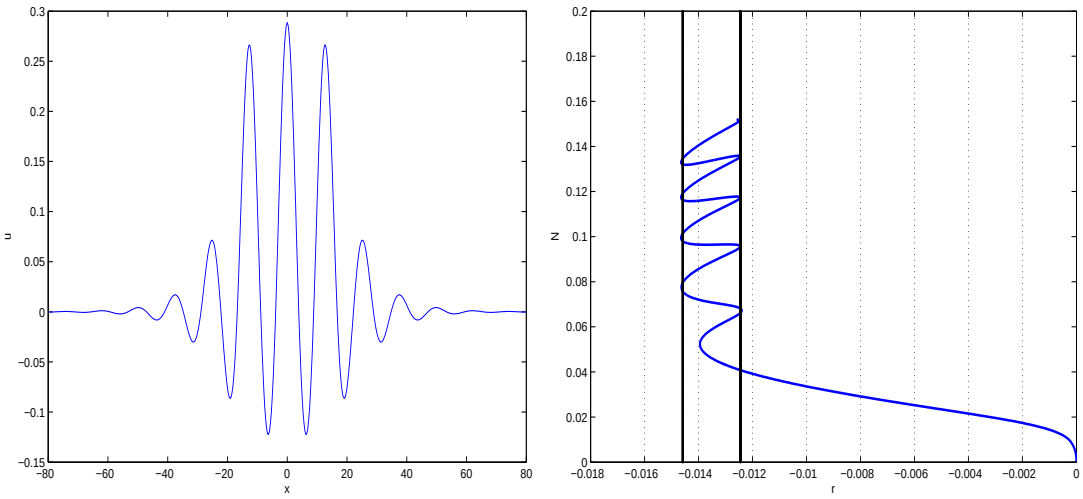

(a) (b)

Figure 6.1: (a) Plot of the three-bumps initial data. (b) A bifurcation diagram for the deterministic SH equation (6.1.1) showing the pinning region within which the solution is stable. We use parameters $r = -0.013, q_c = 0.5, \rho = 0.41$ and $g = 1$ to obtain the bifurcation diagram.

6.2 Numerical discretization of the SH equations.

We apply a Fourier Galerkin projection to the SPDEs (6.1.2), (6.1.3) and (6.1.4) and then use the finite dimensional subspace H_N of H and the projection operator P_N introduced in Section 2.8.1, to obtain a finite dimensional SDEs in the space H_N. The SODEs corresponding to the Fourier Galerkin projection of the SPDEs (6.1.2), (6.1.3) and (6.1.4) are given respectively by

$$du^N(t) = \Big[A_N u^N(t) + f_N(u^N(t))\Big]dt + \nu u^N(t) \circ dW^N(t), \tag{6.2.1}$$

$$du^N(t) = \Big[A_N u^N(t) + f_N(u^N(t))\Big]dt + \nu u^N(t) dW^N(t), \tag{6.2.2}$$

$$du^N(t) = \Big[A_N u^N(t) + f_N(u^N(t))\Big]dt + \nu dW^N(t). \tag{6.2.3}$$

To obtain an approximate solution for $u^N(t)$ in time on the interval $[0, T]$, we use the **ESI** scheme in (5.3.14) to approximate (6.2.1) and the **SETD0** schemes in (5.3.2) and (5.3.3) to approximate (6.2.2) and (6.2.3) respectively.

6.3 Numerical implementation & results.

We perform the numerical simulations of (6.1.2) - (6.1.4) using the following numerical parameters: Number of spatial grid points is 512 with $x \in [-80, 80]$, thus giving the spatial mesh size $\Delta x = 0.3125$. We start the simulation at time zero with a 3 bumps initial data, see Figure 6.1(a) and then evolve forward in time with a time step size equal to $\Delta t = 0.2$ until we reach a final time $T = 8000$. The following range of noise intensity values $\nu = 0, 0.1, \cdots, 1.5$ and correlation lengths $\zeta = 10, 1, 0.1$ were also used.

Correlation lengths of $\zeta = 1$ and 10 gives spatially correlated noise while a correlation length of $\zeta = 0.1$ gives spatially uncorrelated noise, since the length scale is less than Δx.

We first consider the effect of multiplicative Stratonovich noise on the SH equation, that is, we perform simulation on (6.1.2) using a range of control parameters inside, outside and on the boundary of the deterministic pinning region. Inside the pinning region is $r = -0.013$, outside the pinning region is one to the left and the other to the right. The parameter to the left of the pinning region is $r = -0.015$ and to the right of the pinning region is $r = -0.012$. Similarly, on the boundary, we have $r = -0.01453$ to be the control parameter on the boundary of the left-end pinning region and $r = -0.01245$ to be the control parameter on the boundary of the right-end pinning interval.

6.3.1 Effect of Stratonovich noise on the pinning region in the bifurcation for the SH equation.

We carry out simulations with all the control parameter values of interest as stated above and then report the experimental results on a case by case basis.

For all the cases, we will be interested in the behaviour of the solution at the final time T. In particular, we are interested in counting the number of bumps, so that we can compare with the initial function, which is a three-bumps function. In what follows, we present the algorithm used in calculating the number of bumps:

Algorithm for calculating the number of bumps:

- Simulate the SH equation to obtain the solution $u(x,t)$.
- Store the solution at the final time T, that is $u(x,T) = u(x,8000)$.
- Plot the solution $u(x,8000)$ on the y-axis and the spatial domain, $x \in [-80,80]$ on the x-axis.
- Set a threshold value $\theta_t = 0.15$, and plot this value as a horizontal line over the solution $u(x,8000)$, such the solution and the horizontal line both intersect.
- Calculate the number of times the solution $u(x,8000)$ crosses the threshold value and divide it by 2.
- The resulting answer gives the number of bumps.

We remark that although the individual path of the solution $u(x,8000)$ is non-smooth. We perform simulations for R realizations, and then average over the sample R. This is what we term the average number of bumps.

We observe that $R = 20$ is sufficient to obtain a path that appears smooth.

Hence, we define the average number of bumps as follows:

Let the number of bumps for the sth realization be denoted by $\#^s_{bumps}$.

Then, for a given R samples, the average number of bumps is computed from:

$$\frac{1}{R}\sum_{s=1}^{R} \#^s_{bumps}.$$

We now begin to consider the different cases of control parameters for our experiments:

Case 1: Outside the pinning region (left-end): $r = -0.015$

In Figure 6.2, is the plot of the average of number of bumps at final time T = 8000 versus noise intensity values $\nu = 0, 0.1, \cdots, 1.5$, for the simulation of (6.1.2). The error bars along the curve are the computed standard deviations for the number of

bumps over the range of noise intensity values $\nu = [0, 1.5]$. The error bars are obtained by using the mean and standard deviations of the number of bumps.

We have also added on the graph, reference lines which allows us to determine the number of bumps we get at the final time, T for the range of increasing noise intensities. We see in Figure 6.2(a) - 6.2(c) that at noise intensity value $\nu = 0$ which is the deterministic solution dynamics, the solution at the final time T is the zero solution even though the time integration was started with a 3 bumps initial data. We now consider the effects of noise on this deterministic solution dynamics by taking spatially correlated noise with correlation lengths $\zeta = 10$, see Figure 6.2(a) and correlation lengths $\zeta = 1$, see Figure 6.2(b). Results suggest that over the range of noise intensity values $\nu \in (0, 1.5]$, we do not see any effect of noise on the dynamics of the solution. In other words, when we start the numerical simulations with a three-bump initial data, we eventually go to the zero solution as we evolve forward in time. However, when we considered a spatially uncorrelated noise (simulated here with $\zeta = 0.1$), we see in Figure 6.2(c) from $\nu = 0.7$ that the solution curves begin to ascend from the zero solution to the 3 bumps count reference line, and eventually evolve to the periodic solution as noise intensity increases. The case where the solution sticks at the 3 bumps is particularly interesting because that result suggests that, if we perform simulation on (6.1.2) using noise intensity value $\nu = 1$, correlation length $\zeta = 0.1$ and a 3 bumps initial data, we will obtain at the final time $T = 8000$, a solution dynamics of the SH equation (6.1.2) with 3 bumps. We see clearly in Figure 6.5(b) that the 3 bumps function sticks throughout the integration time, which points out that the spatially uncorrelated noise has a stabilizing effect on the bifurcations for the SH equation with multiplicative Stratonovich noise.

This is an interesting phenomenon which is absent in the deterministic scenario and hence indicates a stochastic resonance when the SH equation is forced with multiplicative Stratonovich noise. The implication of this phenomenon is that we will see a shift of the deterministic pinning region as a result of this stochastic forcing.

To support our claim of stochastic resonance in this case, we perform continuation on the control parameter r in AUTO using the Stratonovich-Itô corrected equation in

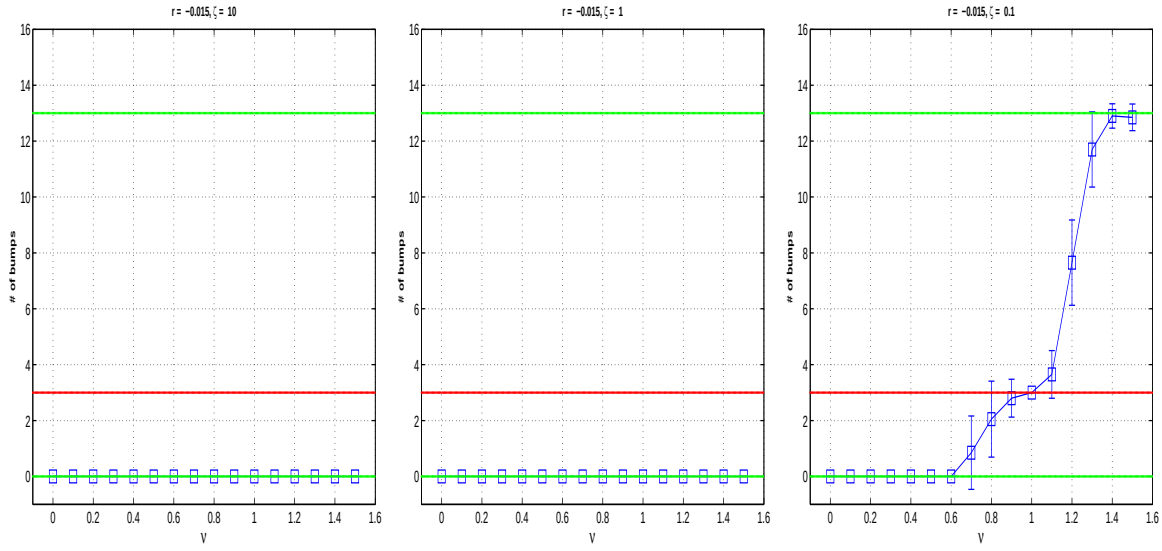

(a) $\zeta = 10$ (b) $\zeta = 1$ (c) $\zeta = 0.1$

Figure 6.2: A plot of the average of number of bumps at final time T = 8000 versus noise intensity ν, for the simulation of (6.1.2) with control parameter $r = -0.015$ (outside the pinning region - left-end). The error bars along the curve are the computed standard deviations for the number of bumps over the range of noise intensity values $\nu = [0, 1.5]$. From left to right is the correlation length used for the computations; in (a) $\zeta = 10$, (b) $\zeta = 1$, (c) $\zeta = 0.1$. Three straight lines have been added to the graph, the three lines denote a reference line for number of bumps count. The lines with the vertical axis value 0, 3 and 13 represent respectively, zero, three, periodic bumps count.

(6.4.2), with the small noise expansion analysis idea in [27]. Details of this is given in section 6.5. We see clearly in Figure 6.3 that the pinning region is shifted to the left. In Figure 6.4 & 6.5, we show on a space-time plot of the spatiotemporal evolution of the solution dynamics of the Stratonovich SH equation (6.1.2) with correlation length $\zeta = 0.1$ and noise intensities $\nu = 0, \cdots, 1.4$. These solutions are average solutions and were obtained over 20 realizations.

Case 2: On the left-end boundary of the pinning region: $r = -0.01453$

Figure 6.6(a) & 6.6(b) displays the result for spatially correlated noise applied to

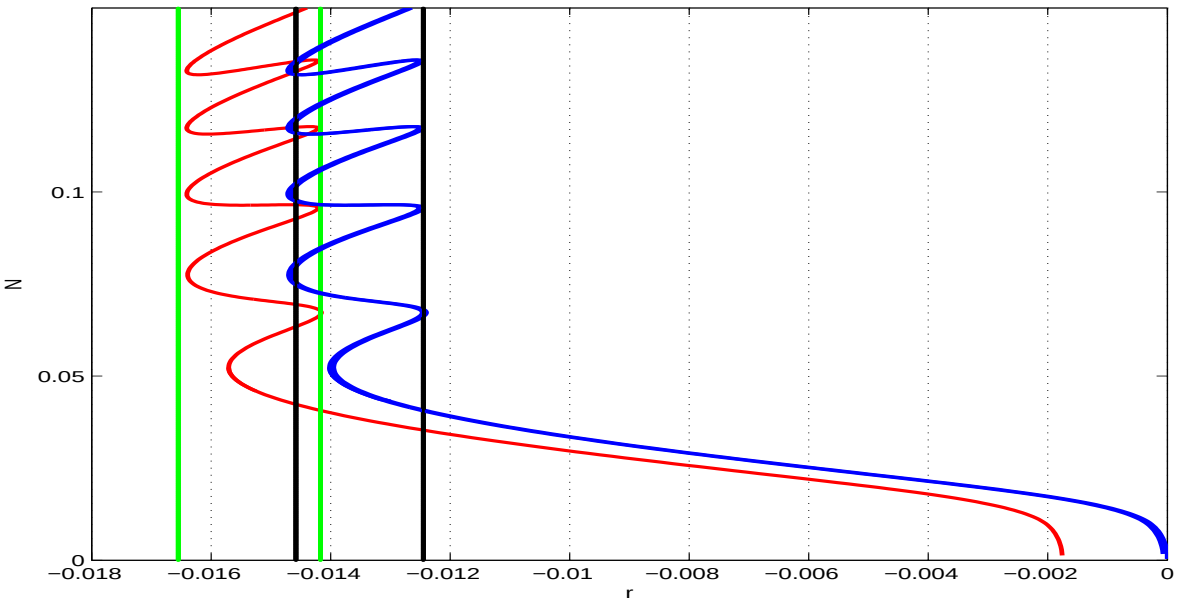

Figure 6.3: Bifurcation diagram for the Stratonovich SH equation with spatially uncorrelated noise. We add in the plot, the bifurcation diagram for the deterministic SH equation for comparison. We see the pinning interval of $-0.1453 \leq r \leq -0.01245$ for the deterministic SH equation and $-0.168 \leq r \leq -0.0146$ for the SH equation with Stratonovich spatially uncorrelated noise.

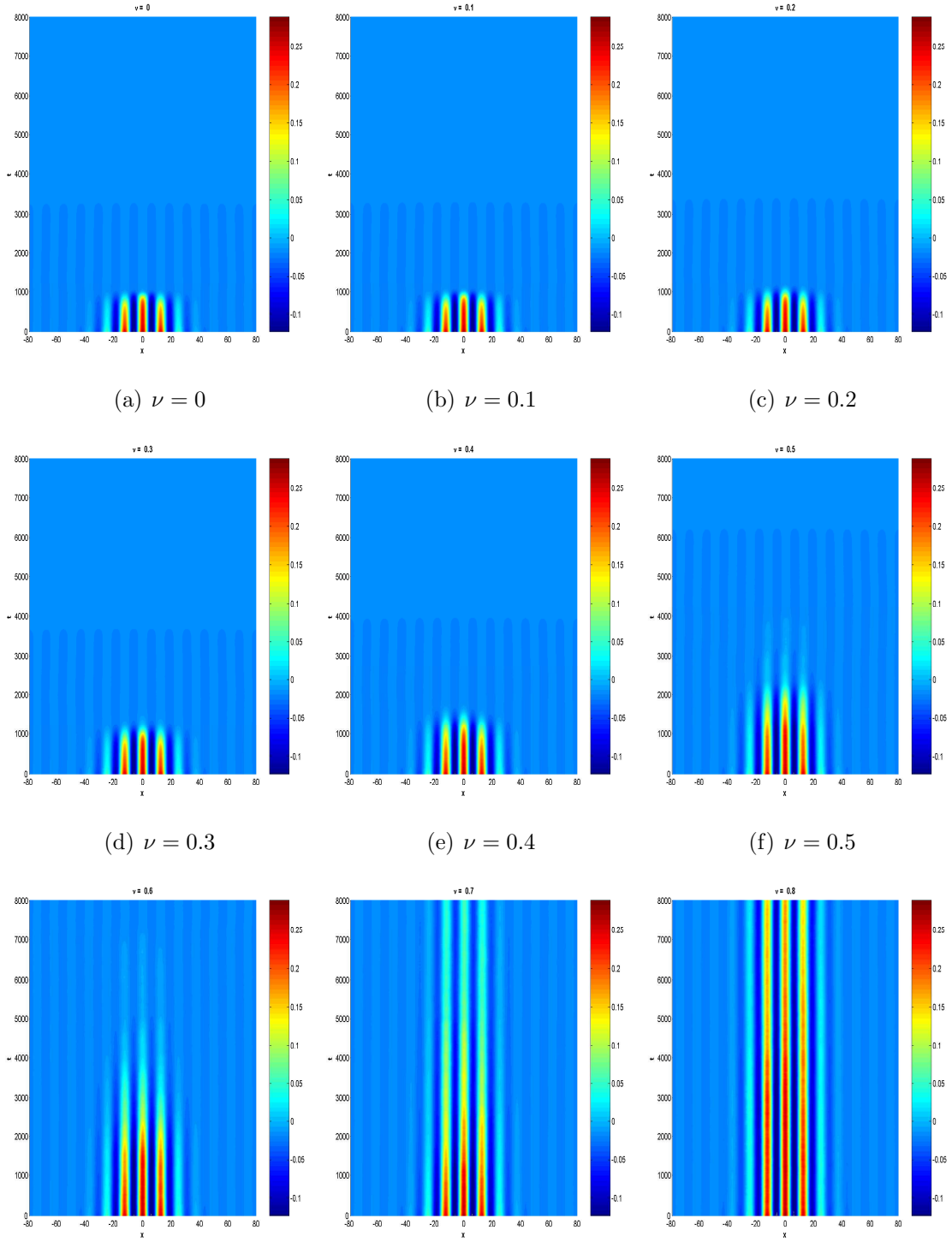

(a) $\nu = 0$ (b) $\nu = 0.1$ (c) $\nu = 0.2$

(d) $\nu = 0.3$ (e) $\nu = 0.4$ (f) $\nu = 0.5$

(g) $\nu = 0.6$ (h) $\nu = 0.7$ (i) $\nu = 0.8$

Figure 6.4: Spatiotemporal evolution of the solution dynamics of the Stratonovich SH equation (6.1.2) using fixed control parameter $r = -0.015$, correlation length $\zeta = 0.1$ and varying noise intensities, $\nu \in [0, 0.8]$. Other parameters are $q_c = 0.5, \rho = 0.41$ and $g = 1$. Solutions were averaged over 20 realizations.

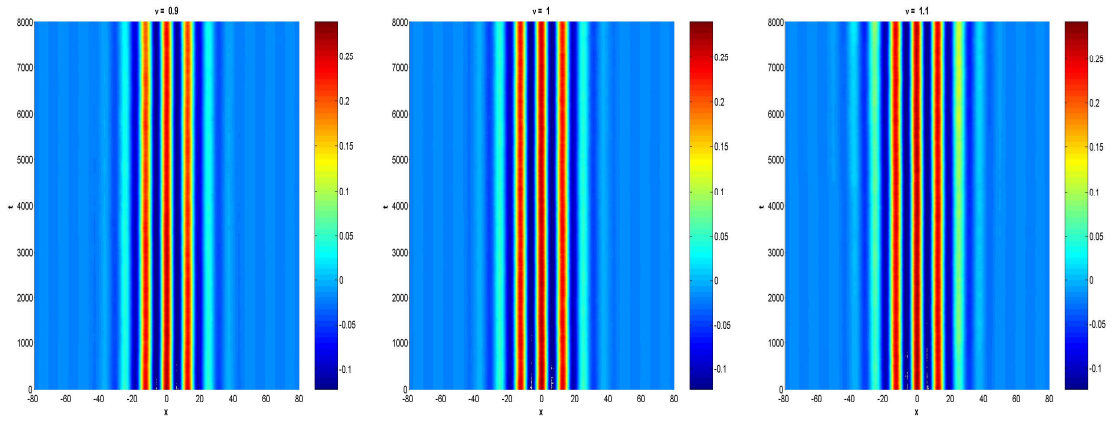

(a) $\nu = 0.9$ (b) $\nu = 1$ (c) $\nu = 1.1$

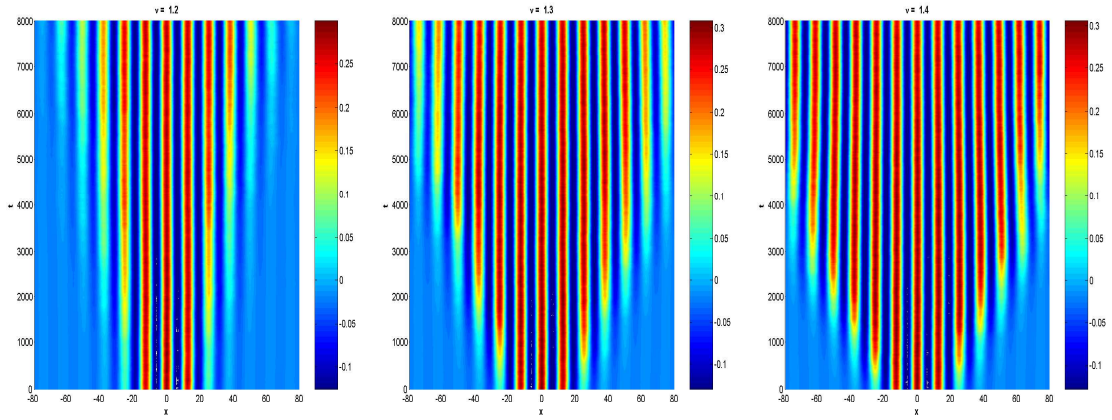

(d) $\nu = 1.2$ (e) $\nu = 1.3$ (f) $\nu = 1.4$

Figure 6.5: Spatiotemporal evolution of the solution dynamics of the Stratonovich SH equation (6.1.2) using fixed control parameter $r = -0.015$, correlation length $\zeta = 0.1$ and varying noise intensities, $\nu \in [0.9, 1.4]$. Other parameters are $q_c = 0.5, \rho = 0.41$ and $g = 1$. Solutions were averaged over 20 realizations.

(6.1.2). We see that the three bumps solution which exists in the deterministic setting, when $\nu = 0$, eventually ceases to exist when noise is taken into account, as we see that all the solutions for the increasing noise intensities do evolve to the zero solution, in other words, the 3 bumps solution destabilizes to the zero solution with the inclusion of spatially correlated noise. However, when spatially uncorrelated noise was used on (6.1.2), the three bumps solution existed in the deterministic setting and then stabilizes for large range of noise intensity parameter values in $\nu = [0, 0.9]$ before evolving to the periodic solution, see Figure 6.6(c). We also noticed that for noise intensity value $\nu \in [0.1, 0.4]$, the behaviour of the average solution is not 3 bumps, and this is might be as a result of realizations evolving to the zero solution.

Case 3: Inside the pinning region: $r = -0.013$

We study the effects of noise on (6.1.2) with control parameter $r = -0.013$, we observe that for spatially correlated noise with $\zeta = 10$, the solution is stable against noise for all the noise intensities examined, see Figure 6.7(a). Figure 6.7(b) shows the result with $\zeta = 1$, we see that the solution is stable against noise for noise intensity values $\nu = [0, 0.7]$ and then slowly evolve towards the periodic solution, although it never arrived to the periodic solution for the remaining noise intensity values we experimented with. Finally, Figure 6.7(c) shows that the solution is at stable against noise although with a smaller range of noise intensities values, that is, $\nu = [0, 0.4]$, when compared with the SH equation with spatially correlated noise. The solution eventually goes to the periodic solution with increasing noise intensity.

Case 4: On the right-end boundary of the pinning region: $r = -0.01245$

Figures 6.8(a), 6.8(b) & 6.8(c) display the result of the SH equation (6.1.2) with control parameter $r = -0.01245$, we observe that for all the correlation lengths considered in this experiment, the solution which is stable in the deterministic scenario is no longer stable even for very small noise, the solution is seen to evolve towards the periodic solution with increasing noise intensity values. We also observed that as $\zeta \to 0$, the three bumps solution evolves at a much faster rate to the periodic solution, which indeed gives an indication that spatially uncorrelated noise has stronger effect on the SH equation (6.1.2).

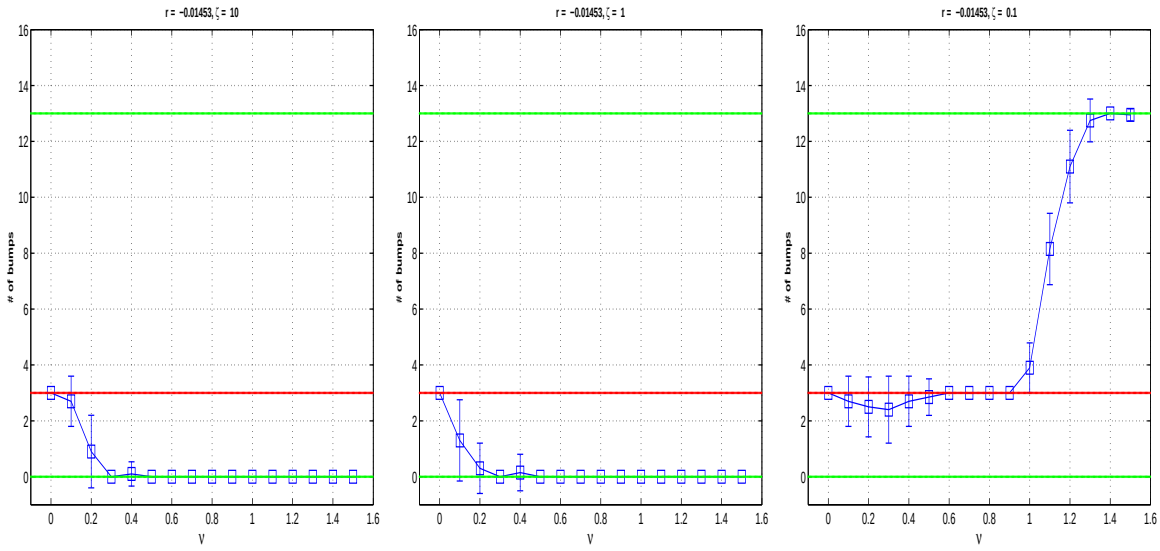

(a) $\zeta = 10$ (b) $\zeta = 1$ (c) $\zeta = 0.1$

Figure 6.6: A plot of the average of number of bumps at final time T = 8000 versus noise intensity ν, for the simulation of (6.1.2) with control parameter $r = -0.01453$ (left-end boundary of the pinning region). The error bars along the curve are the computed standard deviations for the number of bumps over the range of noise intensity values $\nu = [0, 1.5]$. From left to right is the correlation length used for the computations; in (a) $\zeta = 10$, (b) $\zeta = 1$, (c) $\zeta = 0.1$. The description for the straight lines in the graph is given in Figure 6.2.

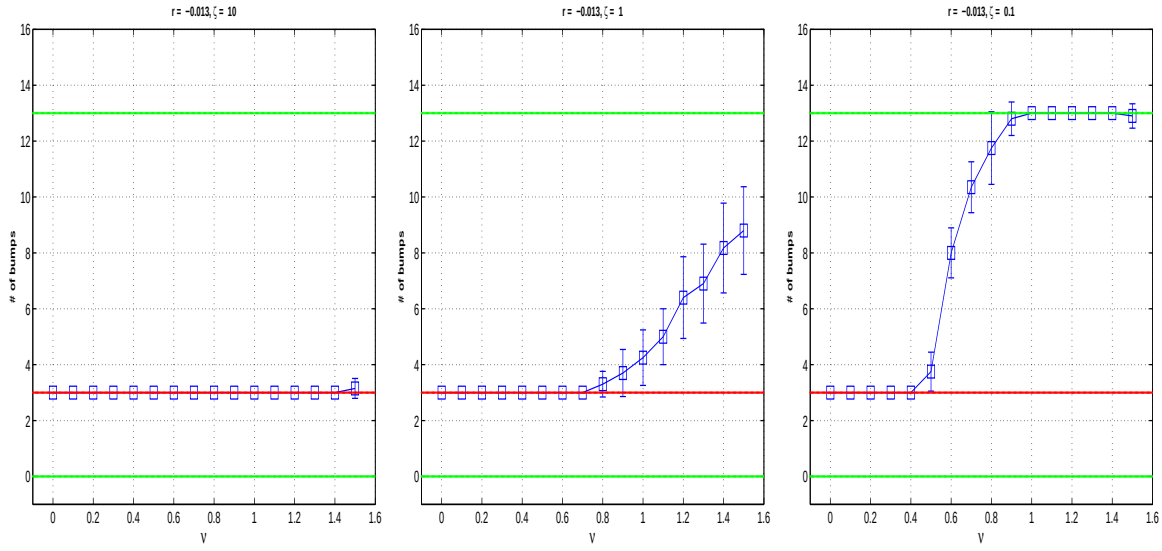

(a) $\zeta = 10$ (b) $\zeta = 1$ (c) $\zeta = 0.1$

Figure 6.7: A plot of the average of number of bumps at final time T = 8000 versus noise intensity ν, for the simulation of (6.1.2) with control parameter $r = -0.013$ (inside the pinning region). The error bars along the curve are the computed standard deviations for the number of bumps over the range of noise intensity values $\nu = [0, 1.5]$. From left to right is the correlation length used for the computations; in (a) $\zeta = 10$, (b) $\zeta = 1$, (c) $\zeta = 0.1$. The description for the straight lines in the graph is given in the caption to Figure 6.2.

Case 5: Outside pinning region (right-end): $r = -0.012$

For this case $r = -0.012$, we see in Figures 6.9(a), 6.9(b) & 6.9(c) that even though we start at a 3 bumps initial data to march the solution forward, the solution at the final time $T = 8000$ is periodic in the deterministic setting, that is, for noise intensity value $\nu = 0$. Inclusion of noise doesn't really show any new interesting dynamics, as can be observed that the solution evolves to the periodic case.

6.3.2 Effects of Itô noise on bifurcation for the SH equation.

In this section we briefly investigate whether Itô noise has any effect on the dynamics of the solution of Itô SH equation (6.1.3) and if it does, does it lead to the stabilizing

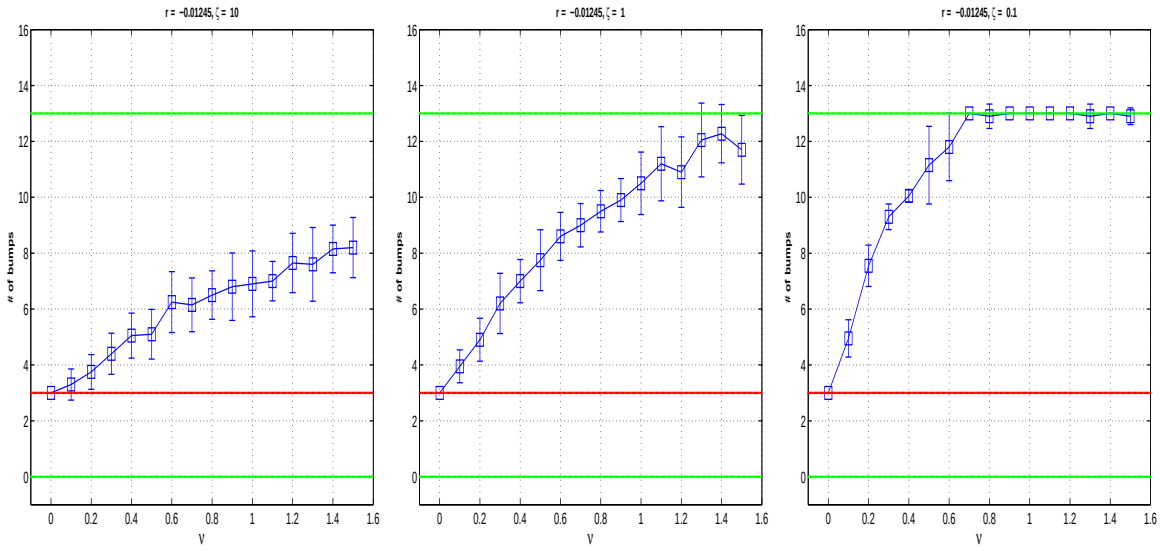

(a) $\zeta = 10$ (b) $\zeta = 1$ (c) $\zeta = 0.1$

Figure 6.8: A plot of the average of number of bumps at final time T = 8000 versus noise intensity ν, for the simulation of (6.1.2) with control parameter $r = -0.01245$ (right-end boundary of the pinning region). The error bars along the curve are the computed standard deviations for the number of bumps over the range of noise intensity values $\nu = [0, 1.5]$. From left to right is the correlation length used for the computations; in (a) $\zeta = 10$, (b) $\zeta = 1$, (c) $\zeta = 0.1$. The description for the straight lines in the graph is given in the caption to Figure 6.2.

effects we observed in the Stratonovich case? We carry out in the same manner the experiment as we implemented in the Stratonovich case. For the Itô case, numerical experiments to study the effects of noise on the control parameter values of interest suggests that multiplicative Itô noise does not produce a phenomenon different from what happens in the deterministic setting. We only report the results of the experiments carried out with control parameter $r = -0.015$, since we are mainly interested in what happens outside the left-end of the pinning region in the bifurcation diagram in Figure 6.1(b). We clearly see that for all the correlation lengths $\zeta = 0.1, 1$ & 10, we do not see any effect of noise on the dynamics of the SH equation when forced with Itô noise, see Figure 6.10. The solution remains at the zero state in the deterministic and for all the ranges of noise intensity considered. For the continuous flow of reading in this chapter, we do not display the figures for the other control parameter values here, since the results are not so particularly interesting.

6.3.3 Effects of additive noise on bifurcation for the SH equation.

In this section, we investigate the effect of additive noise on the SH equation. We perform numerical simulations on (6.1.4) using the control parameter $r = -0.015$ in the same manner as was done for other forms of stochastic forcing. Results shows (figures not displayed in the thesis) that we do not see any interesting effect of noise on bifurcation of (6.1.4) whether the noise is spatially correlated or not. Depending on the model, additive noise has been found in the literature to have stabilized and destabilized a phenomenon. For example in [5] they show that additive noise gave some stabilization effect, while in [22], additive noise was found to have a disordering effect on the convective pattern as the noise intensity is increased in the the two-dimensional SH equation.

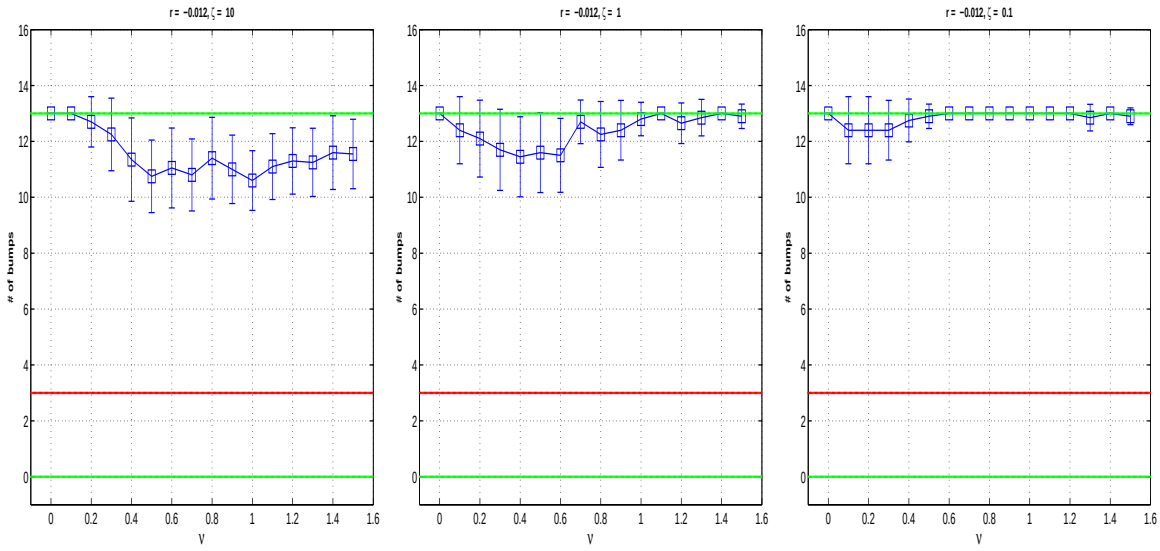

(a) $\zeta = 10$ (b) $\zeta = 1$ (c) $\zeta = 0.1$

Figure 6.9: A plot of the average of number of bumps at final time T = 8000 versus noise intensity ν, for the simulation of (6.1.2) with control parameter $r = -0.012$ (outside the pinning region - right-end). The error bars on the curve connecting the solutions for increasing noise intensities were calculated as the mean standard error. From left to right is the correlation length used for the computations; in (a) $\zeta = 10$, (b) $\zeta = 1$, (c) $\zeta = 0.1$. The description for the straight lines is given in the caption to Figure 6.2.

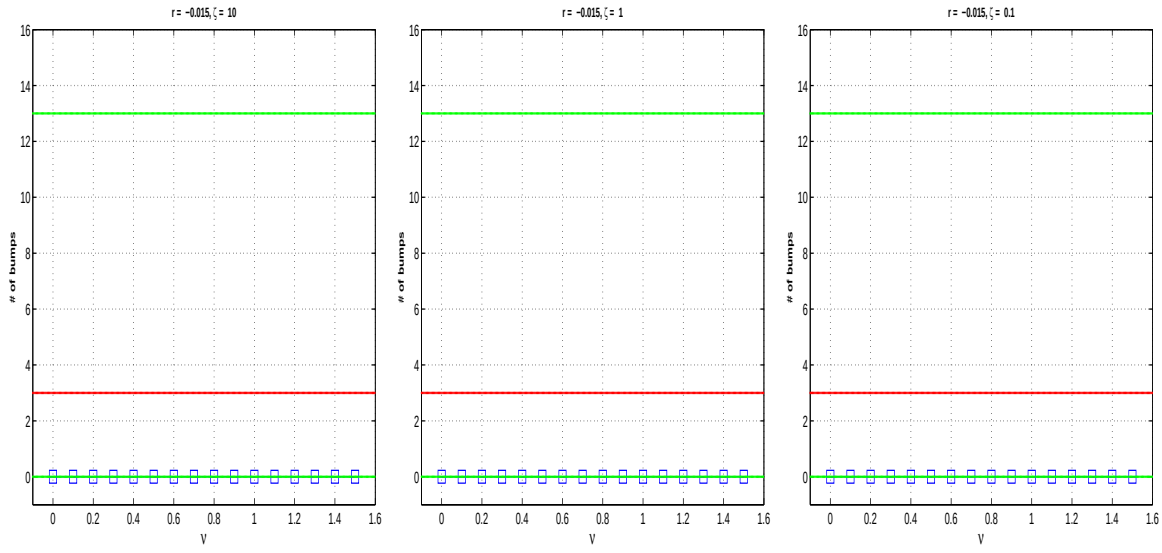

(a) $\zeta = 10$ (b) $\zeta = 1$ (c) $\zeta = 0.1$

Figure 6.10: Itô case: A plot of the average of number of bumps at final time T = 8000 versus noise intensity ν, for the simulation of (6.1.3) with control parameter $r = -0.015$. The error bars along the curve are the computed standard deviations for the number of bumps over the range of noise intensity values $\nu = [0, 1.5]$. From left to right is the correlation length used for the computations; in (a) $\zeta = 10$, (b) $\zeta = 1$, (c) $\zeta = 0.1$. The description for the straight lines in the graph is given in the caption to Figure 6.2.

6.4 Drift correction for Stratonovich SH equation into an Itô equation.

Our objective in this section is to apply a drift-correction formula in (2.1.10) on the Stratonovich SH equation (6.1.2) to obtain an Itô equation for which the solution are equivalent.

The stochastic SH equation interpreted in the Stratonovich sense has a nonzero mean value for the multiplicative noise term, unlike the stochastic SH equation interpreted in the the Itô sense, whereby the multiplicative noise term has zero mean value, as the noise itself. Consequently, converting the Stratonovich SH equation (6.1.2) to the Itô SH equation (6.4.2) implies that we are adjusting the mean of the noise term to zero.

Converting the Stratonovich SH equation to the Itô formulation, allows us to take out the systematic contribution of noise [27] on the corrected equation, which then provides the framework to carry out AUTO computations, see §6.5.

In what follows, we apply the drift correction formula on the Stratonovich SH equation (6.1.2) given by

$$du = \Big[Au + f(u)\Big]dt + \nu g(u) \circ dW(t), \tag{6.4.1}$$

where $A = r - \Big(\Delta + q_c^2\Big)^2$, $f(u) = \rho u^2 - gu^3$, $g(u) = u$, and $W(t)$ is a $\mathbb{Q}$-Wiener process given in (2.3.9).

We convert the Stratonovich SH equation (6.4.1) into an Itô equation by using a drift correction term which uses the trace of $\mathbb{Q}$ denoted as Tr$\mathbb{Q}$ in the correction term coming from the diffusion term of the SPDE. The Tr$\mathbb{Q}$ indeed has the contribution of spatial correlation of the noise.

$$du = \left[Au + f(u) + \nu^2 \mathrm{Tr}\mathbb{Q} g(u)' g(u)\right]dt + \nu g(u) dW(t), \tag{6.4.2}$$

where $\mathrm{Tr}\mathbb{Q} = \sum_n \lambda_n$. The λ_n are the eigenvalues of the $\mathbb{Q}$-Wiener process and it is computed from (2.8.34), since we are considering noise to be white in time and with exponential decaying correlations in space.

Small noise expansion analysis as described in [27] suggests that we can take out

the systematic contribution of noise on the drift term by looking at the average behaviour of (6.4.2). Thus, the average behaviour of the (6.4.2) is approximated by the deterministic equation

$$du = \Big[Au + f(u) + \nu^2 \mathrm{Tr}\mathbb{Q}g(u)'g(u)\Big]dt, \tag{6.4.3}$$

which is essentially the equation we considered for AUTO computations. To show that the solution we get from simulating (6.4.1) and (6.4.2) both have the same result, we perform numerical experiments on both equations using the same parameter values. We see in Figure 6.11(a) that applying the **ESI** method (5.3.14) on (6.4.1) agrees with Figure 6.11(b) where we applied the **SETD0** method (5.3.2) on (6.4.2). We have plotted in Figure 6.11(c), the L^2 norm solutions of the Stratonovich equation (6.4.1) and the Itô equation (6.4.2) and in Figure 6.11(d) is the plot displaying the error between the two solutions which is of magnitude $\approx 10^{-3}$, which indicates that the error is very small.

6.5 Continuation on the control parameter.

For the deterministic case, we carried out continuation on the control parameter r in (6.1.1) using AUTO and present the bifurcation diagram in Figure 6.1(b). To perform continuation on the control parameter r for the deterministic SH equation (6.1.1), we need to consider the solution at equilibrium. That is,

$$0 \;=\; ru - \Delta^2 u - 2q_c^2 \Delta u - q_c^4 u + \rho u^2 - g u^3. \tag{6.5.1}$$

The equation is then reduced to the following four-dimensional systems of ODEs.

$$\begin{cases} \dot{u}_1 = u_2 \\ \dot{u}_2 = u_3 \\ \dot{u}_3 = u_4 \\ \dot{u}_4 = -2q_c^2 u_3 + (r - q_c^4)u_1 + \rho u_1^2 - g u_1^3 \end{cases} \tag{6.5.2}$$

where r is the continuation parameter, g, ρ and q_c are parameters which we take to be 1, 0.41 and 0.5 respectively.

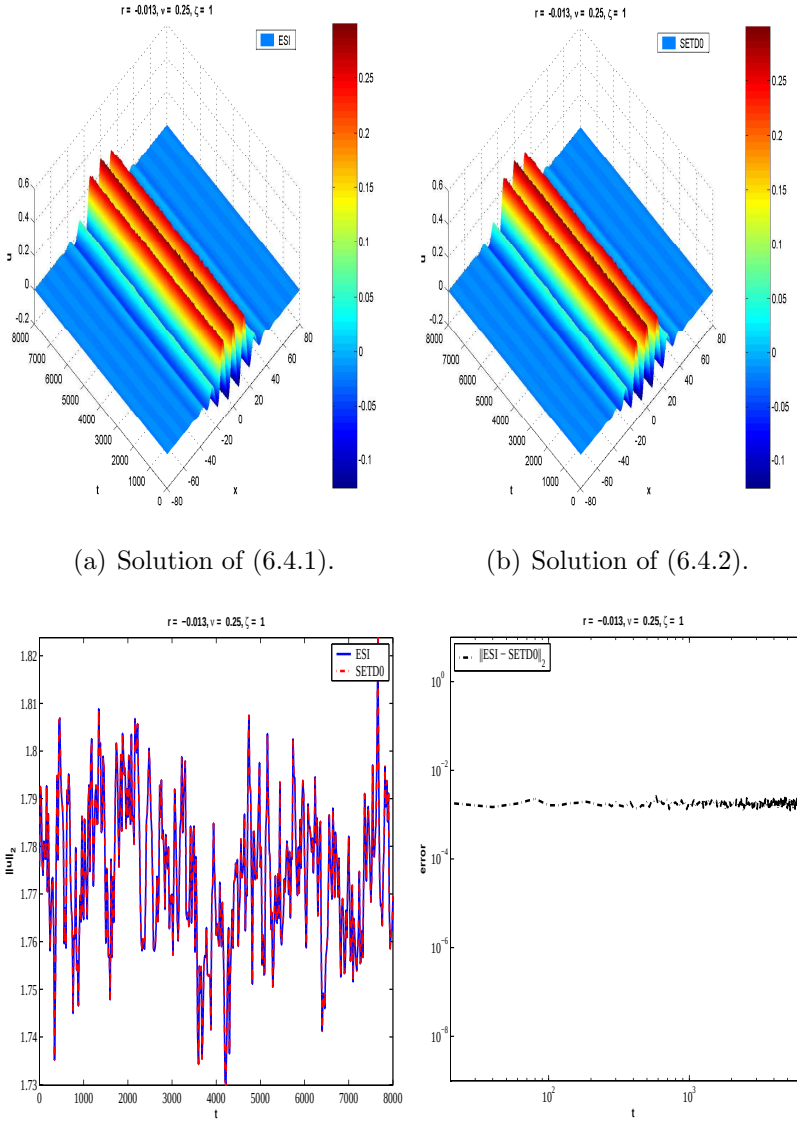

(a) Solution of (6.4.1). (b) Solution of (6.4.2).

(c) $||u||_2$. (d) error vs time.

Figure 6.11: The plots shows the agreement of solution of (6.4.1) and (6.4.2) having performed a drift correction on (6.4.1). For both equations a path of the solution is simulated based on the same path of the Wiener process. In (a) is the solution of equation (6.4.1), in (b) is the solution of the Itô equation (6.4.2) obtained from performing a drift correction on (6.4.1), (c) is a plot of $||u||_2$ versus time; The term $||u||_2$ denotes the norm of the solution of (6.4.1) and (6.4.2) at each point in time over the integration time. (d) is a plot of error versus time; The expression error in Figure 6.11 stands for the L^2 norm of the difference between the solution obtained when (6.4.1) is discretized using the **ESI** scheme and the solution obtained when (6.4.2) is discretized using the **SETD0** scheme.

For the stochastic case, we carry out continuation by applying a numerical small noise expansion analysis on the stochastic SH equation, which means that if we wish to perform continuation on the Itô equation in (6.4.2), we will neglect the stochastic contribution of noise on the diffusion part of the equation and only consider the following equation with an extra term in the nonlinearity of the stochastic SH equation, see equation (6.4.3).

For continuation of the control parameter r on the stochastic SH equation, we denote the factor $\nu^2 \mathrm{Tr}\mathbb{Q}$ in (6.4.3) by K, and we modify the function $\dot{u}_4$ in (6.5.2) as

$$\dot{u}_4 = -2q_c^2 u_3 + (r - q_c^4)u_1 + \nu u_1^2 - g u_1^3 + K u_1. \tag{6.5.3}$$

The resulting four-dimensional system of ODEs were then used in AUTO to obtain the bifurcation diagrams displayed in Figure 6.3.

6.6 Conclusion

We conclude this chapter with the following key results. Bifurcation diagram for the deterministic SH equation suggests that stable localized solutions are contained within the pinning region bounded by $r = -0.01453$ and $r = -0.01245$, see Figure 6.1(b). We showed that the inclusion of Stratonovich spatially uncorrelated noise in the SH equation with control parameter $r = -0.015$ changes the range of the pinning region by shifting the homoclinic branch which contains the localized stable solution a further distance to the left on the bifurcation diagram, see Figure 6.3.

We remark that there is an open question in the case of what influence spatially correlated noise has on the bifurcation of the SH equation because small noise expansion analysis suggests that there exist a control parameter outside the deterministic pinning region for which stabilization occurs.

ν \ r	-0.018	-0.015	-0.01453	-0.013	-0.01245	-0.012
0	0	0	1	1	1	0
0.1	0	0	1	1	0	0
0.2	0	0	0	1	0	0
0.3	0	0	0	1	0	0
0.4	0	0	1	1	0	0
0.5	0	0	1	1	0	0
0.6	0	0	1	0	0	0
0.7	0	0	1	0	0	0
0.8	0	0	1	0	0	0
0.9	0	1	1	0	0	0
1	0	1	1	0	0	0
1.1	0	1	0	0	0	0
1.2	0	0	0	0	0	0
1.3	0	0	0	0	0	0
1.4	0	0	0	0	0	0
1.5	0	0	0	0	0	0

Table 6.1: A compact tabular representation of the dynamics of the solutions of (6.1.2) with spatially uncorrelated noise at final time $T = 8000$ with varying noise intensities $\nu = [0, \cdots, 1.5]$, correlation length $\zeta = 0.1$ and for all the control parameters r used in the experiment. The cells with 0 indicates instability while the cells with 1 indicates stability. By stability, we mean if we start the simulation of the stochastic SH equation with three-bumps initial data, then the dynamics of the solution throughout the integration time is three-bumps in nature, otherwise it is unstable.

Chapter 7

Conclusions.

In Chapter 2, we give some background materials on SODEs and SPDEs used in this thesis. In particular, we give results concerning the existence and uniqueness of solution of Itô SODEs and SPDEs. We also outline standard numerical approximation techniques for the solution of these equations interpreted in the Itô and Stratonovich sense.

In Chapter 3, we give a review on the deterministic ETD schemes and then developed three stochastic versions of the exponential time differencing scheme. Two of the schemes are suited for the simulation of Itô SDEs, we call these the Stochastic Exponential Time Differencing (**SETD0**) and (**SETD1**) schemes; and the other scheme is suited for the simulation of Stratonovich SDEs, we call this the Exponential Stratonovich Integrator (**ESI**). We tested these numerical schemes by numerically investigating their rates of strong convergence. We compared the **ESI** scheme against the standard **Heun** scheme and compared the **SETD0** and **SETD1** schemes against the **EM** and **LR** schemes. We considered four numerical examples all interpreted in the Itô and Stratonovich sense. Numerical results indicate that we get strong orders of convergence of ≈ 0.5 for the **SETD0**, **SETD1**, **EM** and **LR** schemes; and strong orders of convergence of ≈ 1 was obtained for the **ESI** and **Heun** schemes for equations with scalar noise and SODEs driven by one Wiener process. However, we obtain lower strong orders for the Stratonovich schemes when the SODE is driven by two

Wiener processes. This result has been reported in the literature, see [79].
In the literature it has been shown that the rate of convergence of a numerical method can be improved if the strength is noise is considerably small. Thus, we analyzed the effects of small noise on SODEs using a population dynamics scalar SDE. In addition to the numerical schemes used above, we carry out simulations with the **Milstein** scheme. Numerical results show a rate of strong convergence of order 1 for all the numerical methods.
The strong order of convergence that were observed numerically are indeed in good agreement with theoretical results in the literature. We also showed the plots of the solutions from the different stochastic calculus interpretations, and we see that all the solution paths agree, which shows that we can use the drift-correction techniques to carry out Itô-Stratonovich correction and vice-versa, Stratonovich-Itô correction.
The new numerical method we introduced in Chapter 3 called the exponential Stratonovich integrator **ESI** was used to carry out simulations. Simulations were also carried out with the standard **Heun** method and we observe that we get the same dynamics of solutions from using the both schemes. Thus, we investigate the accuracy and efficiency of the **ESI** and **Heun** schemes by examining their strong order of convergence. Indeed numerical results suggest that the **ESI** scheme has approximately the same accuracy and efficiency as the standard **Heun** scheme.

In Chapter 4, we proved theoretical strong convergence results for the **SETD0** schemes applied to parabolic SPDEs with infinite-dimensional additive noise and one-dimensional multiplicative noise. However, we do not prove a convergence result for SPDEs with infinite-dimensional noise. In all these cases, we consider that the SPDEs have only one driving Wiener process. For the numerical approximations of SPDEs, we considered a Fourier based Galerkin approximations for the spatial variables and the **SETD0** scheme for the time variable. We obtained the following strong error estimates, which are in the root mean square sense.

Multiplicative noise SPDE; *see Theorem 4.4.1* .

$$\left(\mathbb{E}\left[\left|\left|u(t_j)-u^N(t_j)\right|\right|^2\right]\right)^{1/2} \leq C\Big(N^{-2}+\Delta t^{\theta}+N^{-r}|\alpha_N^{-1}| + \epsilon\Delta t^{\theta}+\epsilon^2\Delta t^{1/2}+\epsilon N^{-r}|\alpha_N^{-1/2}|\Big).$$

Additive noise SPDE; *see Theorem 4.5.1.*

$$\left(\mathbb{E}\left[\left|\left|u(t_j)-u^N(t_j)\right|\right|^2\right]\right)^{1/2} \leq C\Big(N^{-2}+\Delta t^{\theta}+\epsilon^2\Delta t+N^{-r}|\alpha_N^{-1}|+ \epsilon\Delta t N^{-\gamma}|\alpha_N^{1/2}|+\epsilon N^{-\gamma}|\alpha_N^{-1/2}|\Big).$$

We also show four complimentary results, see Corollaries 4.4.2, 4.4.3, 4.5.2 and 4.5.3. These results show the strong convergence of the **SETD0** scheme applied to a second-order SPDE (for example, the Allen-Cahn equation) and a fourth-order SPDE (for example, the Swift-Hohenberg equation) for one-dimensional multiplicative Itô noise and infinite-dimensional additive noise.

In Chapter 5, we numerically investigated the strong convergence of six numerical methods for the solution of SPDEs. Four of the numerical methods, that is, the **SETD0**, **SETD1**, **LR** and **EM** schemes are suited for the simulation of Itô SPDEs, while the remaining two numerical methods, that is, the **ESI** and **Heun** schemes are suited for the simulation of Stratonovich SPDEs.

We test the convergence of these numerical methods by performing numerical simulations on two SPDE examples. We considered a second-order SPDE, that is, the Allen-Cahn equation and the fourth-order SPDE, that is, the Swift-Hohenberg equation. In addition, we examined the effects of small and large noise for the convergence of the numerical schemes.

Numerical results for the **SETD0** schemes confirms the convergence proof in Chapter 4, for the case of SPDE with one-dimensional noise, we obtain rates of convergence of 1/2 and 1 for the case where noise is large and small respectively. These rates are

in excellent agreement with the theoretically predicted rates of convergence.
The **ESI** scheme was found to be more accurate and efficient than the **Heun** scheme in all the numerical simulations on SPDEs interpreted in the Stratonovich sense.

In Chapter 6, we considered the effects of noise on bifurcations for SPDEs. In particular, we study the effects of spatially correlated and uncorrelated noise on the snaking region for localized states in Swift-Hohenberg equation. We considered the SH equation with both the additive and multiplicative noise in dW. For the SH equation with multiplicative noise, we considered the equation both the Itô and Stratonovich sense. Direct simulations of the SH equation with Stratonovich spatially uncorrelated noise suggest that we obtain a stochastic resonance, that is to say, we obtained an effect which does not exist in the deterministic setting. We see a shift in the snaking region, this means there is a stabilizing effect of spatially uncorrelated noise on the SH equation for the range of control parameters where solutions were shown to be unstable in the deterministic scenario.

Bibliography

[1] G. Ahlers, C. W. Meyer, and D. S. Cannell. Deterministic and stochastic effects near the convective onset. In *Proceedings of the Workshop on External Noise and Its Interaction with Spatial Degrees of Freedom in Nonlinear Dissipative Systems (Los Alamos, NM, 1988)*, volume 54, pages 1121–1131, 1989.

[2] G. Akrivis, M. Crouzeix, and C. Makridakis. Implicit-explicit multistep methods for quasilinear parabolic equations. *Numer. Math.*, 82(4):521–541, 1999.

[3] E. J. Allen, S. J. Novosel, and Z. M. Zhang. Finite element and difference approximation of some linear stochastic partial differential equations. *Stochastics and Stochastics Reports*, 64:117–142, 1998.

[4] L. Bergamaschi, M. Caliari, A. Martnez, and M. Vianello. *A Parallel Exponential Integrator for Large-Scale Discretizations of Advection-Diffusion Models*, volume 3666/2005. Springer Berlin / Heidelberg, 2005.

[5] D. Blömker, M. Hairer, and G. Pavliotis. Some remarks on stabilization by additive noise. *Preprint.*

[6] J. P. Boyd. *Chebyshev and Fourier spectral methods.* Dover Publications Inc., Mineola, NY, second edition, 2001.

[7] E. Buckwar and R. Winkler. Multistep methods for sdes and their application to problems with small noise. *SIAM J. Numer. Anal.*, 44(2):779–803, 2006.

[8] E. Buckwar and R. Winkler. Improved linear multi-step methods for stochastic ordinary differential equations. *J. Comput. Appl. Math.*, 205(2):912–922, 2007.

[9] E. Buckwar and R. Winkler. On two-step schems for sdes with small noise. *PAMM*, 4(1):15–18, 2007.

[10] J. Burke and E. Knobloch. Localized states in the generalized Swift-Hohenberg equation. *Phys. Rev. E (3)*, 73(5):056211, 15, 2006.

[11] J. Burke and E. Knobloch. Homoclinic snaking: structure and stability. *Chaos*, 17(3):037102, 15, 2007.

[12] J. Burke and E. Knobloch. Snakes and ladders: localized states in the Swift-Hohenberg equation. *Phys. Lett. A*, 360(6):681–688, 2007.

[13] K. Burrage, P. M Burrage, and T. Tian. Numerical methods for strong solutions of stochastic differential equations: an overview. *Proceedings of the royal society of London series A: Mathematical, Physical and Engineering Sciences*, 460(2041):373–402, 2004.

[14] H. Busch and F. Kaiser. Influence of spatiotemporally correlated noise on structure formation in excitable media. *Physical Review E.*, 67(4):041105.1–041105.7, 2003.

[15] C. Canuto, M. Y. Hussaini, A. Quarteroni, and T. A. Zang. *Spectral methods in fluid dynamics*. Springer Series in Computational Physics. Springer-Verlag, New York, 1988.

[16] Y. Chen and P. J. McKenna. Traveling waves in a nonlinearly suspended beam: theoretical results and numerical observations. *J. Differential Equations*, 136(2):325–355, 1997.

[17] P. Chow. *Stochastic partial differential equations*. Chapman & Hall/CRC Applied Mathematics and Nonlinear Science Series. Chapman & Hall/CRC, Boca Raton, FL, 2007.

[18] S. M. Cox and P. C. Matthews. Exponential time differencing for stiff systems. *J. Comput. Phys.*, 176(2):430–455, 2002.

[19] G. Da Prato and J. Zabczyk. *Stochastic equations in infinite dimensions*, volume 44 of *Encyclopedia of Mathematics and its Applications*. Cambridge University Press, Cambridge, 1992.

[20] A. M. Davie and J. G. Gaines. Convergence of numerical schemes for the solution of parabolic stochastic partial differential equations. *Mathematics of Computation*, 70(233):121–134, 2001.

[21] F. de la Hoz and F. Vadillo. An exponential time differencing method for the nonlinear Schrödinger equation equations. *Computational Physics Communications*, 179:449–456, 2008.

[22] K. R. Elder, J. Vinals, and M. Grant. Ordering dynamics in the two-dimensional stochastic Swift-Hohenberg equation. *Phys. Rev. Lett.*, 68(3024), 1992.

[23] L. C. Evans. *Lecture notes on an Introduction to Stochastic Differential equations, Department of Mathematics, UC Berkeley.*

[24] B. Fornberg. *A practical guide to pseudospectral methods*, volume 1 of *Cambridge Monographs on Applied and Computational Mathematics*. Cambridge University Press, Cambridge, 1996.

[25] J. G. Gaines. Numerical experiments with S(P)DE's. In *Stochastic partial differential equations (Edinburgh, 1994)*, volume 216 of *London Math. Soc. Lecture Note Ser.*, pages 55–71. Cambridge Univ. Press, Cambridge, 1995.

[26] J. García-Ojalvo. Effects of external noise on the Swift-Hohenberg equation. *Phys. Rev. Lett.*, 71(10), 1993.

[27] J. García-Ojalvo and J. M. Sancho. *Noise in spatially extended systems*. Institute for Nonlinear Science. Springer-Verlag, New York, 1999.

[28] C. W. Gardiner. Handbook of stochastic methods for physics, chemistry and natural sciences. *Springer Series in Synergetics, Springer-Verlag*, 13, 1983.

[29] J. Goodman, T. Hou, and E. Tadmor. On the stability of the unsmoothed Fourier method for hyperbolic equations. *Numer. Math.*, 67(1):93–129, 1994.

[30] D. Gottlieb and S. A. Orszag. *Numerical analysis of spectral methods: Theory and applications*. Society for Industrial and Applied Mathematics, Philadelphia, Pa., 1977. CBMS-NSF Regional Conference Series in Applied Mathematics, No. 26.

[31] D. Gottlieb and S. A. Orzag. *Numerical analysis of spectral methods: Theory and applications*. SIAM, 1977.

[32] W. Grecksch and P. E. Kloeden. Time-discretised Galerkin approximations of parabolic stochastic PDEs. *Bull. Austral. Math. Soc.*, 54(1):79–85, 1996.

[33] I. Gyöngy. Lattice approximation for stochastic quasi-linear parabolic partial differential equations driven by space-time white noise. *I. Potential Analysis*, 9:1–25, 1998.

[34] I. Gyöngy. Lattice approximation for stochastic quasi-linear parabolic partial differential equations driven by space-time white noise. *I. Potential Analysis*, 11:1–37, 1999.

[35] I. Gyöngy and A. Millet. On discretization schemes for stochastic evolution equations. *Potential Anal.*, 23(2):99–134, 2005.

[36] I. Gyöngy and A. Millet. Rate of convergence of implicit approximations for stochastic evolution equations. In *Stochastic differential equations: theory and applications*, volume 2 of *Interdiscip. Math. Sci.*, pages 281–310. World Sci. Publ., Hackensack, NJ, 2007.

[37] I. Gyöngy and A. Millet. Rate of convergence of space time approximations for stochastic evolution equations. *Potential Anal.*, 30(1):29–64, 2009.

[38] I. Gyöngy and D. Nualart. Implicit scheme for stochastic parabolic partial differential equations driven by space-time white noise. *Potential Anal.*, 7(4):725–757, 1997.

[39] E. Hausenblas. Approximation for semilinear stochastic evolution equations. *Potential Analysis*, 18:141–186, 2003.

[40] D. J. Higham. Maple and matlab for stochastic differential equations in finance. *http://www.dipic.unipd.it/faculty/canu/files/tmp/sde/03.pdf*.

[41] D. J. Higham. An algorithmic introduction to numerical simulation of stochastic differential equations. *SIAM Rev.*, 43(3):525–546, 2001.

[42] M. Hochbruck and C. Lubich. On Krylov subspace approximations to the matrix exponential operator. *SIAM Journal on Numerical Analysis*, 34(5):1911–1925, 1997.

[43] W. Horsthemke and R. Lefever. Noise-induced transitions. *Springer*, 1984.

[44] T. Y. Hou and R. Li. Computing nearly singular solutions using pseudo-spectral methods. *J. Comput. Phys.*, 226(1):379–397, 2007.

[45] K. Itô. On stochastic differential equations. *Mem. Amer. Math. Soc.*, 4, 1951.

[46] A. Jentzen and P. E. Kloeden. Overcoming the order barrier in the numerical approximation of SPDEs with additive space-time noise. *Proc. R. Soc. A*, 465:649–667, 2009.

[47] A. Kassam and L. N. Trefethen. Fourth-order time-stepping for stiff PDEs. *SIAM J. Sci. Comput.*, 26(4):1214–1233, 2005.

[48] F. C. Klebaner. *Introduction to stochastic calculus with applications*. Imperial College Press, 2005.

[49] P. E. Kloeden, G. J. Lord, A. Neuenkirch, and T. Shardlow. The exponential integrator scheme for stochastic partial differential equations: Pathwise error bounds. *J. Comp. Appl. Math.*, 235(5):1245–1260, 2011.

[50] P. E. Kloeden and E. Platen. *Numerical solution of stochastic differential equations*, volume 23 of *Applications of Mathematics (New York)*. Springer-Verlag, Berlin, 1992.

[51] P. E. Kloeden, E. Platen, and H. Schurz. *Numerical solution of SDE through computer experiments*, volume 1. Springer-Verlag, Berlin Heidelberg New York, 2003.

[52] S. Krogstad. Generalized integrating factor methods for stiff PDEs. *J. Comput. Phys.*, 203(1):72–88, 2005.

[53] T. Leppanen, M. Karttunen, R. A. Barrio, and K. Kaski. The effects of noise on Turing patterns. *Progress of Theoretical Physics Supplement*, 150(367-370), 2003.

[54] G. J. Lord and J. Rougemont. A numerical scheme for stochastic PDEs with Gevrey regularity. *IMA J. Numer. Anal.*, 24(4):587–604, 2004.

[55] G. J. Lord and T. Shardlow. Postprocessing for stochastic parabolic partial differential equations. *SIAM J. Numer. Anal.*, 45(2):870–889, 2007.

[56] G. J. Lord and A. Tambue. Stochastic exponential integrators for a finite element discretization of SPDEs with additive noise. *http://arxiv.org/abs/1005.5315*, 2010.

[57] G. J. Lord and V. Thüemmler. Freezing stochastic travelling waves. *http://arxiv.org/abs/1006.0428*, 2010.

[58] X. Lu, C. Wang, C. Qiao, Q. Ouyang, and H. Wang. Effect of noise on chemical waves in three-dimensional reaction-diffusion systems with gradient. *Journal of Chem. Phys.*, 128:114505, 2008.

[59] G. Lythe and S. Habib. Dynamics of kinks: nucleation, diffusion and annihilation. *Physical Review Letters*, 84:1070–1073, 2000.

[60] G. Lythe and S. Habib. Kink in stochastic PDE. *Proceedings of the IUTAM symposium on nonlinear stochastic dynamics*, pages 435–444, 2003.

[61] G. Lythe and S. Habib. Kink stochastics. *CISE*, 8(3):10–15, 2006.

[62] Y.-P. Ma, J. Burke, and E. Knobloch. Snaking of radial solutions of the multi-dimensional Swift-Hohenberg equation: A numerical study. *Elsevier Physica D*, 239:1867 – 1883, 2010.

[63] X. Mao. *Stochastic differential equations and their applications*. Horwood Publishing Series in Mathematics & Applications. Horwood Publishing Limited, Chichester, 1997.

[64] S. McCalla and B. Sandstede. Snaking of radial solutions of the multi-dimensional Swift-Hohenberg equation: A numerical study. *Elsevier Physica D*, 239:1581 – 1592, 2010.

[65] G. N. Milstein and M. V. Tret′yakov. Mean-square numerical methods for stochastic differential equations with small noise. *SIAM J. Sci. Comput.*, 18(4):1067–1087, 1997.

[66] G. N. Milstein and M. V. Tret′yakov. Numerical methods in the weak sense for stochastic differential equations with small noise. *SIAM J. Numer. Anal.*, 34(6):2142–2167, 1997.

[67] C. Moler and C. Van Loan. Nineteen dubious ways to compute the exponential of a matrix, twenty-five years later. *SIAM Rev.*, 45(1):3–49, 2003.

[68] C. M. Mora. Weak exponential schemes for stochastic differential equations with additive noise. *IMA Journal of Numerical Analysis*, 25:486–506, 2005.

[69] A. C. Newell and J. V. Moloney. *Nonlinear optics*. Advanced Topics in the Interdisciplinary Mathematical Sciences. Addison-Wesley Publishing Company Advanced Book Program, Redwood City, CA, 1992.

[70] B. Øksendal. *Stochastic differential equations: An introduction with applications*. Springer-Verlag, sixth edition, 2003.

[71] A. Pazy. *Semigroups of linear operators and application to partial differential equations*, volume 44. Applied Mathematical Sciences, Springer-Verlag, 1983.

[72] L. A. Peletier and W. C. Troy. *Spatial patterns*. Progress in Nonlinear Differential Equations and their Applications, 45. Birkhäuser Boston Inc., Boston, MA, 2001. Higher order models in physics and mechanics.

[73] C. Prêvôt and M. Röcker. *A concise course on stochastic partial differential equations*. Springer, 2007.

[74] J. Printems. On the discretization in time of parabolic stochastic partial differential equations. *Math. Model. and Numer. Anal.*, 35(6):1055–1078, 2001.

[75] D. Qiang and Z. Wen-xiang. Stability analysis and application of the exponential time differencing schemes. *J. Comput. Math.*, 22(2):200–209, 2004.

[76] B. D. Reddy. *Introductory functional analysis: with applications to boundary value problems and finite elements*. Springer-Verlag, 1998.

[77] J. C. Robinson. *Infinite-Dimensional Dynamical Systems: An Introduction to Dissipative Parabolic PDEs and the theory of Global Attractors*. Cambridge University Press, 2001.

[78] A. Rocco, J. Casademunt, W. V. Saarloos, and U. Ebert. Diffusion coefficient of propagating fronts with multiplicative noise. *Physical Review E*, 65(012102), 2001.

[79] W. Rümelin. Numerical treatment of stochastic differential equations. *SIAM J. Numer. Anal.*, 19(3):604–613, 1982.

[80] H. Sakaguchi. Noise-induced synchronization for phase turbulence. *Physics Letters A*, 318(6):553–557, 2003.

[81] J. M. Sancho and A. Sánchez. External fluctuations in front dynamics with inertia: The overdamped limit. *The European Physical Journal B*, 16(1):127–131, 2000.

[82] N. D. Sandham. Turbulence simulation. In *Prediction of turbulent flows*, pages 207–235. Cambridge Univ. Press, Cambridge, 2005.

[83] M. A. Santos and J. M. Sancho. Noise-induced fronts. *Physical Review E.*, 59(1):98–102, 1999.

[84] T. Shardlow. Numerical methods for stochastic parabolic partial differential equations. *Numer. Funct. Anal. Optim.*, 20(1-2):121–145, 1999.

[85] T. Shardlow. Nucleation of waves in excitable media by noise. *SIAM Multiscale Model Simul.*, 3(1):151–167, 2004.

[86] T. Shardlow. Numerical simulation of stochastic PDEs for excitable media. *J. Comput. Appl. Math.*, 175(2):429–446, 2005.

[87] D. Smets and J. B. van den Berg. Homoclinic solutions for Swift-Hohenberg and suspension bridge type equations. *J. Differential Equations*, 184(1):78–96, 2002.

[88] R. L. Stratonovich. A new representation for stochastic integrals and equations. *SIAM Journal on Control*, 4(2):362–371, 1966.

[89] J. Swift and P. C. Hohenberg. Hydrodynamic fluctuations at the convective instability. *Phys. Rev. Lett. A*, 15(1):319–328, 1977.

[90] A. Tambue. *Efficient numerical schemes for porous media flow.* PhD thesis, Department of Mathematics, Heriot Watt University, 2010.

[91] L. N. Trefethen. *Spectral methods in MATLAB*, volume 10 of *Software, Environments, and Tools.* Society for Industrial and Applied Mathematics (SIAM), Philadelphia, PA, 2000.

[92] J. B. van den Berg, L. A. Peletier, and W. C. Troy. Global branches of multi-bump periodic solutions of the Swift-Hohenberg equation. *Arch. Ration. Mech. Anal.*, 158(2):91–153, 2001.

[93] J. B. van den Berg and R. C. Vandervorst. Stable patterns for fourth-order parabolic equations. *Duke Math. J.*, 115(3):513–558, 2002.

[94] C. van den Broeck and J. M. R. Parrando. Noise-induced nonequilibrium phase transition. *Physical Review Letters*, 73(3395–3398), 1994.

[95] J. M. G. Vilar and J. M . Rubi. Spatiotemporal stochastic resonance in the Swift-Hohenberg equation. *Physical Review Letters*, 78(2886–2889), 1997.

[96] W. F. Warnick. *Numerical analysis for electromagnetic integral equations*. Artech House, Inc., 2008.

[97] R. Winkler. Stochastic differential algebraic equations of index 1 and applications in circuit simulation. *J. Comput. Appl. Math.*, 163(2):435–463, 2004.

[98] M. Wu and C. D. Andereck. Effects of external noise on the Fréedericksz transition in a nematic liquid crystal. *Physical Review Letters*, 65(591–594), 1990.

[99] Y. Yan. Galerkin finite element methods for stochastic parabolic partial differential equations. *SIAM J. Numer. Anal.*, 43(4):1363–1384, 2005.